Feasibility Of Demand Side Response From Electrolysers To Support Power System Stability

Patrick K.S. Ayivor

Technische Universiteit Delft

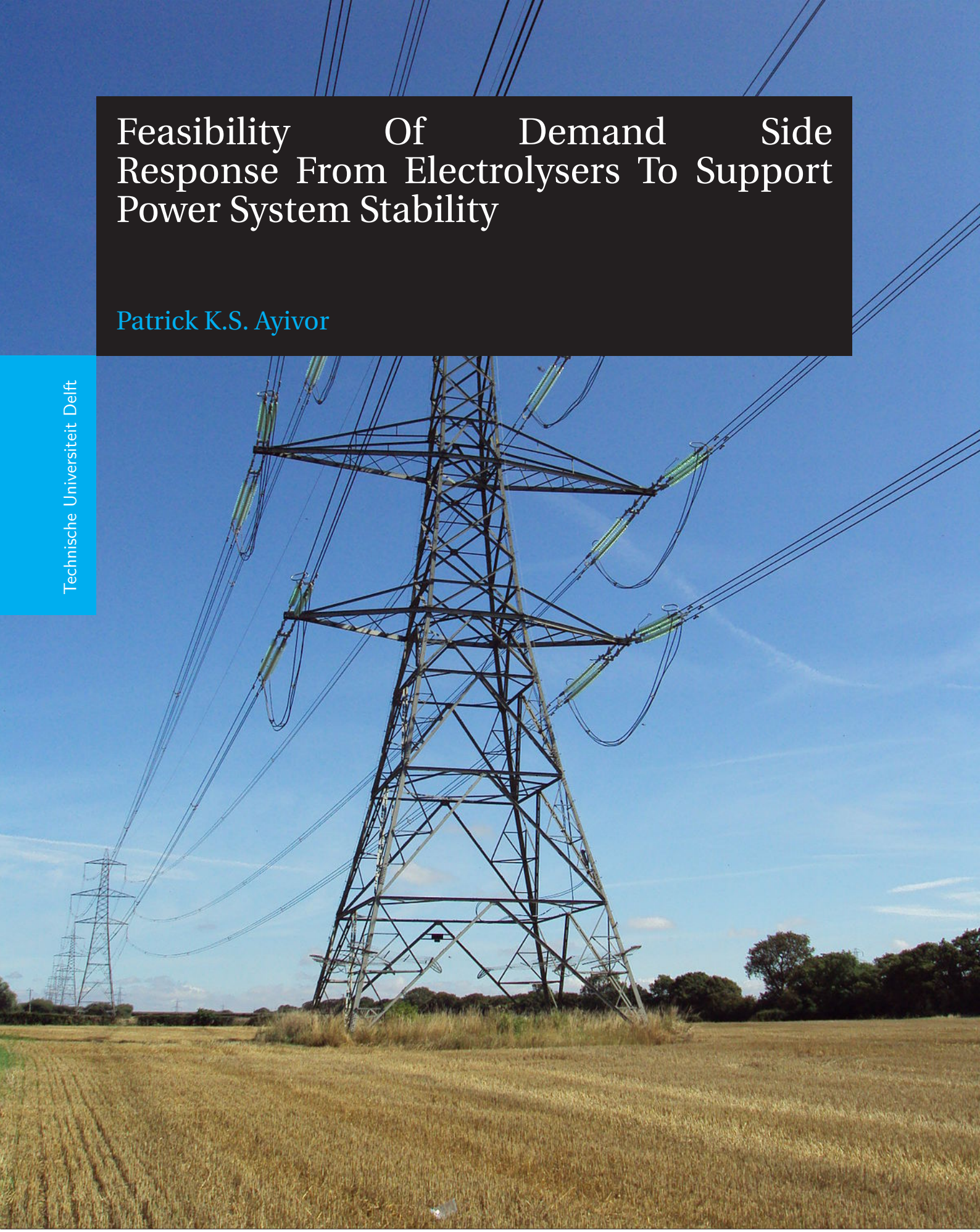

TU Delft Delft University of Technology

Challenge the future

Feasibility Of Demand Side Response From Electrolysers To Support Power System Stability

by

Patrick K.S. Ayivor

A thesis submitted in partial fulfilment of the requirements for the degree of

Master of Science
in Electrical Engineering

at the Delft University of Technology,
to be defended publicly on 18th July 2018.

Supervisor:	Dr. ir. J. L. Rueda Torres	
Thesis committee:	Prof. M.A.M.M van der Meijden	IEPG, TU Delft
	Dr. ir. J. L. Rueda Torres	IEPG , TU Delft
	Dr. Z. Qin	DCE&S, TU Delft

TU Delft Delft University of Technology

ACKNOWLEDGEMENT

"A single tree cannot make a forest" - *Ewe Proverb*.

I wish to thank The Almighty God, the Creator and Ruler, for leading the way in my life. All the glory to Him. I am grateful for my family, Victoria, Regina, Anne, Ernest, Audry, Nuna, Koku, Kwame and Koshi. Your prayers and constant encouragement kept me going.
I am honoured to have the guidance of Prof. Mart van der Meijden, Dr. Jose Rueda and Dr. Da Wang during this thesis project. Thank you for the continuous support, valuable feedback and guidance during this study. I appreciate the time you dedicated to guiding me throughout this study. I am also grateful for the opportunity to learn and also to contribute to ongoing research. Next, I would like to thank Dr. Qin for agreeing to be part of my thesis committee, and taking time to evaluate the my work.

I also wish to express my sincere gratitude to all those who supported me during the period of my research. Most notably, Dr. Jose Chavez, Dr. Bart Tuinema, Matija Naglic, Dr. Lian Liu, Arcadio Perilla and the entire IEPG postdoc team for their valuable insights. Furthermore, I would like to appreciate the timely support of Ellen with conference preparations and administrative tasks. Finally, I would like to appreciate my colleagues and friends who played a part in my stay in The Netherlands: Abdulrassaq, Ernst, Jan, Victor, the entire class of 2018 and host of acquaintances both on and off campus. Thank you all!.

Patrick K.S.Ayivor,
4578880
Delft,
July 2018.

ABSTRACT

The search for new sources of ancillary services and the projected demand for hydrogen as a medium of energy storage has aroused considerable interest in the use of large scale electrolysers for power system ancillary services. As the number of large scale electrolysers is projected to grow, it is important that the dynamics of these plants are well understood in order to integrate them successfully.

In line with this objective, suitable models must be developed to aid studies of electrical power system dynamics with electrolysers configured as sources of ancillary services. This thesis report provides an overview on implementing practical models of large scale electrolysers (>1 MW) for real time digital simulation and also proposes a control scheme to extend the basic capabilities of large scale electrolysers in order to provide ancillary services to the electrical power system.

To illustrate the feasibility of creating such models, case studies are built on a one megawatt-scale plant connected to a high voltage infinite grid via step-down transformers. Real time simulations are performed by using the Real-Time Digital Simulator (RTDS) platform to investigate the response of the electrolyser model to external command signals and power system disturbances. The 1 MW model is also scaled to 300 MW with the view to qualitatively assess its performance, with respect to grid code compliance. The results show that the generic 1 MW model in RTDS can replicate the step response profile of a real electrolyser. The results also support the view that high level control schemes are a key enabler for ancillary services using large scale electrolysers. High level control schemes can enable an optimal operation of the electrolyser load on the basis of market and power system conditions.

CONTENTS

List of Figures

LIST OF TABLES

1

INTRODUCTION

The transitioning of power system towards more sustainable fuels, has led to an increased proportion of renewable generation in the generation mix. This trend is expected to continue in the foreseeable future. This increased penetration of variable renewable energy sources (VRES) such as wind and solar, coupled with the simultaneous phasing out of conventional generation units, has increased further the need for power system flexibility. Maintaining a balance between generation and demand is critical for power system stability. This balance is reflected in a stable frequency within admissible limits around the nominal value. Traditionally, the supply side (large centralised synchronous generation) provided the larger part of short term flexibility procured via ancillary services. In [8], it was observed that in most countries surveyed, the larger portion draw on ancillary services provided from generation sources, however, a significant portion also draws on demand side resources. To ensure power system stability (rotor angle, voltage and frequency stability) in future power systems with high penetration of VRES, new sources of ancillary services must be sought. Concurrent with the transition in the power sector, is another trend, i.e. the growing interest in hydrogen, as an energy carrier. This has become significant in the recent years due to increased awareness of climate change and the emerging trend of multi-sector coupling. Hydrogen has been identified as a clean and flexible energy carrier that can be used to provide both power and heat across multiple end-use sectors [9]. According to [10], hydrogen will play an important role in the future multi-energy system. Hydrogen production methods fall broadly under steam reforming, water electrolysis, photochemical reactions and biological processes [11]. Among these methods, water electrolysis currently constitutes about 4% [12] of total global production and is growing as new Power-to-Gas plants are commissioned. It is estimated that 270,000 tons of hydrogen will be produced in northern Netherlands alone, between 2017 and 2030, to support multiple sectors (industry, mobility, electricity generation, heating etc). This projected increase in demand for hydrogen will be achieved with several megawatts of electrolyser capacity [10]. The evolution of flexibility options to include larger shares of demand side resources, coupled with the increased number and scale of large electrolysers (Power-to-Gas), unlocks new opportunities for sources of power system flexibility (i.e. ancillary services). Power-to-Gas provides an unparalleled scale of energy storage and can enhance power system flexibility. The scale of pilot Power-to-Gas projects built to date range from 100 kW to 10 MW (with the majority less than 1 MW). The capacity required for commercial projects will likely be large scale with capacities in the range of tens to hundreds of MW [12]. The reason for this is the massive scale of energy storage required. For power systems with a high penetration of Variable Renewable Energy Source (VRES), the energy storage requirement is in GWh, and the size of power ramps from VRES output will be in the order of hundreds of megawatts [12]. Electrolysers can act as controllable industrial loads to support power system stability by rapidly varying their electricity consumption. The power consumption of an electrolyser

can be changed within milliseconds (24.3 milliseconds). Settling times of fractions of a second (0.2 seconds) after a set point change, are also possible [13]. Electrolysers can reduce their electrical consumption, operating for unlimited amounts of time (as low as 10 percent of nominal capacity is possible). Data from an experiments with larger units (120 kW and 312 kW) further supports the view that grid services with large electrolysers is possible [14, 15]. Despite having favourable performance characteristics, electrolysers may interact with the power system and existing sources for ancillary services thereby creating new problems. Given the projected scale (1000 MW and above) of these electrolyser plants in the future, this presents a significant risk. Therefore, it is critical that these interactions are well understood in order to integrate large electrolysers into the power system. An understanding of the potential impacts, requires good models which represent real systems with a good level of accuracy. The challenge, however, is that model concepts of these large electrolysers (>1 MW) are not available in current literature [16]. Therefore, bridging this knowledge gap is crucial. The main motivation for this thesis project lies within this challenge.

1.1. PROBLEM STATEMENT

The problem which the study aims to solve can be summarised as follows:
The understanding of interactions of large scale electrolysers within the power system, can be facilitated with practical models. Currently, model concepts of large scale electrolysers (>1 MW) do not exist. Practical generic and scalable models are therefore, needed.

1.2. SCOPE, OBJECTIVES AND RESEARCH QUESTIONS

This thesis project aims to contribute to bridging the existing knowledge gaps, by developing a scalable generic model of a 1MW electrolyser in order to study its impact on the transmission network. The scope of this thesis is to develop a generic scalable model of a large scale electrolyser. The model utilises library components in the RSCAD software. Models which represents the PEM stack, power conversion system, controls and Balance of Plant (BoP) subsystems are developed. A control approach for unlocking the capabilities of the electrolyser for ancillary service delivery is also developed using RSCAD library components. The chemical reactions within the PEM stack are not modelled. Test data available from literature is used to validate the basic model. Simulations are limited to the interactions of the model with the power system and also the model's capabilities within the framework of defined ancillary services. All simulations are carried out on the RTDS platform. The basic model is created and tested with step commands. The basic model is then augmented with a high level control scheme. Based on the matching of performance of the extended model to the ancillary service, minimum requirements for qualifying large electrolysers are proposed. The key issues addressed in this thesis are captured in the following research questions:

- Is it feasible to build a suitable model to represent the electrical response of the electrolyser in RSCAD?
- Which additional control scheme is required to extend the capabilities of electrolysers for ancillary service applications?
- How robust is the controller to disturbances in the power system?
- What are the minimum requirements needed for delivery of ancillary services using electrolysers?

1.3. METHODOLOGY

Mathematical modelling and real time simulation using Real Time Digital Simulation (RTDS) is the selected research methodology. Digital real-time simulation of the electric power system is

the reproduction of output (voltage/currents) waveforms, with the desired accuracy, which are representative of the behaviour of the real power system being modelled. This approach is a cost effective and low-risk method of developing and testing research concepts to be implemented in the power system. The entire study is broken down into five key stages namely: system analysis, RSCAD model development, model verification, model validation and model scale up to 300 MW. Figure 1.1 highlights the stages of the study.

1.3.1. SYSTEM ANALYSIS

The electrolyser system is first decomposed into key subsystems. The mathematical foundations of each subsystem are then analysed and translated into RSCAD using library component combinations. Data from literature is used extensively in this stage to ensure the developed model replicates the real system as closely as possible.

1.3.2. RSCAD MODEL DEVELOPMENT

The model developed in this thesis is a deterministic model which uses computer-based simulation. In order to simplify the model and reduce the computational burden, key assumptions are made in the model development stage. In this model, temperature effects have not been taken into account in the, since the temperature is assumed fixed. Pressure effects are neglected, since the electrolysers typically operate at fixed pressure. Stack temperature is assumed to be uniform in the electrolyser and each cell is assumed to have identical thermal behaviour. The stack model is reduced to identical PEM electrolytic cells connected in series. Therefore, the total stack working voltage can be obtained, by multiplying the cell voltage by the number of series-connected cells. The membrane is considered as being completely saturated with water. The water management in the system assumes a continuous flow of feed and coolant water to maintain a fixed temperature. The larger model (>1 MW) is also assumed to be made up of smaller units whose controllers respond simultaneously without interacting with each other. The smaller units are assumed to be operating at the same current density within the range of 1 to 3 A/cm^2. In real systems the temperature and age of the electrolyser stack, external ambient temperature and the thermal mass of the rest of the plant impact the response to step commands. This variation can be adequately accounted for by adjusting controller parameters to emulate the delays and thermal inertia etc.

1.3.3. MODEL VERIFICATION AND VALIDATION

Model verification is done with data from available literature for key parameters and step responses. In practice, controller gains etc. are adjusted at the time of commissioning and they vary for each installation.

1.3.4. MODEL SCALING TO 300 MW

The final stage of the process entails scaling the model up to 300 MW using built-in functionality of the RSCAD software components. This is an important feature of the modelling task since it can

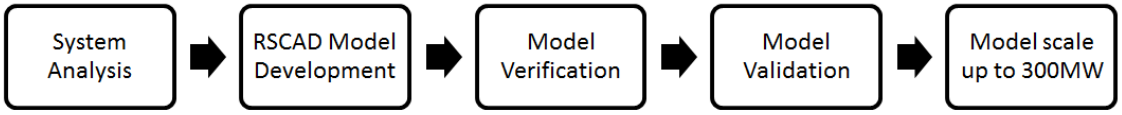

Figure 1.1: The study is divided into five stages, starting with an analysis of the electrolyser system.

facilitate easy scaling to understand the impact of electrolysers of different ratings.

1.4. CONTRIBUTION OF THESIS

This thesis contributes to ongoing research on the possibilities of using large electrolysers to enhance flexibility of power systems with large penetration of VRES. The following are key contributions of this thesis:

- A generic scalable RSCAD model of a large scale electrolyser created in this study will facilitate a deeper understanding of potential impacts of large scale electrolysers (Power-to-Gas).
- A simple hierarchical control scheme (Front End Controller) that unlocks additional capabilities for ancillary services support.
- A proposed set of pre-qualification requirements for large scale electrolysers configured to deliver ancillary services.

1.5. OUTLINE OF THESIS

Chapter 2 presents the mathematical foundations of the PEM electrolyser system at the module layer. The basics of PEM electrolyser operation is also explained. The other key subsystems such as the power conversion system and balance of plant components are also modelled.

Chapter 3 builds on the mathematical models with a detailed analysis of the hierarchical control system which can be used to extend the capabilities of the PEM electrolyser. The approach to determining the low level controller structure and parameters is explained. The structure of the high level controller is also explained along with the tuning approach.

The performance of the model is the focus of chapter 4. An overview of the Real Time Digital Simulator (RTDS) is provided together with an analysis of the responses of the model to step commands, power system disturbances and external signals. The various capabilities of the model both with and without the extended controls, are shown with simulation data. Step responses and the response to typical disturbances are evaluated with selected test cases that are built on typical real life events.

Chapter 5 describes an overview of ancillary services and matches the capabilities of large electrolysers to requirements of various ancillary services. This is done with the view to establish the feasibility of using the model to study ancillary services delivery with large electrolysers. A set of guideline requirements to qualify electrolysers is also proposed.

Chapter 6 concludes the report with a summary of the results and answers to the research questions. Contributions made by this thesis and recommendations for future work are also highlighted.

2

MATHEMATICAL MODELLING

2.1. INTRODUCTION

The objective of this chapter is to provide an overview of the PEM electrolyser system and the mathematical modelling approach used in developing the RSCAD model. The mathematical models developed in this chapter are the basis for control design, modelling and simulation in RSCAD/RTDS. Part of this chapter is drawn from [17], a published conference paper.

2.2. OVERVIEW OF PEM ELECTROLYSER SYSTEM

Hydrogen can be produced by water electrolysis, steam reforming, biological processes or photochemical reactions [11]. The production of hydrogen in this report however, is limited to the electrolysis of water. Water electrolysis is an electrochemical process in which electricity is applied to split water into hydrogen and oxygen. In the first part of the reaction, water is oxidised into protons, electrons and oxygen. The produced oxygen is then transported and removed from the cell. Protons from the oxygen evolution reaction (OER), described by equation 2.1, at the anode are transported through a diaphragm/membrane to the cathode and are reduced to molecular hydrogen in the hydrogen evolution reaction (HER) described by equation 2.2. The overall electrolysis reaction is the sum of two electrochemical half reactions, which take place at the electrodes in an acidic environment according to the following equations:

$$H_2O \rightarrow \frac{1}{2}O_2(g) + 2H^+ + 2e^- \tag{2.1}$$

$$2H^+ + 2e^- \rightarrow H_2 \tag{2.2}$$

Equations 2.1 and 2.2 are the basic reactions that govern the electrolysis reaction. The water splitting process is carried out in devices known as electrolysers. According to [1], four types of electrolysers exist currently:

- PEM electrolysers
- Alkaline electrolysers
- Solid oxide electrolysers (SOE)
- Anion exchange membrane (AEM)

Currently, both PEM and alkaline electrolysers are commercially available. Electrolysis based on AEM has a limited range of products, whereas SOE technology is at the early stage of development. Among the electrolysis technologies, alkaline electrolysis is the most mature. Alkaline technology is

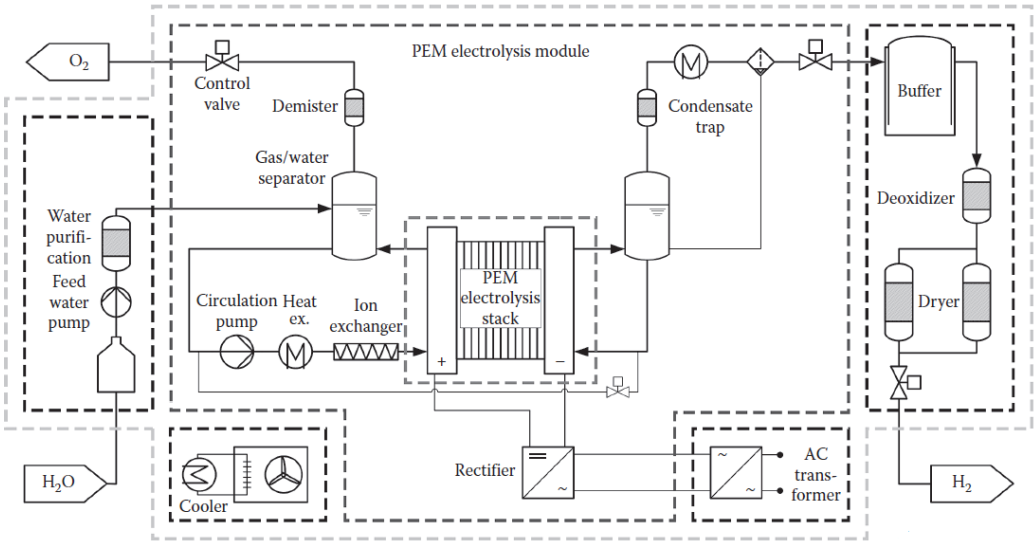

Figure 2.1: General system layout of an electrolyser showing the PEM stack and Balance of plant components (controls not shown). Extracted from [1].

also well suited to Power-to-Gas for smaller-scale projects, however, there are some clear advantages for using PEM technology for large-scale commercial projects. PEM electrolysis holds significant promise for future applications [12]. PEM electrolysers operate at significantly higher current densities, meaning significantly smaller stack volume compared with alkaline technology. This enables significantly smaller Power-to-Gas plant footprints with PEM technology. Today, the capital cost per MW and the efficiency (percentage of electrical energy converted into hydrogen) of most PEM electrolysers is similar to that of alkaline electrolysers [12]. While alkaline electrolysis is a mature technology that has reached a performance plateau, PEM electrolysis technology is at nascent stage with plenty of room for more development to increase power density, efficiency, and cost. PEM electrolyser technology therefore, holds the highest promise for the lowest capital cost along with higher power densities, smaller footprint, larger dynamic range, and a scalable design [12]. The models developed in this thesis are therefore based on the PEM technology. Figure 2.1 depicts the general PEM electrolyser system layout. This diagram is not representative of a general standard, however it captures the relevant components and subsystems. According to [1], an electrolyser system is made up of three layers: the PEM stack layer, which is the unit within which the chemical reaction takes place, the PEM module layer, which includes the stack as well as peripheral components to support stack operation (i.e. supply of reactants and removal of products), and the system layer, which comprises the module layer and other auxiliary subsystems that vary based on the installation site and application. Examples of auxiliary subsystems in the system layer are water purification systems, buffer gas reservoirs, hydrogen purification systems etc.

The PEM stack is the main component within which the production of hydrogen and oxygen takes place. It must be noted however, that the operation of the stack is only feasible with the support of other subsystems. The generic model proposed by this thesis models the PEM system at the module layer, thus the Balance of plant (BoP) components which support the operation of the stack such as feedwater and circulation pumps, are modelled. The multitude of changes required for each installation and site makes it difficult to capture the system layer in a generic model. The key components whose electrical response the generic RSCAD model emulates are, the PEM stack, the power conversion system (rectifier, DC-DC converter and main transformer) and the BoP components. The BoP components modelled include the circulation pump, the cooling system and

electronic loads such as the control system. The chemical reaction within the PEM stack is not modelled.

2.3. ELECTROLYSER SYSTEM MODELLING APPROACHES

According to [18], research over the past decade in the field of PEM electrolysers has led to models of increasing complexity and utility. Research into development of PEM electrolyser technology has focussed on different aspects depending on the research objectives. Significant research has been conducted into improving the PEM stack efficiency and reliability, among others. In line with these objectives, theoretical models or/and graphical ones are developed with the aim of enhancing integration with other systems or improving the device itself. The modelling approaches also vary based on the physical parameters of interest. For example, the models in the electrical domain model voltage and currents, whereas thermal models highlight temperature and entropy flow. According to [19], some models in literature often focus on the impact of specific parameters (membrane conductivity, exchange current densities, temperature, pressure, thermal energy) on the device behaviour, while others take into account all phenomena occurring in the device. However, despite models' variety, simplified electrical and thermal models are mostly used [20]. Lebbal and Lecouche [20] developed a steady-state electrical model and linear dynamic thermal model of a PEM electrolyser. In their approach, electrical model parameters are estimated through a non-linear least square method and thermal model parameters are identified using the properties of a first order linear model. The focus of this work was to develop a model to aid monitoring of PEM cells, thus the model captures the system at the PEM stack layer. Naturally, this approach excludes the power conversion system and other components and therefore, it is of limited use in study of interactions with power systems. A similar approach was used by Atlam and Kolhe [21], who also developed an electrical equivalent circuit model. This developed model can be applied to different sizes of PEM electrolyser as well to different parallel/series combinations of cells. The model can also be applied to electrical systems in order to analyse the electrical response and performance of PEM electrolyser system. This model also captures the electrolyser at the stack layer and is therefore limited. Der Merwe and Petrus [11] also used Electrochemical Impedance Spectroscopy (EIS) to develop an electrical equivalent circuit for the PEM electrolyser. The model captures the electrolyser in good detail at the PEM stack layer but does not capture the power conversion system. Abdin et al. [18] developed a SIMULINK model of a complete PEM electrolyser cell based on modules describing the behaviour of the anode, cathode, membrane and cell voltage in terms of physical parameters related to the materials of construction. This research is focused on improving the PEM cell and excludes other system components such as BoP and power conversion system. Agbli et al. [19] developed a model using Energetic Macroscopic Representation (EMR), a graphical modelling approach which attempts to capture phenomena in different domains. Although the resulting model's output fits well with real data, it does not capture the power supply conversion system (PCS) in sufficient detail. The PCS plays a significant role in the interactions with the power system and other controllers. The PCS is modelled as an energy source using black box approach. This limitation prevents the effective use of the model to study the electrical response of the electrolyser within the framework of ancillary services delivery. Some modelling approaches have expanded the focus to systems which are to be coupled to renewable sources however, the scale is small i.e. <1 MW. For example, Garcı´a-Valverde et al. in [22], proposed a simple model for atmospheric or low-pressure PEM water electrolysers made of three related sub models, but their model captures the electrolysers at the PEM stack layer. Chisea et al. [23] also built a complete model of a 500kW electrolyser system in PSCAD with the aim of demonstrating the capabilities of electrolysers in voltage support applications. The scale of this model, though under 1 MW, may be the closest to a large scale model in literature. The various modelling approaches reviewed appear to focus on different layers of the electrolyser system as a result of different objectives, and are mostly for

sizes of electrolysers which are less than 1 MW. Most of the models are suitable for the limited scope for which they are proposed. However, for purposes of understanding interactions of large scale electrolysers with the power system, more will be required. To address this gap, a model that captures the PEM stack in addition to key subsystems such as power conversion and BoP in sufficient detail and at a power demand scale in the order of megawatts, is needed.

2.4. FUNCTIONAL DECOMPOSITION

As indicated earlier, the PEM stack is the main component within which the production of hydrogen and oxygen takes place, however, the operation of the stack is only feasible with the support of other subsystems. The module layer captures the key parts in sufficient detail for purposes of the thesis objectives. In this layer, three key functions are identified:

- Splitting of water
- Supply of power
- Supply and removal of reactants and products

Therefore, the key components whose electrical response the generic RSCAD model emulates are the PEM stack, the power conversion system (rectifier, DC-DC converter and main transformer) and the BoP components namely, the circulation pump, the cooling system and electronic loads such as the control system. These key components form the basis for the build-up of the model in subsequent sections.

2.5. PEM STACK MODEL

Electrolysis requires a direct current (DC) source to provide the electrical power to drive the process. This section shows the modelling of a PEM (proton exchange membrane) electrolyser stack within the module layer. The main losses in such PEM electrolyser stack are also modelled. It must be noted that that several parameters in the model are difficult to fix, because they vary for each electrolyser device and also because of challenges with obtaining proprietary information. However, practical ranges for these parameters are obtained from available literature. In order to use these models, their parameters have to be estimated. Results of experimental identification techniques such as Electrochemical Impedance Spectroscopy can be converted to an equivalent circuit [11, 24]. Another option is to obtain parameters from datasheets. The model of the PEM module comprises three main parts: the PEM stack, the power conversion system and BoP.

The input DC voltage applied to a PEM cell must overcome the reversible voltage in order to trigger the chemical reaction of water splitting into oxygen and hydrogen. In practice, the cells are electrically connected in series to achieve the required hydrogen output, therefore the total voltage is a sum of the reversible voltage and contributions of the various overpotentials for each cell. Therefore, the voltage applied to the cell, V_{cell}, can be written as:

$$V_{cell} = V_{rev} + V_{act} + V_{diff} + V_{bub} + V_{ohm} \tag{2.3}$$

where V_{rev}, V_{act}, V_{diff}, V_{bub} and V_{ohm} are the reversible, activation, diffusion, bubble and ohmic overpotentials, respectively. Losses within the PEM stack are modelled as overpotentials. In order to build the steady state electrical model of the PEM cell, the reversible voltage and each overpotential are examined.

2.5.1. REVERSIBLE VOLTAGE

The splitting of water is driven by electrical and thermal energy input [1]. The energy input to the process can be represented mathematically as described by equation 2.4. State of the art PEM

electrolysis modules operate at low temperatures (< 373.15 K), implying that the larger part of energy input is obtained from electrical energy. The total energy demand to split water molecules decreases slightly with increasing temperature until the boiling point, where water gets in its gaseous state and the total energy demand increases again [1]. Assuming a lossless electrolysis process, the potential difference at the electrodes of the cell is called the reversible cell voltage. This voltage is the minimum voltage required to drive the process assuming the requisite thermal input is present. Equation 2.4 describes the expression used to calculate the reversible cell voltage.

$$V_{rev} = \frac{\Delta G_R}{z * F} = 1.229V \tag{2.4}$$

where ΔG_R is the Gibbs free energy of the reaction defined as 236.483[kJ per mol], F is the Faraday constant 96,485 [Coulombs per mol] and z is the amount of charges (electrons) transferred during the reaction (i.e. 2). However, without external thermal input, the voltage required to activate the process is higher because of a higher energy requirement for the reaction. This voltage is known as the thermoneutral voltage at standard state (defined as temperature of 25 degrees Celsius and 1 atmosphere pressure). This voltage can be calculated using equation 2.5.

$$V_{th} = \frac{\Delta H_R}{z * F} = 1.481V \tag{2.5}$$

where ΔH_R is the enthalpy of reaction for liquid water defined as -285.83 [kJ per mol] under standard conditions. The reversible voltage can be obtained for various levels of temperature and pressure using equation 2.6.

$$V_{rev} = V_0 + \frac{R * T}{(2 * F)} * ln\left(\frac{P_{H2} * P_{O2}^{0.5}}{a_{H20}}\right) \tag{2.6}$$

where R = 8,314 [Joules per mol Kelvin], F = 96,487 [Coulombs per mol], V_0 =1.23 [V], a_{H2O} = 1 (for liquid water), P_{H2} and P_{O2} are the universal gas constant, Faraday constant, standard reversible voltage, water activity, and the partially pressures (in Megapascals) of hydrogen and oxygen, respectively. This is the theoretical open cell voltage when there is no current flowing through the PEM stack.

2.5.2. LOSSES IN A PEM ELECTROLYSIS CELL

As shown in equations 2.4 and 2.5, the theoretical open-cell voltage (OCV) for the electrolysis of water is 1.229 V (with thermal energy input) or 1.48 V (without thermal energy input). When current flows through the stack however, the actual voltage for water splitting increases above the OCV value, due to irreversible losses within the cell. There are three major mechanisms that lead to losses in a PEM electrolysis cell: activation losses due to slow electrode reaction kinetics, ohmic losses, and mass transfer losses [1]. The above losses can be further categorised into two categories: the faradaic and the non-faradaic processes. The activation losses are faradaic and are linked to the direct transfer of electrons between redox couples at the interface between the electrode and the electrolyte of the oxygen evolution reaction (OER) and the hydrogen evolution reaction (HER). Non-faradaic losses are those that do not result from the direct transfer of electrons across the electrodes due to electrochemical reaction. The ohmic and mass transport losses are related to non-faradaic loss mechanisms.

Ohmic losses are due to resistance to electron flow through the electrodes and cell components as well as resistance to the flow of protons through the membrane and are directly proportional to the amount of current passed through the cell. Mass transport losses are in two main forms: diffusion and bubbles overpotentials. Diffusion losses occur when gas bubbles partly block the pores of current collectors and thereby limiting the supply of reactant water to the process, while bubbles overpotential result when large gas bubbles shield the active area and reduce catalyst utilization.

In electrolysers, the irreversibilities appear in the form of overpotentials or overvoltages that are summed up to the cell potential. The losses at the anode and cathode are represented by the anodic activation overpotential and cathodic activation overpotential respectively. These together form the total activation overpotential. Activation losses are dominant at low current densities [1]. The activation overpotential is caused by the speed of the reactions that occur at the surface of the anode and cathode. A proportion of the voltage supplied is used to drive the chemical reaction that transfers the electrons to or from the electrode. This overpotential is non-linear, varies with the current and predominates at lower currents. The activation voltage drop equation can be obtained from Butler-Volmer and Tafel laws [20]. The activation overpotential, which can be rewritten as a function of the current, is obtained from equation 2.7.

$$V_{act} = \frac{R * T}{\alpha * n * F} * \ln\left(\frac{I}{I_0}\right) \tag{2.7}$$

where α, n, I and I_0 are the transfer coefficient, number of electrons transferred, cell current and the exchange current, respectively. At high current densities (>2mA/cm^2), the production of bubbles shields the active area and reduces the contact area between the electrode and the electrolyte. This reduces catalyst utilization and results in an increase in the local current density and resultant bubbles overpotential. This rise in local current density increases exponentially with increasing current density [1]. The concentration of fluids (gas and water) and diffusion close to the electrodes influence the value of the current. These changes induce the diffusion voltage drop. The diffusion voltage, V_{diff}, can be obtained from equation 2.8.

$$V_{diff} = \frac{R * T}{\beta * n * F} * ln\left(1 + \frac{I}{I_{Lim}}\right) \tag{2.8}$$

where β, n and I_{Lim} are the constant coefficient, number of electrons transferred and the diffusion limit current, respectively. Ohmic losses are directly proportional to the amount of current passed through the cell according to Ohm's law. Ohmic losses, modelled by ohmic overpotential, become dominant at mid current densities. The resistance of the polymer membrane is the main cause of ohmic voltage drop. The resistance value is a function of membrane section area, membrane thickness, hydration ratio (7 = dry enough, 14 = good hydration, 22 = bathed) and temperature. The expression for obtaining ohmic voltage drop is described by the equation 2.9.

$$V_{ohm} = \frac{l_m}{A_m * (0.005139 * \lambda + 0.00326) * \exp\left(1267\left(\frac{1}{303} - \frac{1}{T}\right)\right)} * I \tag{2.9}$$

where λ, l_m, A_m are the membrane hydration ratio, membrane thickness, and membrane section area, respectively.

2.5.3. EQUIVALENT CIRCUIT OF PEM CELL

The electrical response of the PEM stack is characterised by the open cell voltage and overpotentials. The actual cell voltage for water splitting is the sum of the open cell voltage plus, all irreversibilities within the cell. Summing equations 2.4, 2.7, 2.8 and 2.9 yields the mathematical model for the PEM electrolysis cell. The model can then be represented by an electrical equivalent circuit which represents the overpotentials with resistances [25]. The charge double layer phenomenon which takes place at the electrode-electrolyte interface, is modelled by a capacitance in parallel with the activation and mass transport resistances. This representation, shown in figure 2.2, is useful for analysis of dynamic behaviour of the electrolyser. The resistances $Ract$, $Rmass$ and $Rohm$, represent activation, mass transport and ohmic losses, respectively. The reversible voltage is represented by a fixed DC voltage. According to [25], the electrical equivalent is widely used in current literature. For large scale electrolysers the model is further reduced based on the following assumptions:

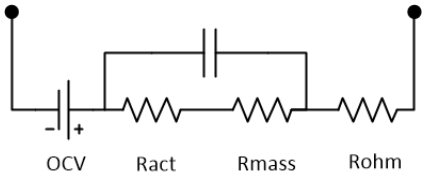

Figure 2.2: Electrical equivalent of PEM cell.

- The mass transfer losses are not significant for low and moderate current densities if the flow field is appropriate for gas removal. Thus, the mass transfer overpotentials can be neglected for current densities up to 3 A/cm^2 [1].
- Activation losses are dominant at low current densities, while the ohmic overpotential becomes dominant at medium current densities [1].
- Pressure and temperature are kept constant. This is normal in practice.

Figure 2.3 shows the reduced equivalent circuit made up of a series connection of a resistance (mainly due to ohmic losses) and a fixed voltage source (the open circuit voltage). The value of this resistance can be estimated from the slope of the I-V curve between the boundaries of the upper and lower operating current densities for a given cell area. It must be noted that larger scale electrolyser units are made up of an aggregation of smaller units (1 to 2 MW) connected in parallel and operating at medium current densities [26], therefore the above simplification assumptions hold for larger systems. The simplified PEM stack model is implemented in RSCAD with the rtds-vsc-BRC3 library model. The open cell voltage is set using the "CC Word" parameter in the settings for the voltage source. This variable can be changed to reflect open cell voltage at different operating temperature and pressure.

2.6. POWER CONVERSION SYSTEM MODEL

The amount of gas produced by an electrochemical process is related to the electrical charge consumed by the cell. This relationship is described by Faraday's law in equation 2.10.

$$m = (Q/F) * (M/z) \tag{2.10}$$

where m is the mass of the substance generated at an electrode in grams, Q is the total electric charge passed through the substance in coulombs, $F = 96{,}500$ [Coulombs per mol] is the Faraday constant, M is the molar mass of the substance in grams per mol, and z is the valency number of ions of the substance (number of electrons transferred). Under ideal conditions, the electric charge, passing through the electrolysis cell, is directly related to the amount of hydrogen and oxygen produced. For each mole of hydrogen produced, two electrons circulate through the external circuit. It is also known that equation 2.11 describes the relationship between total charge, current and time.

$$Q = I * t \tag{2.11}$$

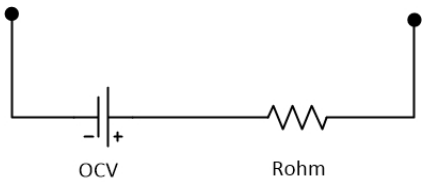

Figure 2.3: Simplified equivalent circuit of PEM cell.

where I is the current in Amperes, and t is the time in seconds. By rearranging terms of equation 2.10 and substituting in Q from equation 2.11, we obtain the hydrogen output per unit time (kilogram per second).This expressed by equation 2.12.

$$H_{2out} = M/(2 * F) * I \tag{2.12}$$

It can be seen that the hydrogen output is directly proportional to the current fed to the electrolysis cell or stack. Therefore, in order to control hydrogen generation output (which is the primary function of the Power-to-Gas plant), the current to the stack must be precisely controlled. The stack current is also proportional to the total active power demand of the electrolyser. Therefore, in order to control the total demand of the electrolyser, the stack current is the main control variable. The typical configuration of the power conversion system is shown in figure 2.4. The AC-DC and DC-DC conversions are implemented in a number of ways by different manufacturers. The generic RSCAD model allows the rectifier stage to be configured as diode rectifier or as an Active Front End (AFE) converter. In this thesis, the AC-DC conversion is implemented with a 3-phase active rectifier followed by a DC-DC converter for simplicity of control [27].

2.6.1. DC-DC CONVERTER

The current fed into the electrolyser stack is controlled by the DC-DC converter configured as a buck converter. The model assumes average current mode (ACM) control. ACM control has several advantages over peak current control such as the elimination of the external compensation ramp, increased gain for current loop at low frequency range and improved immunity to noise in the sensed current signal [28]. The average current mode control is also used in multiphase DC/DC converters to ensure accurate current sharing [28]. It is however, unable to provide peak switch current limiting. For high current applications which require low output current ripple, the interleaved mode of operation is used. As shown in figure 2.5, this approach includes additional switch network pairs (diode and switching device) with output inductors which are connected in parallel to share a common output capacitor and load. In the model developed in this thesis, flexibility to activate the multiple-cell buck converter topology is built in.The cells are switched with the same duty ratio, but with a relative phase shift introduced between each cell in order to reduce the magnitude of the output ripple at the output of the converter. With this approach it has been demonstrated that the output ripple is reduced [29]. In practice, two or more DC-DC converters are connected in parallel to realise high output currents. For the generic model in this thesis, three parallel-connected DC-DC converters are used.

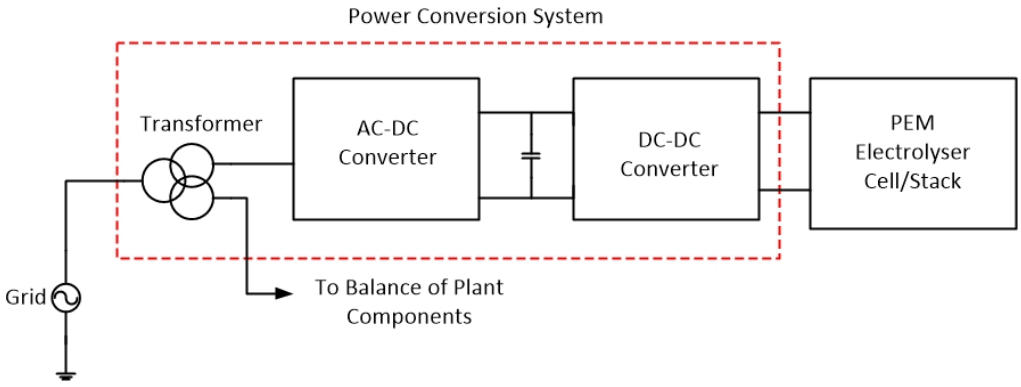

Figure 2.4: Components of power conversion system (controls not shown).

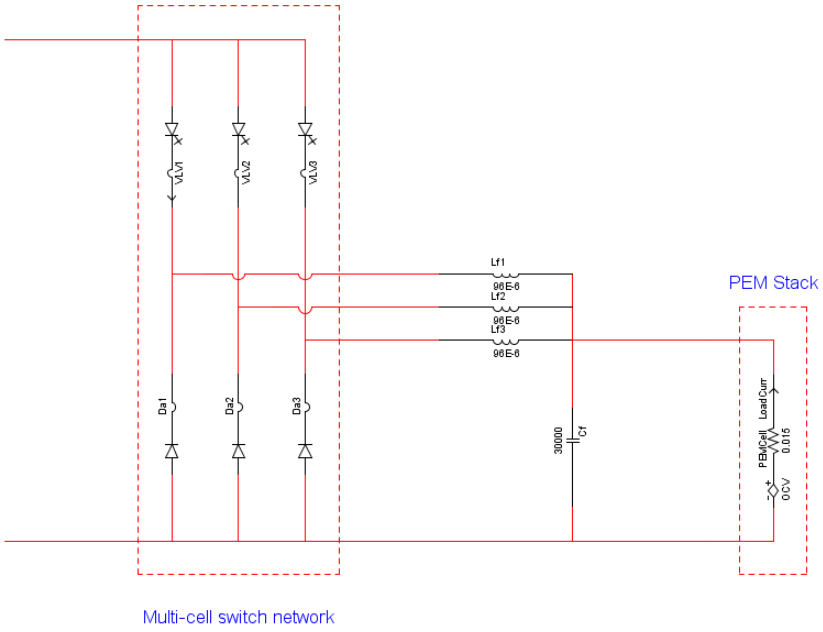

Figure 2.5: Multi-cell buck converter implementation in RSCAD. The switches used in the converter are fully controllable gate turn-off thyristors (GTO).

CONVERTER MODEL

The basic topology of a buck converter is shown in figure 2.6. Assuming ideal components and average mode current control (ACM), it can be said that the dynamic response of the converter is determined by the inductor current [2]. The filter inductance is usually large, therefore it is reasonable to assume that the inductance is equivalent to a controlled current source, as shown in figure 2.7. The equivalent replacement achieves an order reduction of the large signal model of the converter, and makes the model approximation a first-order model. According to [2], equation 2.13 describes the current source model.

$$i_L = f(d, R_L) = \frac{d \cdot V_{DC}}{R_L} \cdot \left(1 + k_1 \cdot e^{\left(\frac{k_2 \cdot R_{LB}}{R_L}\right) \cdot d}\right) \tag{2.13}$$

where k_1 and k_2 in the controlled current source are proportional coefficients, which are related to system parameters. V_{DC} is the input voltage. For this RSCAD model, continuous conduction mode (CCM) is assumed because the significantly high operating currents (in thousands of Amperes) do not permit practical operation in discontinuous conduction mode since this will result in very high voltage drops across the output filter inductance. Derivation of the transfer function of the converter is further simplified by neglecting the exponential term in equation 2.13. According to

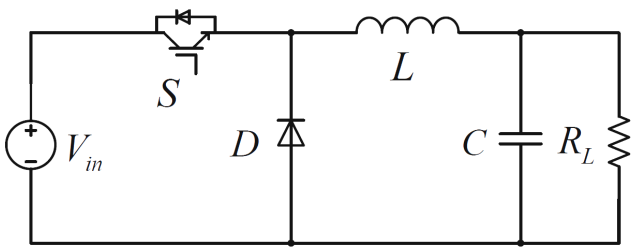

Figure 2.6: Buck converter topology. Extracted from [2].

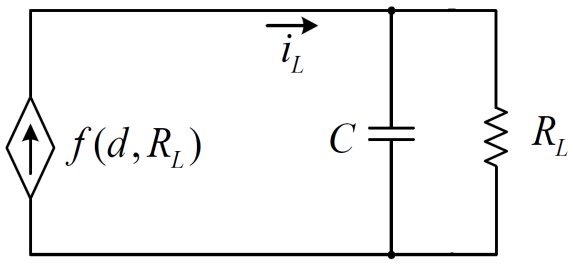

Figure 2.7: Average model of buck converter (without control loop). Extracted from [2].

[2], when load resistance is low, this term has little effect. Typical ranges for resistance values of the PEM Stack are less than one ohm [27]. From figure 2.7, the inductor current can be expressed in terms of currents flowing in the parallel combination of the resistor and output filter capacitor. Applying the Laplace transform and current divider formula yields equation 2.14.

$$i_{STACK} = i_L \cdot \left(\frac{1/sC}{1/sC + R_L} \right) \tag{2.14}$$

Simplifying equation 2.14 further, yields the open loop transfer function of the converter, expressed by equation 2.15.

$$G_{ic}(s) = \frac{i_{STACK}}{i_L} = \left(\frac{1}{1 + sCR_L} \right) \tag{2.15}$$

where R_L represents the total resistance of the PEM stack and C, the total output filter capacitance.

2.6.2. AC-DC CONVERTER (ACTIVE FRONT END)

An Active Front End (AFE) is a grid-connected converter which facilitates transfer of power between an AC power input and an intermediate DC link. It has the ability to transfer power in both directions, operating as a rectifier when transferring power from the AC side to the DC link and as an inverter in the reverse. In Active Front End (AFE) converters, the diode bridge rectifier is replaced by a rectifier comprising insulated-gate bipolar transistor (IGBT) modules. AFE converters provide very low current and voltage distortion at the point of connection and also have voltage boost capability with power factor control. The AC to DC converter used in the first version of the electrolyser model is a three-phase diode bridge rectifier, however the final model uses an active front end because of the above mentioned characteristics which favour power system ancillary service delivery. It must be noted that the converter is operated solely in rectifier mode since it is assumed that the PEM stack does not generate power.

PRECISE MODEL

This section is derived from work done in [3]. To simplify the analysis ,the AFE is analysed without the load from the DC-DC converter. It is assumed that the load current is a disturbance which is compensated for by a feedforward term in the control scheme.

The active front-end converter topology used in this thesis is a two-level, voltage source converter. It has six switches and the DC side is connected with a capacitor, which acts as a voltage source. The main circuit of the active front-end converter modelled in this thesis, is shown in figure 2.8. Parameters shown in the figure are explained as follows:

- V_a, V_b, V_c are the instantaneous grid voltages for A,B and C phases respectively.
- V_{am}, V_{bm}, V_{cm} are the converter output voltages for phases A,B and C measured with respect to point m in figure 2.8.

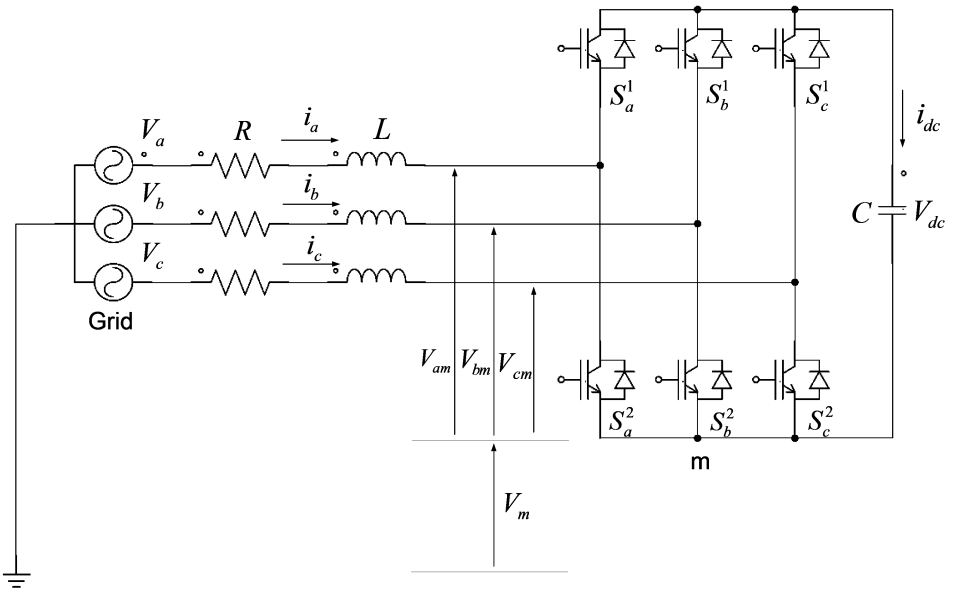

Figure 2.8: Active front end converter showing switches, input reactor and DC link capacitor. Extracted from [3].

- i_a, i_b, i_c are the instantaneous currents flowing into the AFE converter for A,B and C phases respectively.
- V_m is the voltage at point m measured with respect to ground.
- L is the inductance of the reactor.
- C is the capacitance of the DC Link capacitor.
- V_{dc} is the DC link voltage.
- i_{dc} is the instantaneous current flowing through the capacitor.

The voltage source converter (VSC) can be modelled as a voltage source. Therefore, the converter topology shown in figure 2.8 can be represented by two voltage sources linked by the input reactor. Based on the simplified model shown in 2.9, applying Kirchhoff's voltage law for sources and

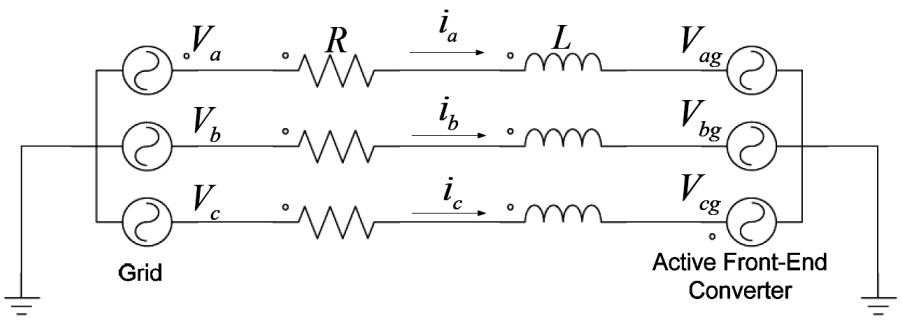

Figure 2.9: Simplified representation showing the AFE and the grid modelled as voltage sources. Extracted from [3].

elements in phase A loop, yields equation 2.16.

$$V_a = L \cdot \frac{di_a}{dt} + R \cdot i_a + V_{am} + V_m \tag{2.16}$$

Similarly for phases B and C, equations 2.17 and 2.18 hold.

$$V_b = L \cdot \frac{di_b}{dt} + R \cdot i_b + V_{bm} + V_m \tag{2.17}$$

$$V_c = L \cdot \frac{di_c}{dt} + R \cdot i_c + V_{cm} + V_m \tag{2.18}$$

Equation 2.19 holds for a balanced system assuming there is no zero sequence current, therefore:

$$i_a + i_b + i_c = 0 \tag{2.19}$$

Substituting equation 2.19 into equations 2.16 and 2.18 yields equation 2.20.

$$V_m = \frac{1}{3}(V_{am} + V_{bm} + V_{cm}) \tag{2.20}$$

In order to proceed with modelling the converter in stationary frame, the switching function for the upper switch in the phase i leg of the converter is defined as c_i in equation 2.21, where i = a, b, c.

$$c_i = \left\{ \begin{array}{l} 1 - ON \\ 0 - OFF \end{array} \right\} \tag{2.21}$$

The converter is controlled such at every instant a line voltage (i.e. terminals of two phases) is connected to the DC link. This requires two closed switches in the switching bridge (one from the upper group and the other from the lower group). It must be noted however, that the two active switches cannot be from the same phase since the switch states for the upper and lower groups are complementary. This constraint prevents short circuiting of the phases. Based on this concept, equations 2.22, 2.23 and 2.24 hold.

$$V_{am} = c_a \cdot V_{dc} \tag{2.22}$$

$$V_{bm} = c_b \cdot V_{dc} \tag{2.23}$$

$$V_{cm} = c_c \cdot V_{dc} \tag{2.24}$$

Substituting equations 2.22, 2.23 and 2.24 into equation 2.20 yields equation 2.25.

$$V_m = \frac{1}{3}(c_a + c_b + c_c) \cdot V_{dc} \tag{2.25}$$

Proceed to substitute equations 2.22 and 2.25 into equation 2.16 and simplify to yield equation 2.26.

$$L \cdot \frac{di_a}{dt} = R \cdot i_a - \frac{V_{dc}}{2} \cdot d_a + V_a \tag{2.26}$$

where d_a is defined as:

$$d_a = \frac{4}{3} \cdot c_a - \frac{2}{3} \cdot c_b - \frac{2}{3} \cdot c_c \tag{2.27}$$

Similar expressions described by equations 2.28 and 2.29 can be written for phase B and C respectively.

$$L \cdot \frac{di_b}{dt} = R \cdot i_b - \frac{V_{dc}}{2} \cdot d_b + V_b \tag{2.28}$$

$$L \cdot \frac{di_c}{dt} = R \cdot i_c - \frac{V_{dc}}{2} \cdot d_c + V_c \tag{2.29}$$

where d_b and d_c are defined as:

$$d_b = -\frac{2}{3}\cdot c_a + \frac{4}{3}\cdot c_b - \frac{2}{3}\cdot c_c \tag{2.30}$$

$$d_c = -\frac{2}{3}\cdot c_a - \frac{2}{3}\cdot c_b + \frac{4}{3}\cdot c_c \tag{2.31}$$

The instantaneous current flowing into the capacitor can be expressed as a function of the line currents and switching functions for each phase leg. It can also be verified that equation 2.33 holds. Therefore, substituting equation 2.33 into equation 2.32 yields equation 2.34.

$$C\cdot\frac{dV_{dc}}{dt} = i_{dc} = c_a\cdot i_a + c_b\cdot i_b + c_c\cdot i_c \tag{2.32}$$

$$c_a\cdot i_a + c_b\cdot i_b + c_c\cdot i_c = \frac{1}{2}\cdot(d_a\cdot i_a + d_b\cdot i_b + d_c\cdot i_c) \tag{2.33}$$

$$C\cdot\frac{dV_{dc}}{dt} = \frac{1}{2}\cdot(d_a\cdot i_a + d_b\cdot i_b + d_c\cdot i_c) \tag{2.34}$$

Simplifying further with the assumption of a balanced system with no zero sequence currents, equation 2.34 can be rewritten as equation 2.35.

$$C\cdot\frac{dV_{dc}}{dt} = \left(d_a + \frac{d_b}{2}\right)\cdot i_a + \left(d_b + \frac{d_a}{2}\right)\cdot i_b \tag{2.35}$$

Combining equations 2.35, 2.26 and 2.28, yields the precise model of the converter. In the stationary reference frame, this model is expressed by equations 2.36 and 2.37.

$$C\cdot\frac{dV_{dc}}{dt} = \frac{1}{2}\begin{bmatrix} d_a \\ d_b \\ d_c \end{bmatrix}^T \cdot \begin{bmatrix} i_a \\ i_b \\ i_c \end{bmatrix} \tag{2.36}$$

$$L\cdot\frac{d}{dt}\begin{bmatrix} i_a \\ i_b \end{bmatrix} = R\cdot\begin{bmatrix} 1 & 0 \\ 0 & 1 \end{bmatrix}\begin{bmatrix} i_a \\ i_b \end{bmatrix} - \frac{V_{dc}}{2}\cdot\begin{bmatrix} d_a \\ d_b \end{bmatrix} + \begin{bmatrix} V_a \\ V_b \end{bmatrix} \tag{2.37}$$

AVERAGE MODEL

To further simplify the model for control design purposes, the average model of the converter is used. At a sufficiently high switching frequency the average model can well emulate the precise model [3]. Based on this approach, d_a, d_b and d_c in the precise model are replaced with $\overline{d}_a$, $\overline{d}_b$ and $\overline{d}_c$, where $\overline{d}_a$, $\overline{d}_b$ and $\overline{d}_c$ represent the average of d_a, d_b and d_c, respectively, over one switching period. The average model is described by equations 2.38 and 2.39.

$$C\cdot\frac{dV_{dc}}{dt} = \frac{1}{2}\begin{bmatrix} \overline{d_a} \\ \overline{d_b} \\ \overline{d_c} \end{bmatrix}^T \cdot \begin{bmatrix} i_a \\ i_b \\ i_c \end{bmatrix} \tag{2.38}$$

$$L\cdot\frac{d}{dt}\begin{bmatrix} i_a \\ i_b \end{bmatrix} = -R\cdot\begin{bmatrix} 1 & 0 \\ 0 & 1 \end{bmatrix}\begin{bmatrix} i_a \\ i_b \end{bmatrix} - \frac{V_{dc}}{2}\cdot\begin{bmatrix} \overline{d_a} \\ \overline{d_b} \end{bmatrix} + \begin{bmatrix} V_a \\ V_b \end{bmatrix} \tag{2.39}$$

ACTIVE FRONT END CONVERTER MODEL IN SYNCHRONOUS ROTATING FRAME

In the precise model, which is based on a stationary reference frame, the variables (voltages, currents) vary with time and this complicates control design. In addition, the interaction between the three phases represents another drawback. This challenge is overcome to a large extent by modelling the converter in using rotating reference frame. Transforming the model using the synchronous rotating frame yields control variables which are constant and thus are more feasible to control using simple controllers. The well-known transformation facilitates this conversion from stationary reference frame to synchronous rotating reference frame. This transformation is captured by the matrix in equation 2.40. The transformation matrix is an orthogonal matrix, therefore equation 2.41 holds.

$$T_{abc/dq0} = \sqrt{\frac{2}{3}} \cdot \begin{bmatrix} \cos\theta & cos\left(\theta - \frac{2\pi}{3}\right) & cos\left(\theta + \frac{2\pi}{3}\right) \\ -\sin\theta & -\sin\left(\theta - \frac{2\pi}{3}\right) & -\sin\left(\theta + \frac{2\pi}{3}\right) \\ \frac{1}{\sqrt{2}} & \frac{1}{\sqrt{2}} & \frac{1}{\sqrt{2}} \end{bmatrix} \tag{2.40}$$

$$T_{dq0/abc} = \left(T_{abc/dq0}\right)^{-1} = \left(T_{abc/dq0}\right)^{T} \tag{2.41}$$

The assumption of a balanced system (i.e. no zero sequence current) allows a simplification of the three by three transformation matrix to the two by two matrix [3] in equation 2.42.

$$T_{dq/ab} = \sqrt{\frac{2}{3}} \cdot \begin{bmatrix} cos(\theta) & -\sin(\theta) \\ \sin\left(\theta - \frac{\pi}{6}\right) & cos\left(\theta - \frac{\pi}{6}\right) \end{bmatrix} \tag{2.42}$$

Applying the simplified transformation on equations 2.38 and 2.39 yields the average model of the converter in rotating reference frame, as shown in equations 2.43 and 2.44.

$$C \cdot \frac{dV_{dc}}{dt} = \frac{1}{2} \begin{bmatrix} \overline{d_d} \\ \overline{d_q} \end{bmatrix}^{T} \cdot \begin{bmatrix} i_d \\ i_{q_0} \end{bmatrix} \tag{2.43}$$

$$L \cdot \frac{d}{dt} \begin{bmatrix} i_d \\ i_q \end{bmatrix} = \begin{bmatrix} -R & \omega L \\ -\omega L & R \end{bmatrix} \begin{bmatrix} i_d \\ i_q \end{bmatrix} - \frac{V_{dc}}{2} \cdot \begin{bmatrix} \overline{d_d} \\ \overline{d_q} \end{bmatrix} + \begin{bmatrix} V_d \\ V_q \end{bmatrix} \tag{2.44}$$

This model is the basis for design of the decoupled current control explained in chapter 3.

2.6.3. TRANSFORMER

The model of the grid transformer can vary depending on the winding configuration used in the application. In the generic model, a three winding transformer (delta primary and wye secondary windings) is assumed. The model is linear and assumes magnetising branch current of 1 percent of the rated current and positive sequence leakage reactance of 6 percent for all windings. This is in line with typical values for large transformers [30]. The grid transformer is implemented with the library model (rtds-3P3W-TRF) of a three-phase three-winding transformer as shown in figure 2.10. The library component allows for modelling of losses.

2.7. BALANCE OF PLANT MODEL

The operation of a PEM stack is only possible with additional components and subsystems. In order to capture the full electrical response it is important to model these additional components which are collectively known as Balance of plant (BoP). To model BoP, a simple load model which has similar characteristics to the detailed load model is chosen.

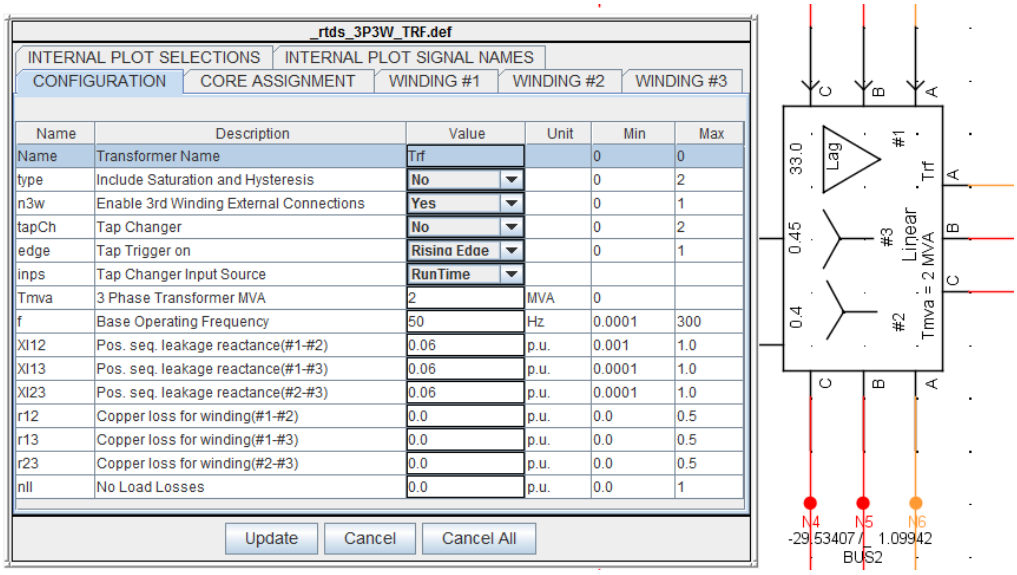

Figure 2.10: Transformer model representation and configuration panel in RSCAD.

The sum of all power inputs to the electrolyser is given by equation 2.45, where P_{AC} is the electrical power supplied to the rectifier and P_{BOP} is the power consumed by BoP components, including circulation pumps.

$$P_{electrolyser} = P_{AC} + P_{BOP} \tag{2.45}$$

The aggregated electrical response of the BoP components is assumed to be constant. This assumption is based on the view that most of the electronics loads such as control systems etc. have a fixed consumption. Secondly, the circulation pump is assumed to work continuously. This is based on the fact that the electrolyser is operated with forced convection in order to enhance water transport to, and gas removal from, the electrodes. This ensures a low temperature gradient over the stack [1]. The formation of bubbles at the electrode along with its attendant problems are avoided with this mode of operation. According to [31], the electrical power required by a pump as a function of capacity, pressure and efficiency is expressed by equation 2.46.

$$P_{pump} = \frac{Q * \Delta p}{36 * \eta} \tag{2.46}$$

where P_{pump} is the electrical power input to the motor, Q is the pump capacity in cubic meters per hour, Δp the pressure differential in bars and η is the combined efficiency of the motor, transmission and pump. Assuming a steady flow of water at a fixed pressure differential and a fixed efficiency, it can be observed that the power consumption is fixed. Taking this assumption and neglecting power consumption of other components, the aggregated BoP can be represented fairly accurately by a static load. The static load model expresses the characteristic of the load at any instant of time as algebraic functions of the bus voltage magnitude and frequency [32]. For the BoP, equations 2.47, 2.48 and 2.49 hold.

$$P = P_0 * (V')^a \tag{2.47}$$

$$Q = Q_0 * (V')^a \tag{2.48}$$

$$V' = \frac{V}{V_0} \tag{2.49}$$

where P, Q and V are active and reactive components of the load and bus voltage magnitude, respectively. P_0, Q_0 and V_0 represent initial values of P, Q and V. The parameters a and b are set at 0

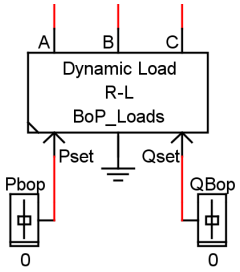

Figure 2.11: Balance of plant loads model implementation in RSCAD.

to represent constant power loads. In practice, BoP components are fed from a separate AC supply and operate at steady state and are therefore not impacted by the demand set point changes sent to the electrolyser. The implementation of the BoP is done with the load model library component within RSCAD (rtds-udc-DYLOAD) shown in figure 2.11. For electrolysers in the 1 to 2MW range, the BoP components contribute about 10 percent of the total load, however for larger units it may be progressively smaller. The BoP load parameter can be set with sliders which can be varied during the simulation. This flexibility exists within the model to allow simulation of changes in BoP load power consumption in real time.

3

CONTROL SCHEME

3.1. INTRODUCTION

The feasibility of delivering ancillary services with electrolysers depends on the control scheme put in place. This chapter describes the hierarchical control scheme, which translates external signals into low level reference signals for converters in the power conversion system. The main objectives of the control scheme are to maximise hydrogen production and enable ancillary services capabilities in a stable manner. The control approach can be expanded to capture multiple objectives, however its structure will differ. The proposed scheme in this thesis retains a simple structure which allows manipulation of the target system variables to achieve the above stated objectives. The scheme, which enables controlled exchange of active and reactive power between the electrolyser system and the power system, has two levels: the low level rectifier controls and the high level control, i.e. Front End Control (FEC). The proposed hierarchical scheme enables control of hydrogen production and also extends the capability of an electrolyser to deliver ancillary services. The control approach draws on concepts proposed in [4].

3.2. INTERNAL MODEL CONTROL

The controller structure in this thesis is based on the Internal Model Control (IMC) philosophy. IMC relies on the principle that accurate control can be achieved only if the control system encapsulates (either implicitly or explicitly) some representation of the process to be controlled. In this thesis, the IMC approach is applied to determine the controller structure. According to [33], the IMC approach results in the controller being parameterised in terms of plant parameters and desired closed loop bandwidth. This approach is described in detail in [34]. Applying this approach yields the controller transfer function in the form described by equation 3.1.

$$F(s) = \frac{\alpha^n}{(s+\alpha)^n - \alpha^n} \hat{G}^{-1}(s) \tag{3.1}$$

where *F(s)* represents the controller structure, α the desired controller bandwidth in radians per second, $\widehat{G}$ an estimation of the plant process and n, the order of $\widehat{G}$. This approach is simple and effective, however it has certain limitations. This approach can result in poor load disturbance rejection and instability, for plants with zeros in the right half plane. The approach also assumes the plant is accurately modelled, which is not always the case in reality.

3.3. LOW LEVEL CONTROL

3.3.1. DC-DC CONVERTER - LOAD CURRENT CONTROL

The goal of the load current inner control loop is to control the current fed to the PEM stack. This directly controls the hydrogen output as well as the total active power demand of the electrolyser stack (assuming lossless converters). There are a number of current control approaches for closed loop control, however, the average current mode (ACM) control method is commonly used [2]. ACM control has distinct advantages which are well suited to controlling parallel-connected DC-DC converters [35]. Therefore, ACM is assumed for this model. Flexibility however exists to modify the control system. With ACM, the average inductor current is the control variable. The error signal is generated by comparing it to a reference current which is set either by the user or by an external signal from a high level control (outer loop). The dynamic response of an average model of the DC-DC converter using current mode control, is determined by the inductor current [2]. It can be observed from figure 2.7 that the output inductance does not affect the output of the model, so it can be omitted. This results in a simple parallel RC network in series with a current source which represents the control input. Based on equation 2.15, the control input-to-output current transfer function can be approximated by equation 3.2.

$$G_{ic}(s) = \left(\frac{1}{1+sCR_L}\right) \tag{3.2}$$

where R_L represents the total resistance of the PEM stack and C is the output filter capacitance. Given that the order of the plant is one (i.e. n = 1), equation 3.1 can be simplified to obtain equation 3.3.

$$F(s) = \frac{\alpha}{s} \cdot \hat{G}^{-1}(s) \tag{3.3}$$

Substituting equation 3.2 into equation 3.3 and simplifying the expression yields equation 3.4.

$$F(s) = \alpha CR_L + \frac{\alpha}{s} \approx k_{lp} + \frac{k_{li}}{s} \tag{3.4}$$

This is equivalent to a PI controller where $k_{lp} = \alpha CR_L$ and $k_{li} = \alpha$. Thus, the generic structure of the load current controller is a PI controller. The Pulse Width Modulator (PWM) can be modelled as a gain [35]. The current sensor transfer function $R_f(s)$, is assumed to be linear and is set to one (i.e. gain of 1 with no phase shift) to simplify the analysis. For current sensors such as hall effect sensors, this is an adequate representation [36]. Combining the transfer functions and applying unity feedback yields the closed loop transfer function of the inner load current control loop, described by equation 3.5.

$$G_{li}(s) = \frac{I_{LOAD}}{I_{ref}} = \frac{k_m \cdot k_{lp} \cdot \left(s + \frac{k_{li}}{k_{lp}}\right)}{C \cdot R_L \cdot \left(s^2 + \frac{(k_m \cdot k_{lp}+1)}{C \cdot R_L} \cdot s + \frac{k_m \cdot k_{li}}{C \cdot R_L}\right)} \tag{3.5}$$

where k_{lp}, k_{li}, k_m, I_{LOAD} and I_{ref} are the proportional gain, integral gain of the load current controller, PWM gain, current reference and actual current of the PEM stack, respectively. Figure 3.1 shows the structure of the inner current control loop implemented in RSCAD.

3.3.2. ACTIVE FRONT END CONVERTER - GRID CURRENT CONTROL

DECOUPLED CURRENT CONTROL

The Active Front End (AFE) rectifier controls the currents absorbed from the grid and also the output DC link voltage. These control functions are realised with a nested loop architecture comprising an inner loop which enables stable and fast control of grid current, and an outer loop which sets the references for the inner loops such that performance objectives are realised. Recall that the active front end can be modelled as a three phase voltage source since it is a voltage source converter. From

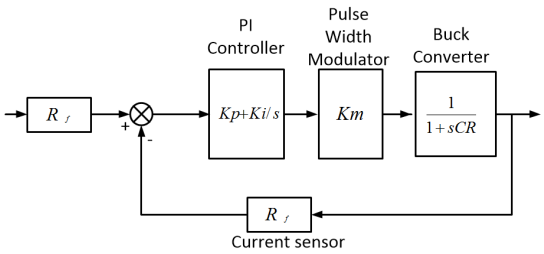

Figure 3.1: Structure of inner load current control loop.

figure 2.9 it can be observed that the line current (current flowing in the input reactor) is controlled by the voltage drop across the reactor inductance interconnecting the two voltage sources (grid and converter). Assuming the grid voltage is constant, controlling the phase angle and the amplitude of converter side voltage indirectly controls the phase and amplitude of the line current. The average value of the current in the DC link is proportional to the active power conducted through the converter, while the reactive power is related to the phase shift between grid current and grid voltage. With decoupled control, both can be controlled independently. This section explains decoupled current control scheme which facilitates the independent control of active and reactive power flows between the converter and the grid. The derivations are based on work done in [3].
In rotating reference frame, active and reactive power (both in per unit) can be expressed by equations 3.6 and 3.7.

$$P_{pu} = V_{sd} \cdot i_d + V_{sq} \cdot i_q \tag{3.6}$$

$$Q_{pu} = V_{sq} \cdot i_d - V_{sd} \cdot i_q \tag{3.7}$$

where, V_{sd} is the d-axis component of grid side voltage, V_{sq}, the q-axis component of grid side voltage, i_d, the d-axis component of grid current and i_q, the q-axis component of grid current. To facilitate simple separation of d-axis and q-axis current components, we assume the rotating reference frame's d-axis is aligned with the AC grid voltage using a Phase Locked Loop (PLL). With this assumption, the q-axis component of the grid voltage is zero and the d-axis component is equal to the magnitude of the grid voltage. Equations 3.6 and 3.7 reduce to equations 3.8 and 3.9 respectively.

$$P_{pu} = V_d \cdot i_d \tag{3.8}$$

$$Q_{pu} = -V_d \cdot i_q \tag{3.9}$$

Assuming the grid voltage is relatively constant it can be observed that independent control of active and reactive power is achieved by controlling the d-axis and q-axis components of the grid current. According to [37], this approach is popular and also well suited to control using simple PI controllers since the controlled quantities (i.e. grid currents) become DC quantities when transformed into the rotating reference frame. The proposed control scheme for the AFE is developed based on this concept. From the model in equation 2.44, it can be observed that there is coupling between the d-axis and q-axis axis components. The elimination of the cross coupling terms is therefore necessary to enable independent control of d-axis and q-axis current components. To obtain the mathematical expressions for the control signals, equation 2.44 is expanded into d-axis and q-axis equations yielding equations 3.10 and 3.11.

$$\frac{V_{dc}}{2} \cdot \overline{d_d} = -L \cdot \frac{di_d}{dt} - R \cdot i_d + \omega \cdot L \cdot i_q + V_d \tag{3.10}$$

$$\frac{V_{dc}}{2} \cdot \overline{d_q} = -L \cdot \frac{di_q}{dt} - R \cdot i_q - \omega \cdot L \cdot i_d + V_d \tag{3.11}$$

From equations 3.10 and 3.11, it can be seen that controlling $\overline{d}_d$ and $\overline{d}_q$ directly enables control of the d-axis and q-axis components of the converter-side voltage which indirectly enables control of the grid currents. To simplify the design process, the d-axis is used for subsequent analysis and derivation with the assumption that the relationships hold for the q-axis. The transfer function of the input reactor is a first order transfer function, therefore applying the IMC approach to determine the controller structure yields a simple PI controller. For the d-axis, set the output of the controller, u_d, equal to the d-axis current terms in equation 3.10 to obtain equation 3.12. Assuming a PI controller structure, equation 3.13 holds.

$$u_d = L \cdot \frac{di_d}{dt} - R \cdot i_d \tag{3.12}$$

$$u_d = k_p \cdot (i_{dref} - i_d) + k_i \cdot \int (i_{dref} - i_d) \cdot dt \tag{3.13}$$

where:
k_p = proportional gain of current controller
k_i = integral gain of current controller
i_{dref} = d-axis current reference
i_d = d-axis current

Equating 3.12 and 3.13, applying Laplace transform and simplifying yields the closed loop transfer function for the d-axis component of the inner loop, described by equation 3.14.

$$\frac{I_d(s)}{I_{dref}(s)} = \frac{k_p \cdot \left(s + \frac{k_i}{k_p}\right)}{L \cdot \left(s^2 + \frac{(R+k_p)}{L} \cdot s + \frac{k_i}{L}\right)} \tag{3.14}$$

This expression also holds for q-axis current control loop. To obtain the duty ratio signals for the switches in the A,B and C phases of the converter, substitute equation 3.12 into equation 3.10 to yield equation 3.15.

$$\frac{V_{dc}}{2} \cdot \overline{d_d} = -u_d + \omega \cdot L \cdot i_q + V_d \tag{3.15}$$

A similar approach for q-axis yields equation 3.16.

$$\frac{V_{dc}}{2} \cdot \overline{d_q} = -u_q - \omega \cdot L \cdot i_d + V_q \tag{3.16}$$

Rearranging equations 3.15 and 3.16 yields the expression for the duty ratio of the switches in d-domain and q-domain respectively. Equation 3.17 holds for d-axis while equation 3.18 holds for q-axis.

$$\overline{d_d} = \frac{-u_d + \omega \cdot L \cdot i_q + V_d}{\frac{V_{dc}}{2}} \tag{3.17}$$

$$\overline{d_q} = \frac{-u_q - \omega \cdot L \cdot i_d + V_q}{\frac{V_{dc}}{2}} \tag{3.18}$$

Converting the duty ratio from rotating reference frame (dq) to stationary (abc) under the assumption of no zero sequence component, yields the duty ratio signals for the three phases of the AFE. The implementation of equations 3.17 and 3.18 in RSCAD is shown in figure 3.2. The firing

pulses for each phase leg switch are generated by comparing the duty ratio modulation signals with a fixed-frequency triangular wave in a comparator. The switching states for each switch are generated based on the amplitude of the modulating signal compared to the triangular wave at each sampling instant. The generation and synchronisation of firing pulses are done with Sinusoidal Pulse Width Modulation (SPWM) and a Phase Locked Loop (PLL), respectively. This approach is common in control schemes for two-level voltage source converters (VSC) and as such will not be analysed in detail. Figure 3.3 shows a high level representation of the scheme implemented in RSCAD. The frequency of the triangular wave is fixed but can be changed based on the switching frequency of the system being modelled.

DC LINK VOLTAGE CONTROL

The DC link voltage is a function of the difference between instantaneous power flowing into the converter and that drawn by the load. The DC link voltage is also equal to the voltage across the capacitor therefore, the instantaneous capacitor current can be expressed as a function of the DC link voltage using equation 3.19. This approach enables the modelling of the DC link as a pure capacitor [38]. From this expression, it can be seen that controlling the instantaneous current flowing into the DC link capacitor will lead to control of the DC link voltage. This is the underlying principle behind the DC link control. For this analysis, the load current is excluded because it is compensated for by a feed-forward term which is added to the d-axis current reference. Applying Laplace transform to equation 3.19 yields the output voltage-to-current transfer function, as described in equation 3.20.

$$i_c = C_{dc} \cdot \frac{dV_{dc}}{dt} \tag{3.19}$$

$$G_{dc}(s) = \frac{V_{dc}(s)}{I_{dc}(s)} = \frac{1}{s \cdot C_{dc}} \tag{3.20}$$

To obtain the controller structure for the DC voltage controller, the IMC approach is applied assuming a first order plant transfer function. Applying equation 3.20 to equation 3.1 assuming $G_{dc}(s)$ is equal to $\widehat{G}$, the expression for the DC link voltage controller is:

$$F(s) = \alpha \cdot C_{dc} \approx k_{vp} \tag{3.21}$$

Where α is the controller bandwidth in radians/second and C_{dc} is the DC link capacitor. This controller structure is a proportional control. In practice however, an integrator is included to ensure steady state error is eliminated [39]. The structure of the DC link voltage controller is

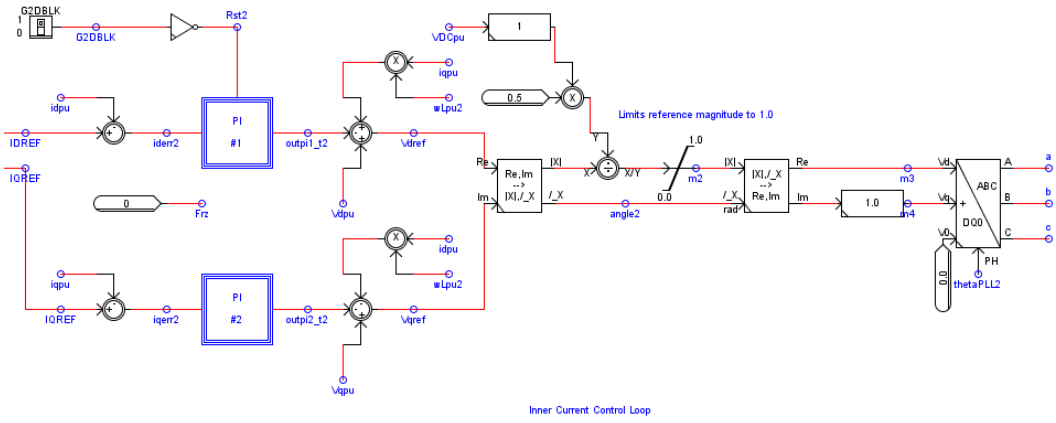

Figure 3.2: Implementation of inner current control loop in RSCAD.

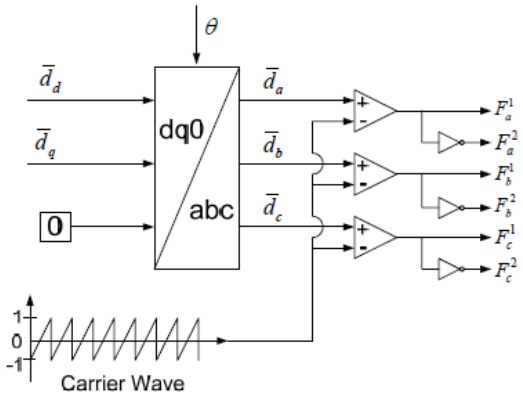

Figure 3.3: Block diagram of scheme used to generate and synchronise firing pulses, comprising comparators, a fixed frequency triangular wave and the transformation block. Extracted from [3].

therefore a PI controller. Setting the capacitor current as the output of the PI controller, equations 3.22 and 3.23 can be written.

$$i_{dc} = u_{dc} = C_{dc} \cdot \frac{dV_{dc}}{dt} \tag{3.22}$$

$$u_{dc} = K_{vp} \cdot \left(V_{dcref} - V_{dc}\right) + K_{vi} \cdot \int \left(V_{dcref} - V_{dc}\right) \cdot dt \tag{3.23}$$

where k_{vp}, k_{vi}, V_{dcref} and V_{dc} are the proportional gain, integral gain of the DC link voltage controller, reference and actual voltage of the DC link respectively. Applying Laplace transform and unity feedback to the series connection of the DC link model and PI controller blocks, yields the closed loop transfer function for the voltage control loop. This transfer function is expressed by equation 3.24.

$$\frac{V_{dc}(s)}{V_{dcref}(s)} = \frac{k_{vp} \cdot \left(s + \frac{k_{vi}}{k_{vp}}\right)}{C_{dc} \cdot \left(s^2 + \frac{k_{vp}}{C_{dc}} + \frac{k_{vi}}{C_{dc}}\right)} \tag{3.24}$$

From equation 3.8, instantaneous active power control between the converter and the grid, is realised by controlling the d-axis component of the current, which is in turn controlled by the duty ratio of the switches. Recall that the instantaneous voltage on the DC link is a function of the instantaneous difference between power flowing in and out the DC link. The d-axis component of the grid current is in two parts: the capacitor current and the load current. By setting the reference for both components, control of active power exchange with the grid and DC link voltage is realised. From equations 2.43 and 3.22, equation 3.25 can be written.

$$u_{dc} = C \cdot \frac{dV_{dc}}{dt} = \frac{1}{2} \cdot \left(\overline{d_d} \cdot i_d + \overline{d_q} \cdot i_q\right) \tag{3.25}$$

In order to maintain the desired DC link voltage, the inner current loop reference must be set by the outer voltage control loop such that the current reference is adequate for the capacitor and load requirement. To obtain the setting for the capacitor, equation 2.43 is rearranged to obtain equation 3.26, such that i_d the dependent variable. Multiplying numerator and denominator by V_{dc} yields an equivalent expression described by equation 3.27.

$$i_d = \frac{u_{dc} - \frac{1}{2} \cdot \overline{d_q} \cdot i_q}{\frac{1}{2} \cdot \overline{d_d}} \tag{3.26}$$

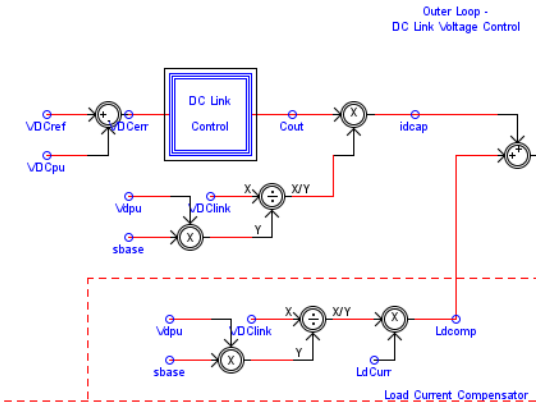

Figure 3.4: DC link control and load compensator implementation in RSCAD

$$i_d = \frac{V_{dc} \cdot u_{dc} - \frac{V_{dc}}{2} \cdot \overline{d_q} \cdot i_q}{\frac{V_{dc}}{2} \cdot \overline{d_d}} \tag{3.27}$$

According to [40], equations 3.28 and 3.29 hold in real operation of active front end converters.

$$\frac{V_{dc}}{2} \cdot \overline{d_d} \approx V_d \tag{3.28}$$

$$\frac{V_{dc}}{2} \cdot \overline{d_q} \approx V_q \tag{3.29}$$

Therefore, current setpoint for the DC link capacitor current to maintain a desired DC link voltage is calculated with equation 3.30.

$$i_{d1} = \frac{V_{dc} \cdot u_{dc} - V_q \cdot i_q}{V_d} \tag{3.30}$$

The setpoint to compensate for the load current, can be calculated from the per unit active power balance equation assuming steady state DC link voltage. The setpoint for the load obtained with equation 3.31.

$$i_{d2} = \frac{V_{dc} \cdot I_{LOAD}}{V_d} \tag{3.31}$$

The d-axis current reference is therefore a sum of the two reference setpoints. According to [38], the bandwidth of the voltage controller is set approximately 10 times slower than that for the inner loop current controller. The load current represents the additional active current component over and above what is required to maintain a stable DC link voltage. This is because the PEM stack consumes DC current to generate gas. It is possible to tune the DC voltage controller to respond to step changes in load current however, the cascade configuration of the outer and inner control loops may not perform well with this approach. Therefore, to compensate for the cascaded voltage and current controls and ensure a fast response, a feed forward term , which is proportional to the load current, is added to the d-axis current reference of the inner controller. According to [41], this compensates for the load disturbance accurately and prevents big fluctuations in DC link voltage during step changes to load current reference. The DC link voltage control implemented in the RSCAD model is shown in figure 3.4.

3.3.3. CONTROLLER TUNING

The two-level cascaded control scheme described in the previous section relies on fast decoupled current control for the inner loops and outer loops which aim to achieve stabilisation and regulation

functions by setting appropriate references for the inner loops. The tuning of the controller gain and time constant parameters is usually a trade-off between speed of response and stability for small disturbances as well as robustness to large signal disturbances [41]. For this control scheme to work properly, the controllers are tuned such that the speed of response increases towards the inner loops i.e. the inner loops are the fastest. The bandwidth of the inner loop is also chosen several orders lower than the switching frequency of the converter in order to avoid interference from switching frequency noise. These broad guidelines were used in tuning the generic model. Appendix A contains the controller parameters for the test cases. These parameters were calculated with software tools (MATLAB). As with all other model parameters, they can be changed to emulate the desired responses.

3.4. HIGH LEVEL CONTROL - FRONT END CONTROL

Extending the capability of large scale electrolysers will require additional control functions. The objective of this high level control is to enable flexibility such that electrolysers are able to adjust their power consumption according to external signals e.g. market and power systems signals. These complementary adjustments of power consumption by large scale electrolysers can add flexibility to the grid with high penetration of VRES. This high level control is also known as the Front End Controller (FEC). The FEC topology developed in this thesis is based on a generic architecture proposed in [4]. The generic architecture is shown in figure 3.5. The FEC is configured to deliver support to the power system without compromising the main function of the electrolyser i.e. production of hydrogen gas. The high level controller attempts to address gaps in the functionalities of lower level controllers within the framework of control objectives i.e. maximum hydrogen production and ancillary services. As technology develops, this high level functionality may be integrated with existing lower level controllers and evolve into a single-device controller. In [4], the generic controller comprises three modules:

- **Communication module**: This is an internet-based module designed to communicate with a higher-level grid management system including load aggregators. This module utilises communications protocols which translate requests from grid management systems.
- **Optimisation module**: This module optimises power adjustments in response to external signals and grid disturbances (i.e. voltage and frequency transients). This module implements two types of optimisation: fast and slow loops. Optimization focused on market participation is called slow-loop optimisation, whereas optimisation in response to grid events is called fast-loop optimisation. The time resolution of the slow and fast loops are aligned with market and power system requirements respectively. These external loops generate references for the low level controls in the power conversion system.
- **Interpretation module**: This module facilitates interpretation of the power setpoint determined by the optimisation module to a signal compatible with low level controllers of the load. The interpretation module also contains an accurate model of the controlled load, to ensure normal and safe operation of the load within prescribed limits.

HIGH LEVEL CONTROLLER CUSTOMISATION

The FEC design in this thesis incorporates the above generic module functions without explicitly retaining the modular structure shown in figure 3.5. This customisation however does not result in loss of functionality. The customised controller also has flexibility for different types and volumes of ancillary services. The nature of interactions between the high level control, the power system and low level electrolyser controls is shown in figure 3.6. The FEC proposed for control of the electrolyser implements mainly the optimisation module functions. The interpretation module function, which

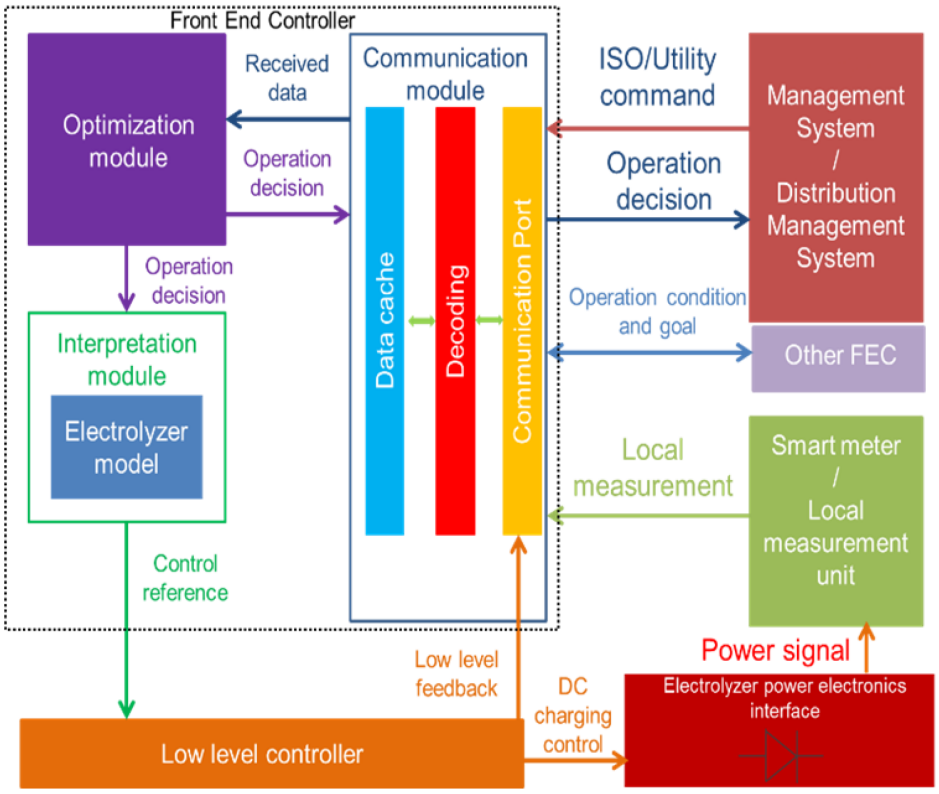

Figure 3.5: Proposed front end controller (FEC) architecture comprising communication, optimisation, and interpretation modules. Extracted from [4]

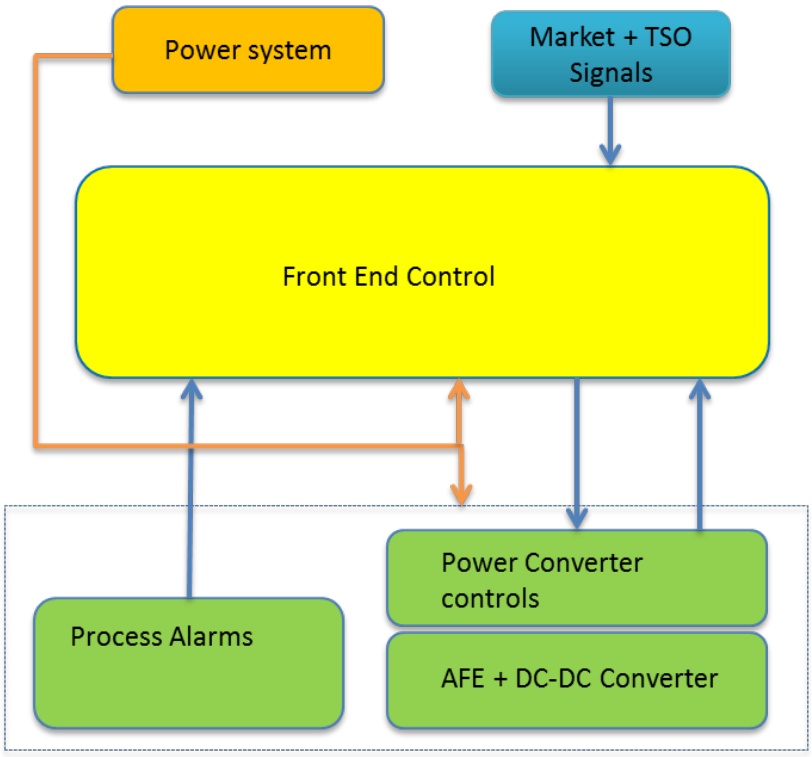

Figure 3.6: FEC interacts with power system, the market, low level controls and process alarms.

ensures the plant is operated within built in limits, is embedded in the low level and high level controls in the form of limiters. The communications function of the FEC is not modelled in this thesis.

FAST OPTIMISATION LOOP

The fast optimisation loop is designed to track and respond to grid disturbances based on predefined rules. The main signals of interest are the power system frequency and the bus voltage at the Point of Common Connection (PCC). The fast optimisation loops track deviations in voltage and frequency and adjust active and reactive power setpoints according to a predefined droop. For frequency support, the active power setpoint offset and reference are generated using equations 3.32 and 3.33 respectively:

$$-K_{droop} \times \Delta f = \Delta P \tag{3.32}$$

$$P_{ref} = P + \Delta P \tag{3.33}$$

where Δf, K_{droop}, P_{ref}, P and ΔP, are the frequency deviation from 50Hz, droop constant, active power reference, measured active power and active power offset, respectively. The droop constant is calculated based on the contractual active power capacity (in MW) committed and maximum frequency deviation allowed for a particular time period. A similar approach is adopted for voltage support. In the case of fast voltage support, a deviation from the reference bus voltage generates an error, which is used to offset the q-axis current reference in the inner loop. This offset can also be applied to the reactive power setpoint to either inject or absorb more reactive power to restore the bus voltage level. Figure 3.7 shows the implementation of the fast optimisation loop for frequency support in RSCAD.

SLOW OPTIMISATION LOOP

The slow loop embeds the functionality that responds to price signals and slower commands from the system operator. It must be noted, however, that this optimisation is specific to higher level objectives of the stakeholders. This optimisation is difficult to generalise since it will depend on commitments made in contracts between parties involved. However, within the scope of this thesis, it is assumed that the production of hydrogen to meet demand at the lowest cost is the main priority. In this RSCAD model, the controller assumes setpoints for active and reactive power are already optimised by higher level control at the dispatch center. The optimised setpoints are then translated to low level control signals for the low level controllers to execute.

3.4.1. IMPLEMENTATION IN RSCAD

The slow loops shown in figure 3.8, set the reference for low level converters based on two options preset by the user. The first option allows adjustment of active and reactive power settings received

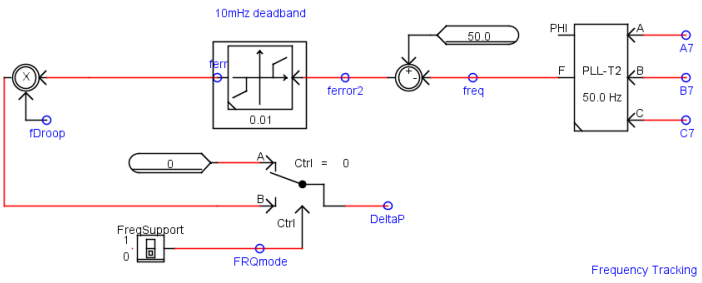

Figure 3.7: Frequency tracking module implementation in RSCAD.

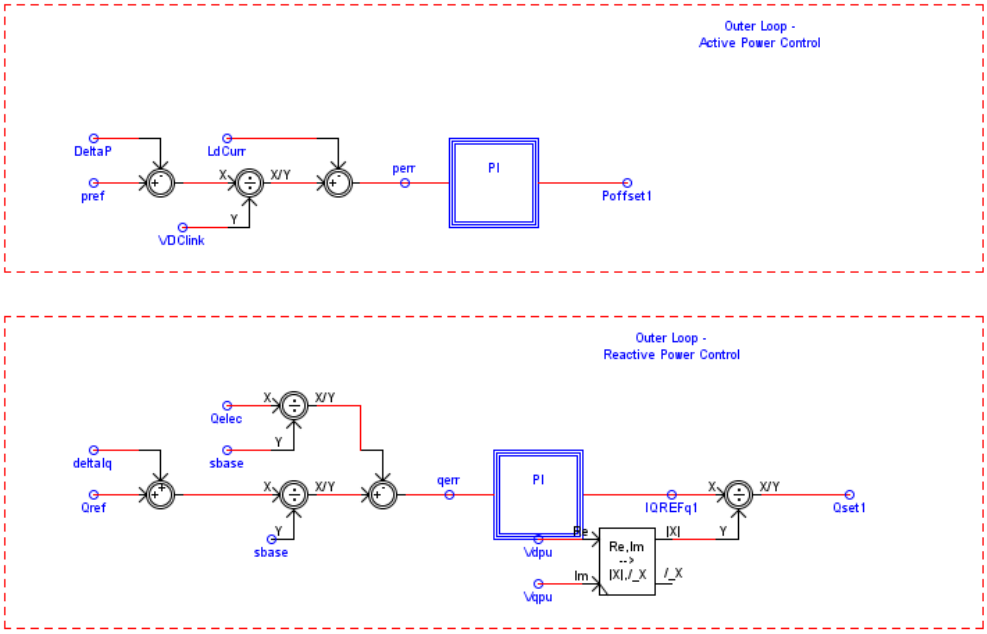

Figure 3.8: Active and reactive power control loop implementation in RSCAD.

from, for example, the system operator. The second option sets references based on price signals and active power bid size in MW. The references are set within the constraints of converter capacity, maximum frequency and bus voltage deviation. The controllers are simple PI controllers tuned to achieve responses required by the respective ancillary services. The second option adds an additional layer of complexity by enabling optimisation of the setpoint based on price signals. The flowchart which describes the optimisation is shown in figure 3.9.

The model allows the user to control the direction and size of active power ramp in order to deliver frequency support and congestion management. The electrolyser can be made to prioritise hydrogen gas production based on committed active power capacity and direction of ramp required (i.e. ramp up only or ramp down only). A third option, which is the norm in the market, is the symmetrical bid. This option allows both up and down ramps in response to frequency deviations. This option also has built in flexibility to adjust the operating point to maximise hydrogen production when price is favourable. It achieves this by comparing the market price of hydrogen to a reference price and adjusting the setpoint accordingly. For example, if the price of hydrogen is favourable and active power capacity committed for frequency support is less than the maximum, the algorithm makes use of the extra capacity by increasing the setpoint and producing more gas. This capability can be used to force the electrolyser to respond to both price and power system systems signals simultaneously, thereby meeting multiple objectives. As indicated earlier, this optimisation in reality can be more complex, however for purposes of this thesis it is simplified.

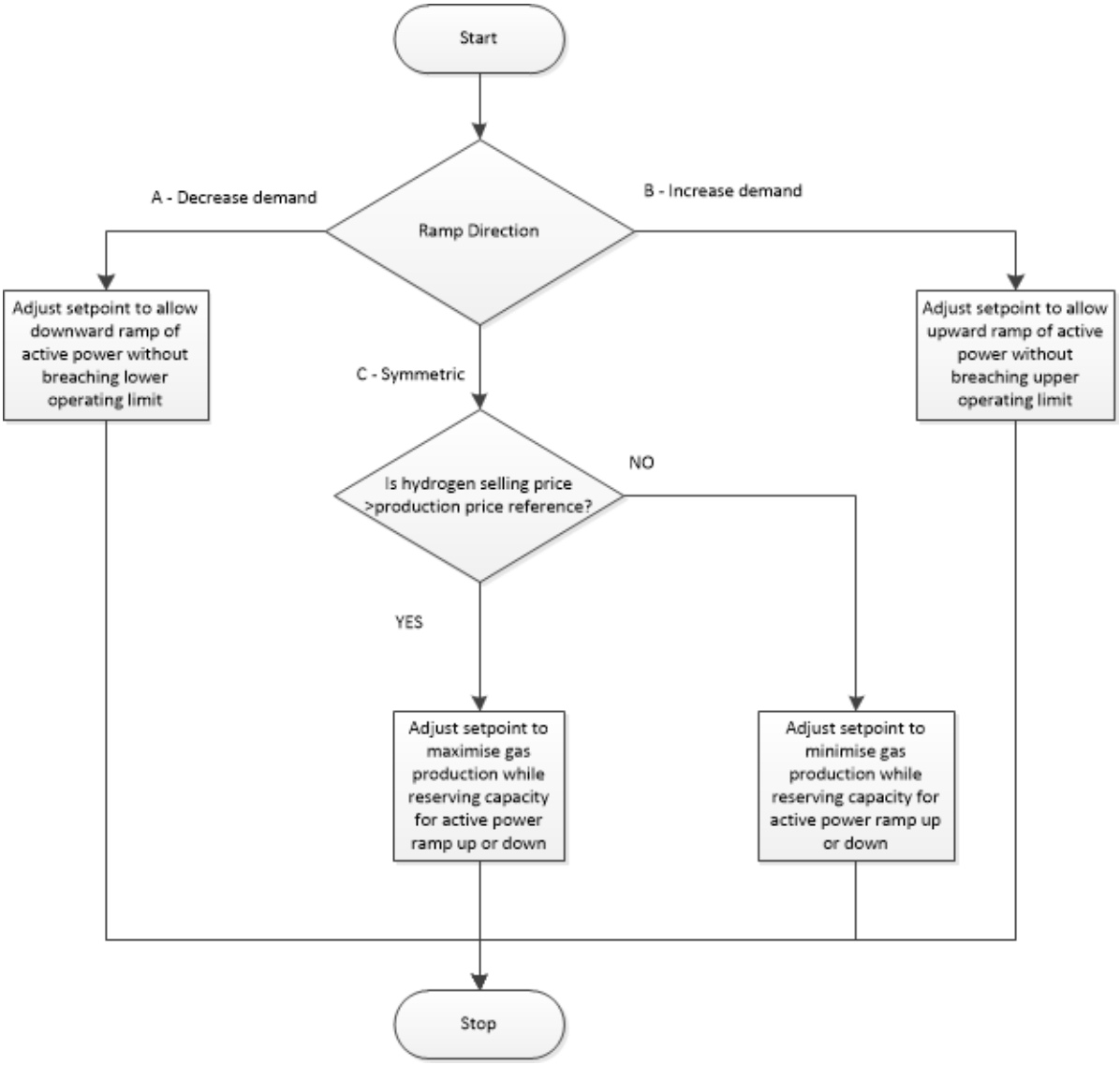

Figure 3.9: Setpoint optimisation flowchart.

4

MODEL PERFORMANCE AND SCALING

This section of the report provides an overview of the Real Time Digital Simulator (RTDS) and also analyses the responses of the electrolyser model to step commands, power system disturbances and external signals. The objective is to demonstrate the electrolyser's response or capabilities with and without the front end controller. The selected cases are built around events or disturbances which are highly likely. The set of cases however, does not represent the exhaustive collection of possible scenarios. First, the model's response to basic step commands is simulated without the high level controller in the loop. This is to verify the basic model's response. The augmented model with the FEC in the loop is then simulated for various types of power system disturbances and external control signals. The impact of stack resistance variations on step response is also evaluated. The generic responses shown can be tuned to emulate the response of the real electrolysers with a good level of accuracy. In practice the controller parameters are customized for each installation, therefore in the generic model, parameter tuning is done with simple rules to achieve a reasonable performance. This provides a good level of visibility into typical response of electrolysers based on the generic model and also the robustness of the proposed hierarchical control scheme.

4.1. OVERVIEW OF RTDS PLATFORM

Real-time simulation of the electric power system is the reproduction of output (voltage/currents) waveforms, with the desired accuracy, that are representative of the state or behaviour of the real power system being modelled [5]. The states of the system being simulated are computed at discrete time intervals using a fixed time step. If the time to complete the computation of the system is shorter or equal to the selected time-step, the simulation is considered to be real-time. If it is longer than one or more time-steps, the simulation is considered as non-real-time or off-line The main advantage of the Real Time Digital Simulator (RTDS) lies in its ability to process high speed calculations continuously in real time. These calculations are done at a much faster rate than with off-line simulation programs. Complex networks are simulated using a typical time-step of 25–50 microseconds. Small timestep sub-networks operating with timesteps in the range of 1–4 microseconds simulate fast switching power electronic devices [6]. The thesis approach of modelling and simulating large scale electrolysers in real-time, presents a cost effective and low-risk method, to aid the study of potential effects of large scale electrolyser integration. Real-time digital simulation in power systems applications are in two categories: fully digital real-time simulation loop and hardware-in-the-loop (HIL) real-time simulation. In a fully digital real-time simulation, the entire system (including control, protection, and other accessories) is modelled inside the simulator. No external interfacing or inputs/outputs (I/Os) is required. On the other hand, the HIL simulation involves having parts of the simulation replaced by actual physical components.

The HIL mode of the simulation allows interaction with real devices (hardware under test) via input/output (I/O) interfaces. In some cases, the HIL system involves real controller hardware that interacts with the rest of the simulated system. This is called controller hardware-in-the-loop (CHIL). This approach is used for controller prototyping. A fully digital simulation is often used for understanding the behaviour of a system under certain conditions, whereas an HIL simulation is aimed at reducing the risk of investment through the use of a prototype, once the underlying theory is established [5]. The scope of this thesis is limited to a fully digital real time simulation.

4.1.1. SYSTEM DESCRIPTION

A real-time simulator usually has a scalable architecture. Incremental computing power is enabled by adding rack-mounted units. The Real Time Digital Simulator (RTDS) comprises hardware and software. The system has multiple processors, a host computer and I/O interfaces and other supporting systems (e.g. power supplies, synchronisation and communications network). The processor cluster operates in parallel to run the simulation in real time. The host computer is used to prepare the model of the system off-line, compile and load it on the target platform. It also facilitates monitoring the results of the real-time simulation. The I/O terminals interface with external hardware and the communication network to exchange data between multiple targets when the model is split into multiple subsystems.

HARDWARE

The RTDS system utilises custom-built hardware assembled in units. In earlier versions, these units are called racks. The architecture of the RTDS system is shown in figure 4.1. The racks contain several slot-mounted processor cards known as PB5 cards, each containing two processors operating in parallel. This serves as the main computational engine. A maximum of 12 processors can be housed in one rack. A PB5-based rack enables processing of one or two network solutions in one rack. A network solution can include a maximum of ninety single-phase nodes or thirty 3-phase buses. Two subsystems, each with 90 nodes can be processed on one rack. This approach, however, requires additional PB5 processors to solve the other component models within the simulated network. Signal exchange between the PB5 cards is accomplished through a common backplane as shown in figure 4.1, or via optical ports which are located on the cards. Scaling to simulate larger networks is achieved by adding more racks. The current generation of simulation hardware for the RTDS is called NovaCor. The NovaCor platform is based on a chassis architecture, each containing a powerful multi-core processor and allowing scalable access through the licensing of cores. NovaCor has 2 to 3 times the capacity of PB5 [6]. Figure 4.2 shows the NovaCor hardware chassis. The PEM electrolyser model can be run on both PB5 and NovaCor platforms.

In addition to the main processors, each simulator rack contains a workstation interface card. The workstation interface card (GTWIF) facilitates Ethernet communication between the host (i.e. Windows-based PC) and the target (i.e. PB5 or NovaCor). It also handles synchronisation functions together with the Global Bus Hub (GBH). The other functions handled by the workstation interface card include:

- Loading, starting and stopping cases
- Timestep generation
- Coordination of all backplane transfers during simulation
- Rack hardware diagnostics
- Communication with RSCAD (diagnostic and simulation data)

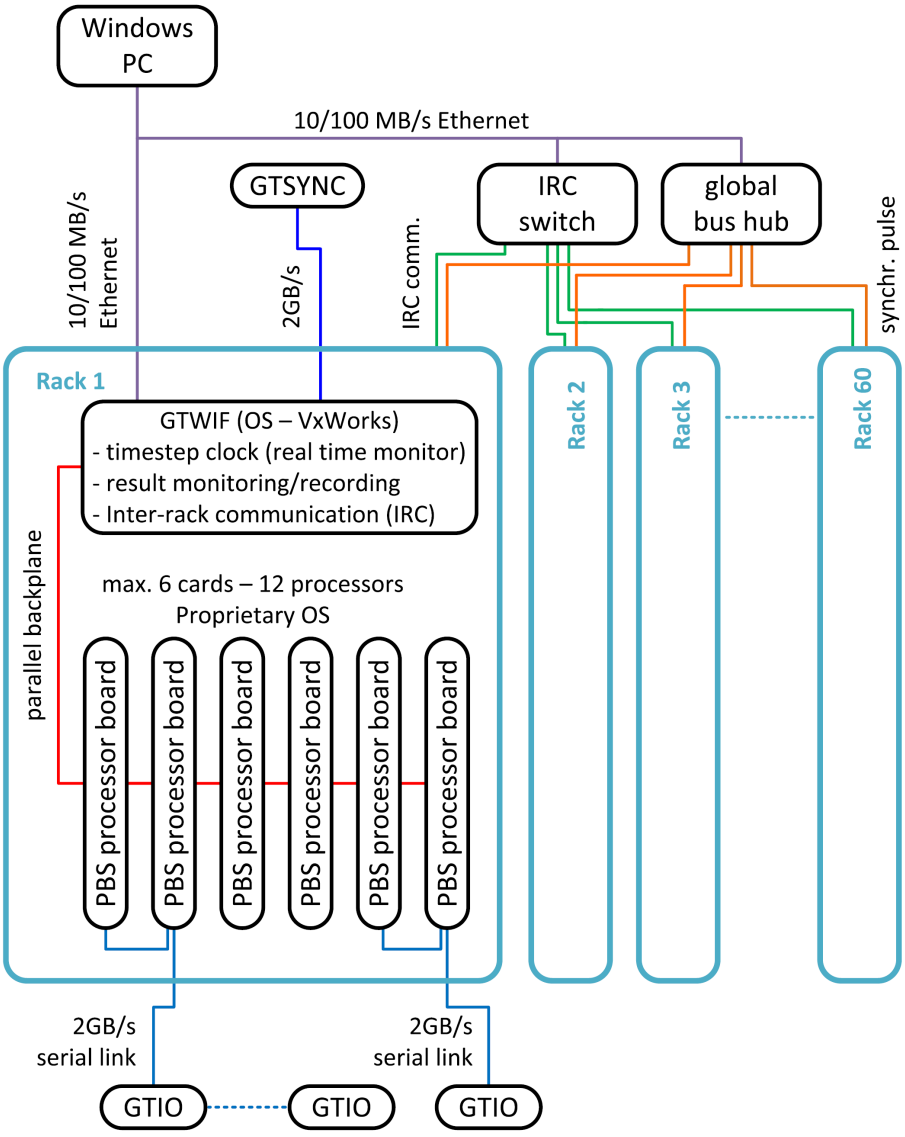

Figure 4.1: Basic hardware architecture of RTDS simulator. Extracted from [5].

Figure 4.2: NovaCor chassis. Extracted from [6].

The Inter-Rack Communication (IRC) switch acts as a high speed switch for inter-rack communication. The IRC switch is mainly used in systems with a large number of chassis or racks. The IRC switch can enable direct data communication between as many as 60 chassis [6]. The benefits of the IRC switch increases with the number of chassis or racks. The IRC switch offers greater connectivity, flexibility and simplified wiring.

The global bus hub is used for for real-time synchronisation of multiple chassis when three or more chassis/racks are installed in a simulator. Each chassis/rack connects to the GBH via a fibre optic cable. It must be noted that, GBH communication is separate from the Ethernet communication. For purposes of synchronising the simulation with external time references such as Global Positioning System (GPS), the GTSYNC card is used.

The Giga-Transceiver Input/Output (GTIO) cards act as the interface between the RTDS simulator and an external device. They are fed from optical ports on the NovaCor chassis or PB5 processor cards. The fiber optic link has a bandwidth of 2 Gbit per second and allows the GTIO cards to be located remotely from the RTDS cubicles. GTIO cards enable connections to external hardware via analogue (GTAI/GTAO cards) and digital (GTDI/GTDO cards) interfaces.

In addition to the aforementioned hardware, the simulator also includes the GTNET card which handles communication via high level Ethernet protocols depending on the application (e.g. IEC 61850). Field Programmable Gate Arrays (FPGAs) have also been recently added to RTDS hardware. The GTFPGA unit, enables highly capacity computations in parallel with the RTDS Simulator. The GTFPGA Unit is also interfaced with the RTDS via an optical fibre cable. The GTFPGA unit has embedded flexibility which allows various firmware to be run on the hardware for different purposes. RTDS belongs to the Type A class of simulators which rely on custom-built hardware.

SOFTWARE MODULES

For Type-A simulators such as RTDS, a graphical user interface with built in component model libraries is included as an integral part of the package. These software tools enable the creation and simulation of models. The RSCAD software has a number of modules which allows models to be created for both large time-step and small timestep simulations. The small time-step enables modelling of fast switching dynamics in power electronics systems. Interfacing of small and large time step is also possible via the use of interface transformers. A facility is also provided within RSCAD for creating custom components (CBuilder) and performing conversions (e.g. from PSCAD to RSCAD). For this project, the Draft and Runtime modules were used mainly. Figure 4.3 shows the electrolyser developed in the RSCAD Draft module. This module is used to create power system models prior to compiling and running simulations. After creation of the model in the Draft module, it can be simulated using the Runtime module. The electrolyser simulation setup in the Runtime module is shown in figure 4.4. It captures the PEM electrolyser along with the front end controller and segments which represent signals from the system operator and the ancillary services/hydrogen market.

RTDS uses Dommel's algorithm. This algorithm, described in detail in [42], is used to model all the components of the circuits. Active sources are modelled as equivalent sources with several types of impedances, including positive and zero sequences [5]. Appendix A describes in detail how to compile and run the test various cases using the relevant software modules.

4.2. TEST NETWORK

The performance of the model is tested with a simple network comprising a voltage source, high voltage transmission line, transformer and the electrolyser. The network is adequate for analysing response of the model to setpoint changes driven by power system disturbances, external signals and local basic commands and also for analysing the feasibility of ancillary services. The network shown in figure 4.5, comprises a 110 kV source which represents the infinite grid, connected to the

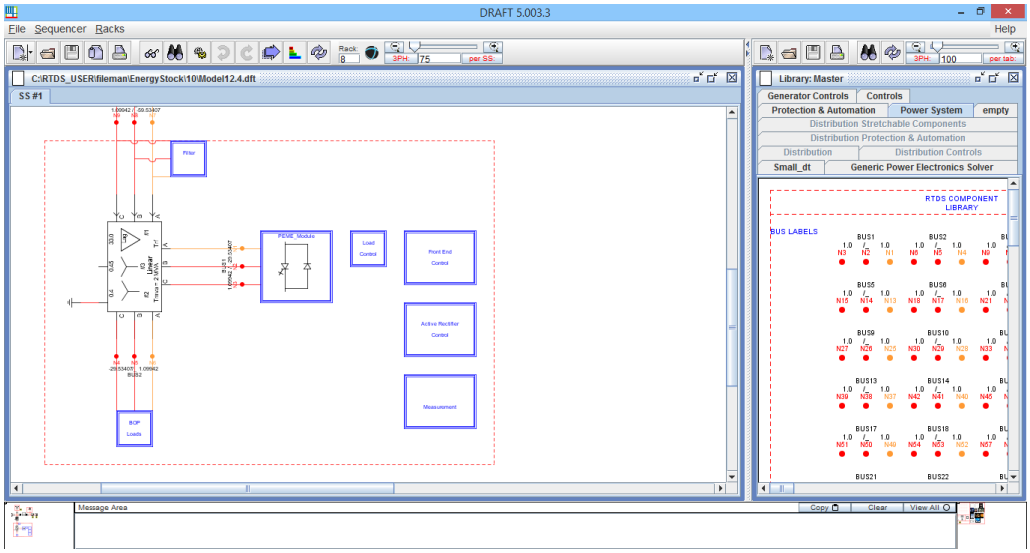

Figure 4.3: Electrolyser model in Draft module of RSCAD.

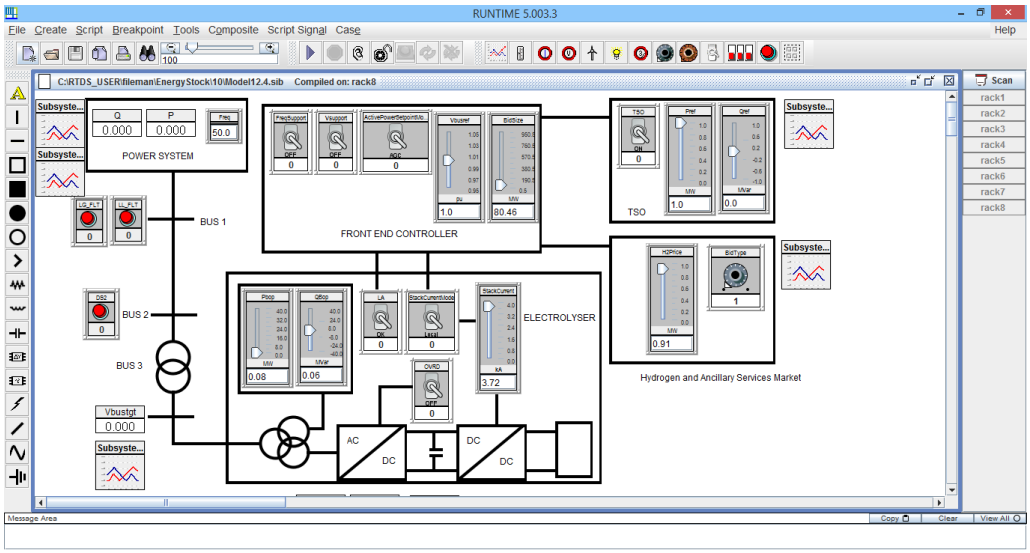

Figure 4.4: Electrolyser model in Runtime module of RSCAD.

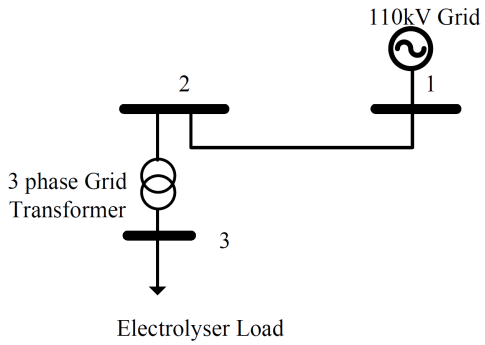

Figure 4.5: Test system showing electrolyser connection to 110kV infinite grid via step down transformer.

33 kV-rated load (electrolyser) via a 5 kilometre transmission line and step down transformer. This network is a replica of the real network to which the electrolyser will be connected.

4.3. TEST CASE DEFINITIONS

The selected cases fall in three categories. The first set covers response to basic step commands. The second set simulates typical power system disturbances such as faults. The third set simulates the responses to external control signals such as hydrogen price or signals from the system operator. The list of cases is as follows:

BASIC RESPONSE

- Test 1: Step increase/decrease in PEM stack current

RESPONSE TO POWER SYSTEM DISTURBANCE

- Test 2: Grid frequency disturbance – 0.1 Hz system frequency deviation within one 1 second
- Test 3: Bus voltage disturbance – voltage fluctuation due to load disturbance.
- Test 4: Single line to ground fault
- Test 5: Double line to ground fault
- Test 6: Symmetrical three phase ground fault

RESPONSE TO EXTERNAL SIGNALS

- Test 7: Response to system operator command - Active Power
- Test 8: Response to system operator command - Reactive Power
- Test 9: Response to change in hydrogen price

It is also assumed that the capacity of electrolyser remains the same for each scenario. The above case studies are simulated such that the results replicate the estimated response of the electrolyser model to defined events, fairly accurately.

4.3.1. BASIC RESPONSE

TEST 1: STEP INCREASE/DECREASE IN PEM STACK CURRENT

From equation 2.12, it can be deduced that an increase in hydrogen production requires an upward adjustment of current fed to the PEM stack. This leads to an increase in active power drawn from the power system as well. This is the basic operating principle used to store excess generated energy

as hydrogen gas. Thus, electrolysers configured to increase demand and hydrogen output based on a signal from a high level controller or dispatch center must be able to ramp up demand within a certain time frame. The model is capable of emulating the response of an electrolyser whose stack current setpoint has been adjusted upward via a step command. Figures 4.6 and 4.7 show the RSCAD model's response to the step change for stack current increase and decrease respectively. This command is typically initiated locally by a user from a control panel or remotely from a high level controller such as the FEC or system control centre. The electrolyser responds by adjusting the current fed to the stack in less than 1 second. This response can be tuned to model the response of a variety of electrolysers.

This feature is particularly of interest in frequency containment reserve (FCR) applications in future power systems since electrolysers are known to have relatively faster response compared to generator governors [13]. The fast response time characteristics also holds potential for improving nadir frequency after a disturbance. Comparing the response profile and settling time to that for a real electrolyser shown in figures 4.8 and 4.9, it can be concluded that the generic model replicates the real system fairly accurately.

4.3.2. RESPONSE TO POWER SYSTEM DISTURBANCE

TEST 2: GRID FREQUENCY DISTURBANCE – 0.1HZ FREQUENCY DEVIATION WITHIN ONE 1 SECOND

This case study involves simulating a deviation in system frequency. This scenario will typically occur when there is an imbalance in generation and demand. The simulation involves making a step change in the grid model frequency input via a slider in real time. All other parameters kept the same as in the pre-disturbance case. It can be observed that the electrolyser model ramps down active power within 1 second. The amount of demand reduction is determined by the gain setting of the droop control. A similar response is obtained for an increase in frequency. Depending on the user preference or ancillary service contract, between 10% to 90% of the electrolyser's capacity can be adjusted. The response of the control system is stable after the frequency disturbances, as shown in figure 4.10.

TEST 3: BUS VOLTAGE DISTURBANCE – VOLTAGE FLUCTUATION DUE TO LOAD DISTURBANCE

This test case involves simulating a deviation in bus voltage at the point of common connection (i.e. Bus 3 in figure 4.5. This is the bus to which the electrolyser is directly connected). The simulation involves closing a circuit breaker which connects a large load to Bus 2. The increased current flowing through the transmission line results in a larger voltage drop across it. As a result the bus voltage at Bus 2, the receiving end, reduces. The response of the model with and without voltage support deactivated is shown in figure 4.11. When voltage support is inactive, the bus voltage does not recover while the load is still connected. However, under the same conditions with voltage support activated, the bus voltage improves. The improvement is due to the increased injection of reactive power by the converter. In order to have this feature functional, the converter must be dimensioned to have extra capacity over and above what is required for active power transfer. The control system prioritises active power because that is related directly to hydrogen gas production. This limits the amount of reactive power available at each instant in time.

4.3.3. RESPONSE TO FAULTS

A fault in a power system is any failure which interferes with the normal flow of current. Most faults on transmission lines are caused by lightning, which results in the flash-over of insulators [43]. The high voltage between the conductors and the grounded tower causes ionisation, which creates a path to ground for the charge induced by the lightning. The low impedance path to ground allows flow of current from the conductor through the ground, and back to the neutral of the transformer or generator. There are two main classes of faults, symmetrical and unsymmetrical faults. This section

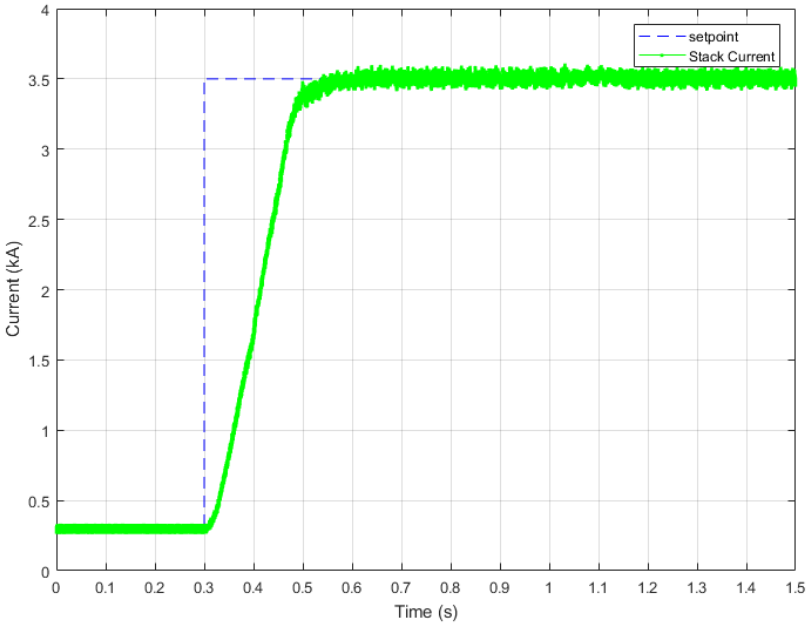

Figure 4.6: Response of electrolyser model to load current set point increase.

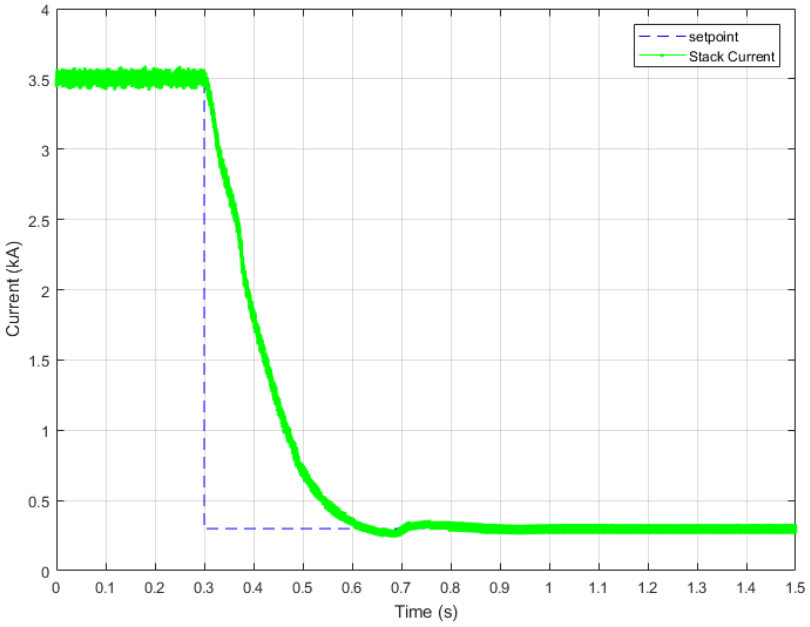

Figure 4.7: Response of electrolyser model to load current set point decrease.

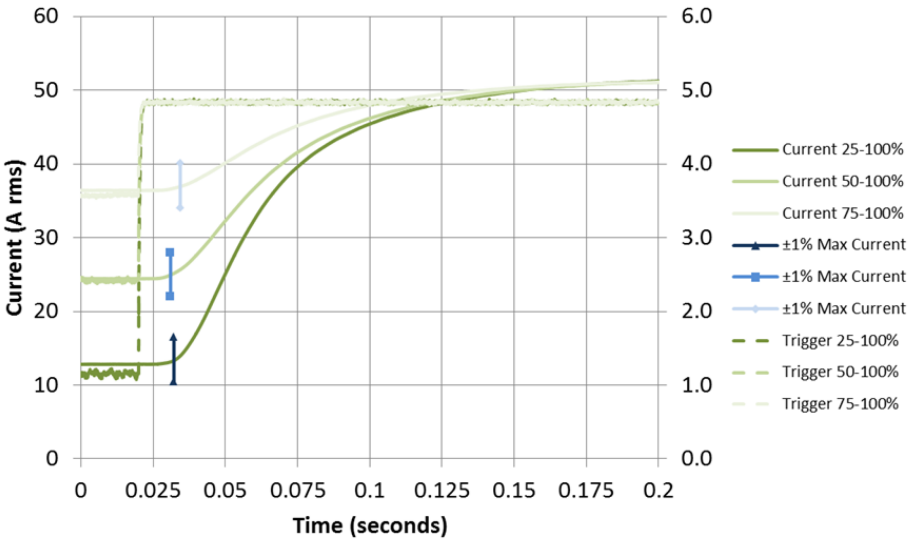

Figure 4.8: Response of real electrolyser to load current setpoint increase.

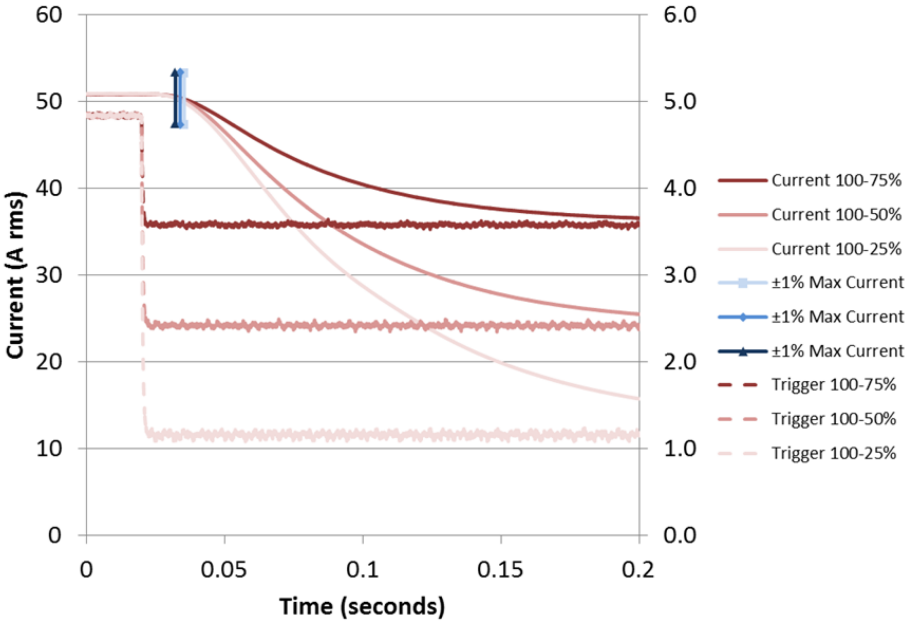

Figure 4.9: Response of real electrolyser to load current setpoint decrease.

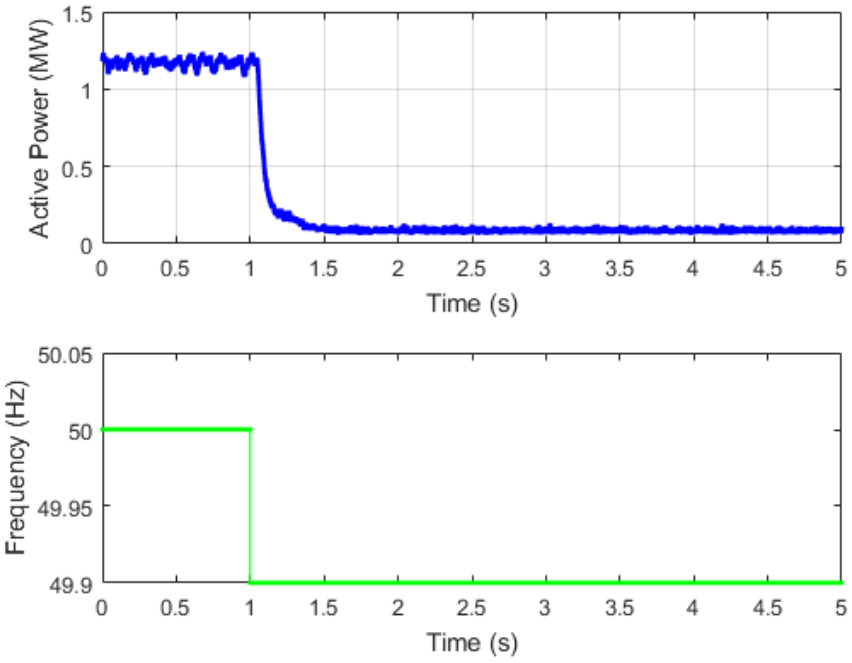

Figure 4.10: Response of electrolyser to 0.1Hz change in power system frequency.

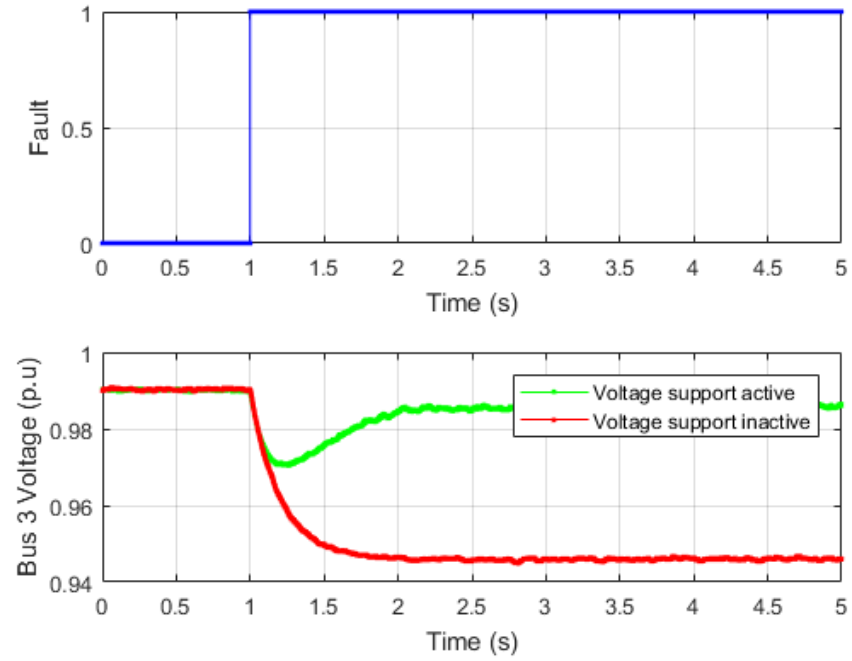

Figure 4.11: Response to bus voltage disturbance with and without voltage support. Voltage support actively contributes to improving the voltage level.

simulates both types of faults. Focus is placed on mainly the faults which are likely to occur. So for example, line to line faults not involving ground, which are less common, are not simulated.

TEST 4: SINGLE LINE TO GROUND FAULT – FAULT AT BUS 1 (DURATION 100 MILLISECONDS)

Unsymmetrical faults are very common in power systems. According to [43], about 70–80% of faults are single line to ground faults. It is therefore useful to understand how these faults impact the performance of the proposed control scheme. The simulation involves creating a fault on phase A at Bus 1 in figure 4.5. The fault impedance is 0.1 ohm and the fault is cleared in 100 milliseconds. The case, simulated for both scenarios with voltage support activated and deactivated, is shown in figure 4.12. It can be observed that the recovery for the case with voltage support activated, is approximately 400 milliseconds seconds faster than the case without voltage support.

TEST 5: DOUBLE LINE TO GROUND FAULT – FAULT AT BUS 1 (DURATION 100 MILLISECONDS)

In this case study, a double line-to-ground fault is created near Bus 1 and is cleared in 100 milliseconds. The simulation involves creating a ground fault on phase A and B close to Bus 1. The fault impedance is 0.1 ohm. It can be observed from figure 4.13 that the response is similar to that for a single line to ground fault. The controller enables a faster recovery of the bus voltage back to pre-disturbance levels.

TEST 6: SYMMETRICAL THREE PHASE GROUND FAULT – FAULT AT BUS 1 (DURATION 100 MILLISECONDS)

Figure 4.14 shows the response of the control system to a symmetrical three phase fault created at Bus 1 for 100 milliseconds. This type of fault, though not very frequent, is more severe in terms of potential damage to power system components. As with the other types of faults, an improvement in recovery time, albeit with some overshoot, can be observed. The overshoot, however, is still within the 1.05 p.u. upper limit for voltage deviation. It must be noted that this response can be improved by further tuning of the control system parameters.

4.3.4. RESPONSE TO EXTERNAL SIGNALS

TEST 7 & 8: RESPONSE TO SYSTEM OPERATOR COMMAND - ACTIVE POWER AND REACTIVE POWER RAMP UP/DOWN

The generic model is also capable of receiving active power setpoint commands from an external source such as a central dispatch center. These setpoints are translated by the FEC into signals for the low level controllers. The response of the system to ramp up and ramp down commands is shown in figures 4.15 and 4.16, respectively. This feature in the model enables secondary and tertiary frequency control and congestion management capabilities. In addition to the active power adjustments, the electrolyser's Voltage Source Converter (VSC) can be used to support the power system. The converter control can be instructed to inject or absorb reactive power on demand. The power conversion system can also be instructed to operate at unity power factor. This reactive power control capability is largely independent of the active power control. Figures 4.15 and 4.16 show the capability to adjust active power while maintaining operation of the converter at unity power factor (i.e. zero reactive power). This feature is further extended in the generic model to control bus voltage at the point of common connection (PCC). The model has the flexibility of indirectly supporting voltage on other buses by adjusting reactive power based on measurements from remote buses. Figures 4.17 and 4.18 show results of a simulation of a command from the system operator to inject and absorb reactive power respectively. The impact of this adjustment is observed in the increase and decrease in voltage at the PCC i.e. bus 3. Active power varies slightly mainly due to increased losses. The voltage improves within 5 seconds of initiating the command. For faster voltage support, the fast optimisation loop is used via activation of the fast voltage support feature.

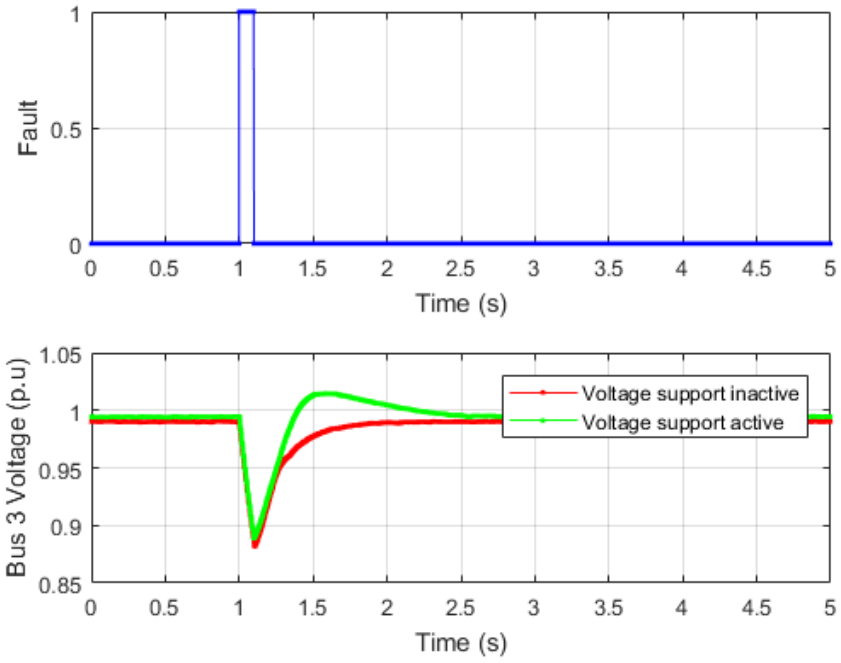

Figure 4.12: Response to single line to ground fault at bus 1, with and without voltage support. Voltage support actively contributes to improving the recovery time of bus voltage.

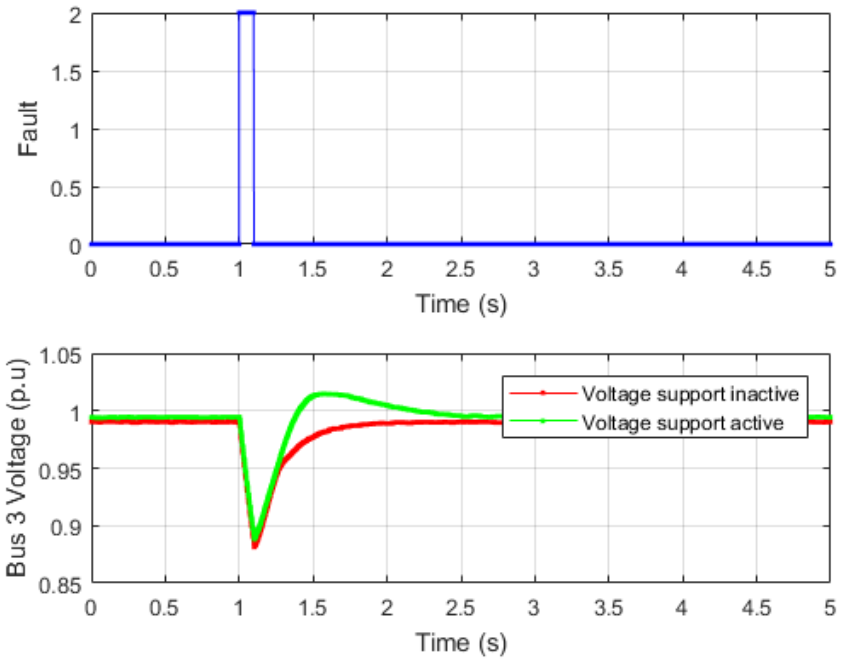

Figure 4.13: Response to double line to ground fault at bus 1, with and without voltage support. Voltage support actively contributes to improving the recovery time of bus voltage.

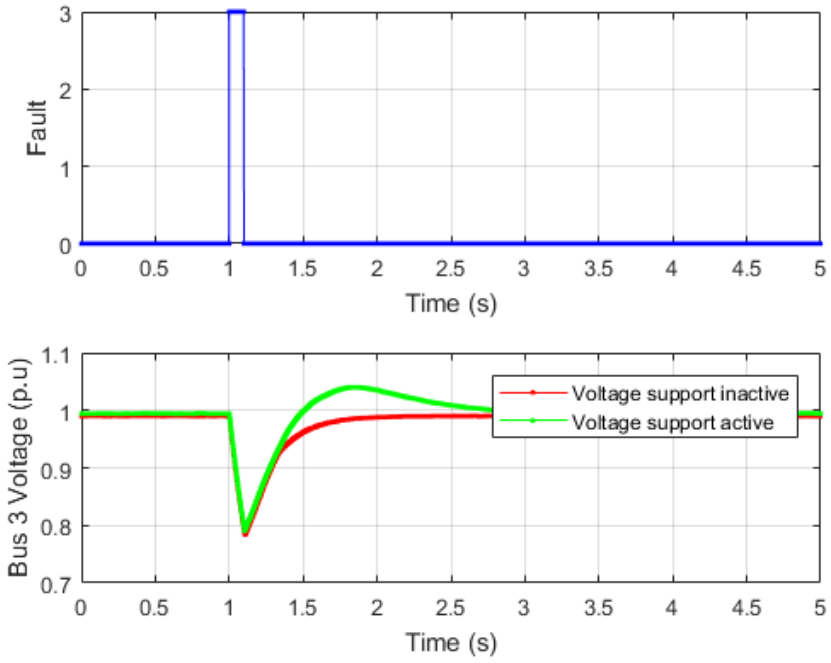

Figure 4.14: Response to three phase ground fault at bus 1, with and without voltage support. Voltage support contributes to the recovery time of bus voltage.

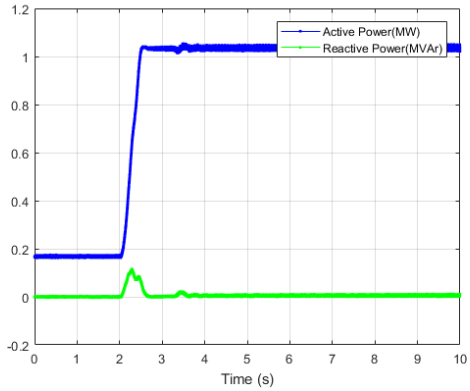

Figure 4.15: Active power ramp up command.

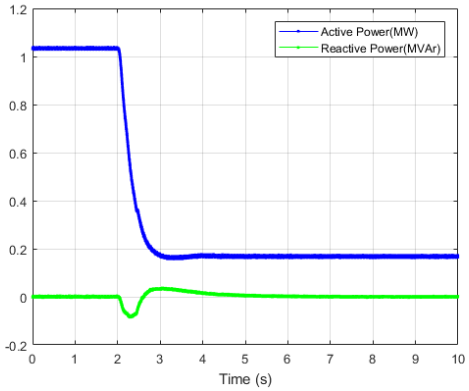

Figure 4.16: Active power ramp down command.

TEST 9: RESPONSE TO CHANGE IN HYDROGEN PRICE

The simulation of price signals is also possible with the high level controller. Figure 4.19 shows the automatic adjustment in active power demand as a result of a change in hydrogen pricing. In this scenario, the FEC tracks the hydrogen price on the market and compares it to a reference price (for example cost of production). Once the selling price is favourable, the setpoint of the electrolyser is automatically adjusted upwards to maximise hydrogen production. This price signal may also be a function of the cost of electricity. Previous research [44] indicates that, regardless of any additional cost elements, electricity costs have a major impact on hydrogen price if produced via electrolysis. This is a typical case which is likely to occur once the hydrogen economy within the framework of the multi-energy system takes off fully.

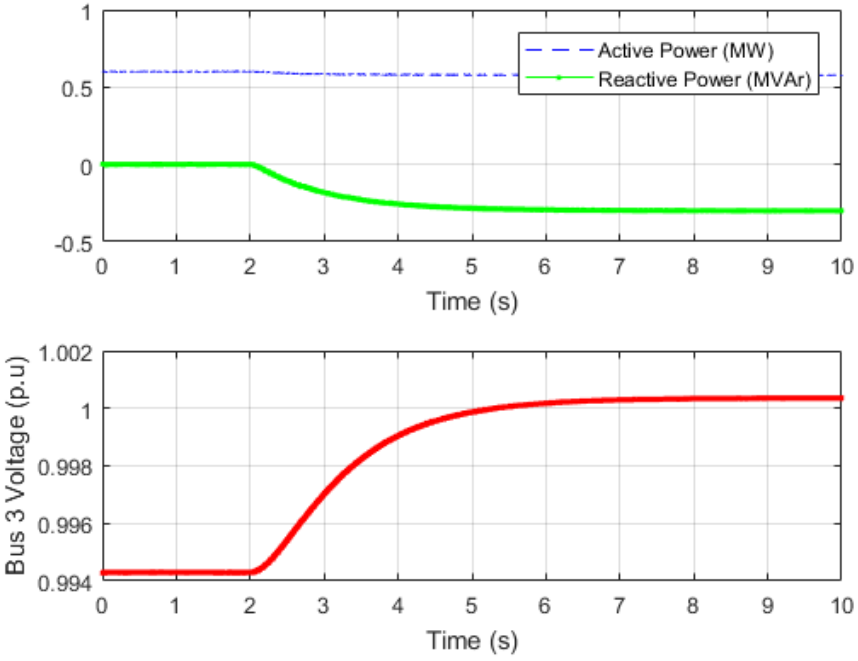

Figure 4.17: Response of PCC bus voltage to reactive power injection command from system operator.

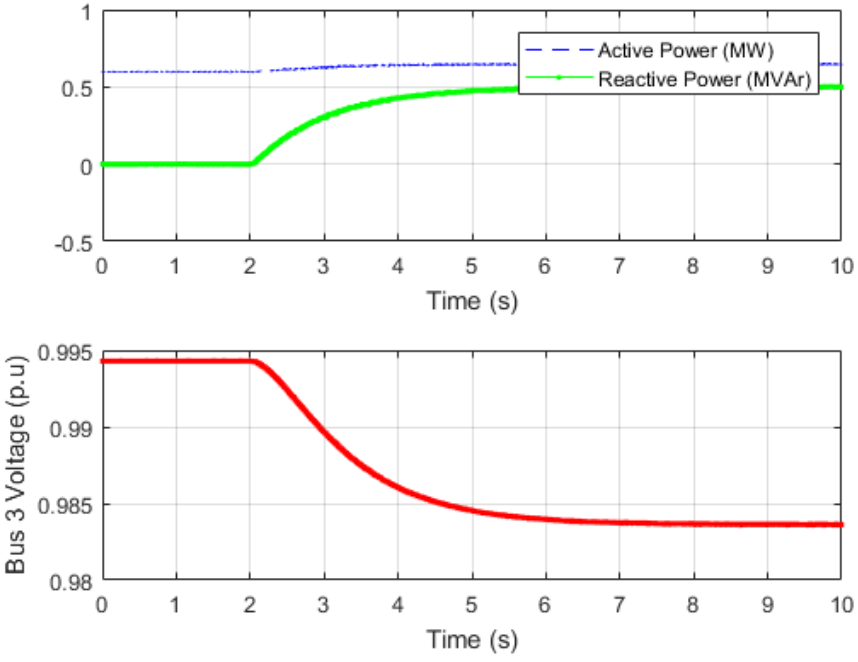

Figure 4.18: Response of PCC bus voltage to reactive power absorption command from system operator.

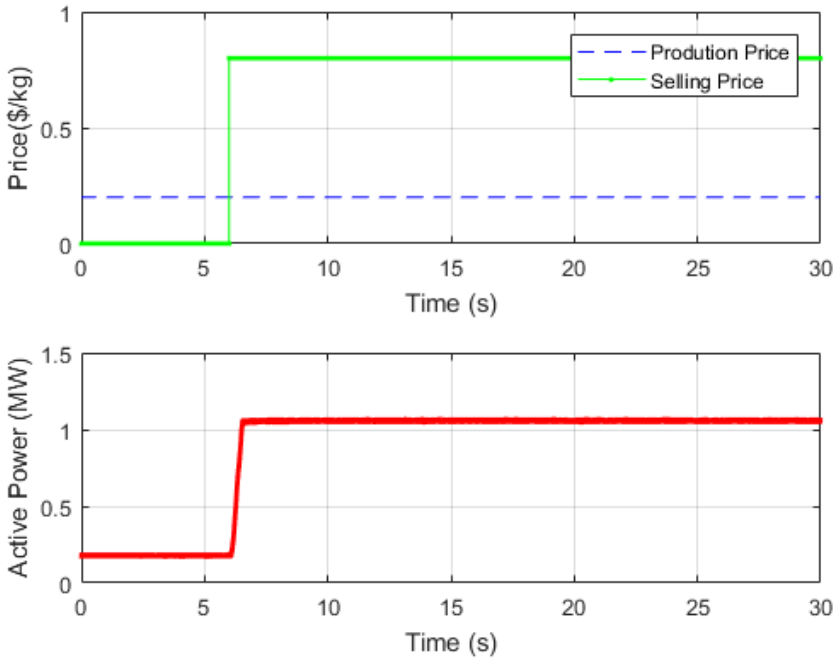

Figure 4.19: Automatic upward adjustment of active power to produce more gas, in response to hydrogen price signal.

4.4. MODEL SENSITIVITY TO STACK PARAMETER VARIATION

In the operation of the electrolyser, it is possible that stack parameters may vary due to environmental factors or defects in the stack. This section highlights the impact of variations in stack resistance on the performance of the electrolyser. The base case has the stack resistance set to 0.015 ohm and the open circuit voltage is set to 145 Volts DC. The stack resistance is increased/decreased by 10% and 20%. From figures 4.20 and 4.21, it can be observed that variations in stack resistance did not result in wide deviations from the base case performance. Reference tracking and speed of response remain largely unchanged. The total active power drawn by the electrolyser however, changes slightly with varying resistance, as shown in figure 4.22. This is consistent, since active power losses vary linearly with resistance for a given current. Increasing stack resistance results in higher losses and lower efficiency of the stack. Observations of system's performance indicate it is stable in the presence of a reasonable amount of stack parameter uncertainty.

4.5. MODEL SCALING

Practical sizes of electrolysers will be in the MW range in the near future. It is also known that commercial electrolysers larger than 5 MW, are an aggregation of smaller basic blocks which range from 1 to 2 MW, connected in parallel [26]. This knowledge is applied in scaling the RSCAD model. In the model, it is assumed that there are no interactions between the controllers of the various sub units and all controllers respond simultaneously to the same input command. Therefore, by the principle of superposition, N units of 1 MW electrolysers will provide N MW total demand. Scaling of the electrolyser model can be achieved by multiplying the primary current of the VSC interface by the required scale factor. This can be done by setting the scaling parameters (enscl, scupr, namsc, sclwr, scini) of the VSC interface transformer model (Rtds-vsc-IFCTRF1) in the RSCAD component library. It must however be noted that scaling the model will require adjusting other component ratings in the power system e.g. transformers. Figure 4.23 shows the scaling of the model to produce

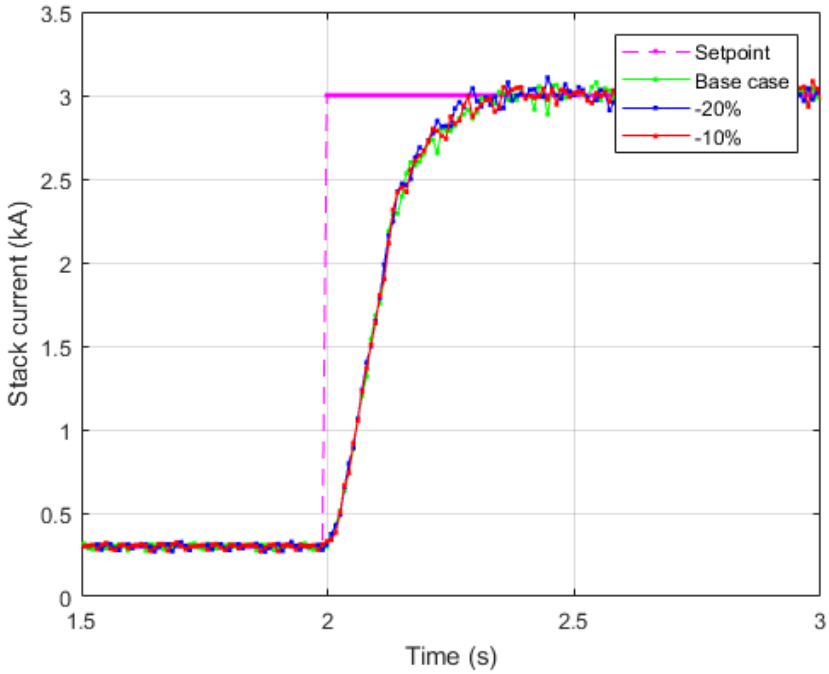

Figure 4.20: Stack current step response with varying stack resistance. Reference tracking and speed of response remain unchanged for a step decrease in load current.

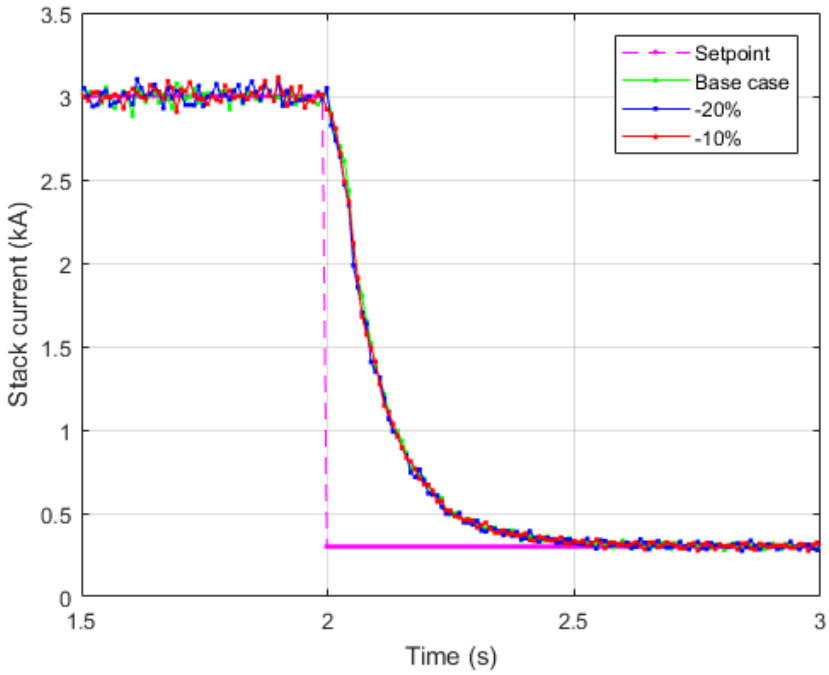

Figure 4.21: Stack current step down response with varying stack resistance. Reference tracking and speed of response remain unchanged for a step increase in load current

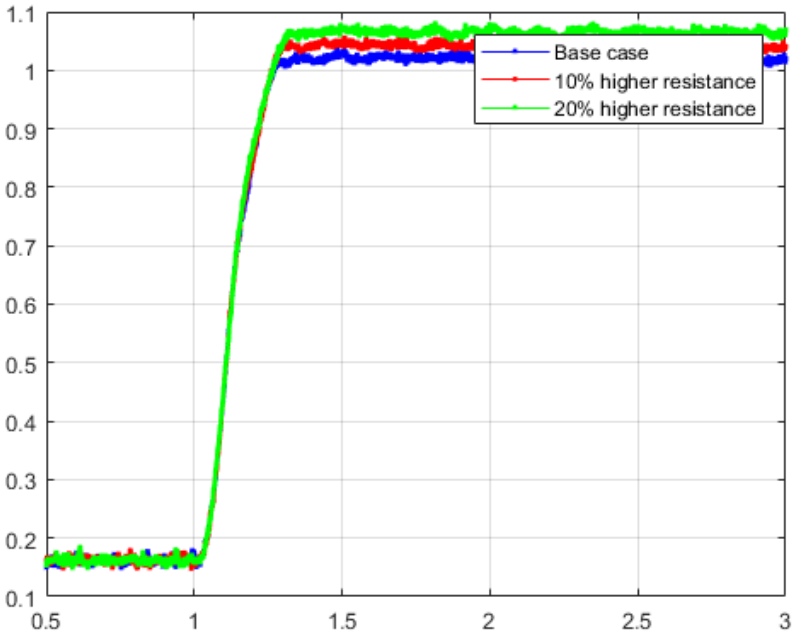

Figure 4.22: Active power variations with increasing stack resistance. Higher resistance leads to higher losses

a demand of 100 MW. The scaling effect produces approximately 100 MW at the interface with the infinite grid. The same scaling can be done to achieve 300 MW. The response time of a 300 MW version can also be adjusted to match the system being modelled. Figures 4.24 and 4.25, show the active power ramp up and ramp down of a 300 MW scaled-up version of the model. It must be noted that the 300 MW model can only support qualitative assessments since it does not yet exist.

Experts in the Power-to-Gas field indicate that THD for a 1MW electrolyser is approximately 1% and 2.2% for current and voltage, respectively. The basic model with low level control (i.e. 1 MW unit) is able to achieve THD of less than 2% for voltage and less than 3% for current, as shown in table 4.1. The scaled up 300MW version however, has a significantly higher THD for both current and voltage. Figures 4.26 and 4.27 show the THD levels for the 300 MW model. The scaling methodology used in the model, works by multiplying the primary current of the interface transformer by a factor determined by the user. This approach facilitates scaling without increased computational burden. The limitation with this approach is that, any distortion present in the current waveform is amplified proportionally. This presents a challenge since the increased distortion may impact results for larger electrolysers. Another approach using multiple independent units in parallel was simulated. In this approach an extended model, shown in figure 4.28, is used. The model comprises two independent PEM stacks, PCS and controls. Results of the analysis can be found appendix B. From the summary of results in table 4.1, it can be observed that the single unit of 1 MW has a lower current THD compared to the unit with two 0.5 MW units in parallel.

	1 unit	2 units	2 Units (S)
Voltage THD (%)	1.83	0.74	0.74
Current THD (%)	2.38	2.87	3.18

Table 4.1: Comparison of THD at PCC for single unit and dual units. The single unit performs better than the dual units for synchronised (denoted by (S) and separate operation.)

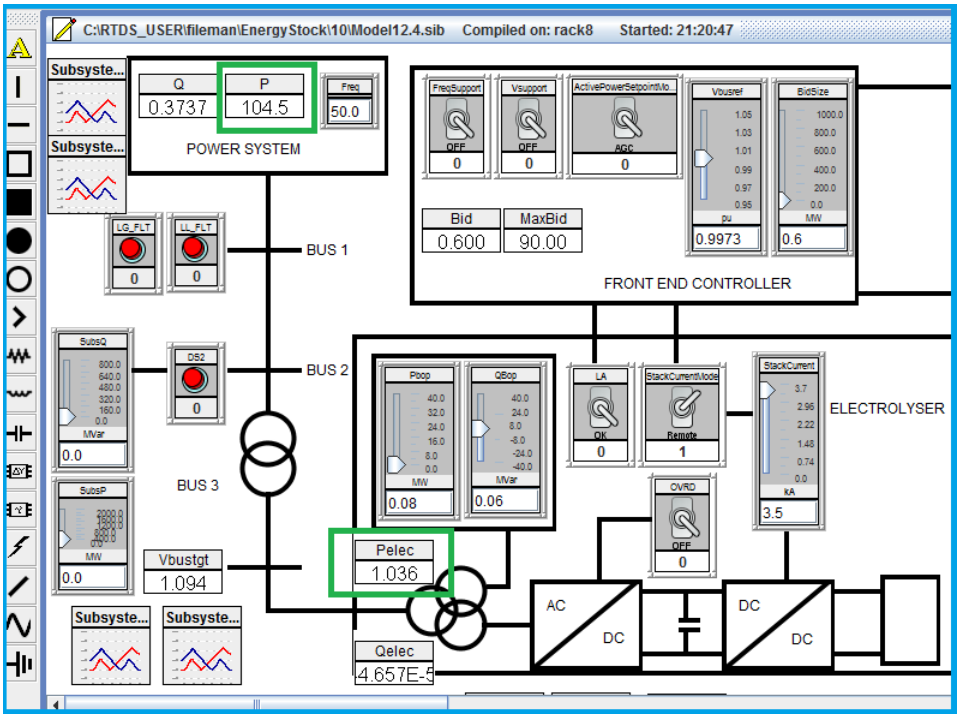

Figure 4.23: Green boxes highlight the basic unit capacity of 1.036 MW and the scaled power observed of 104.5 MW at grid interface.

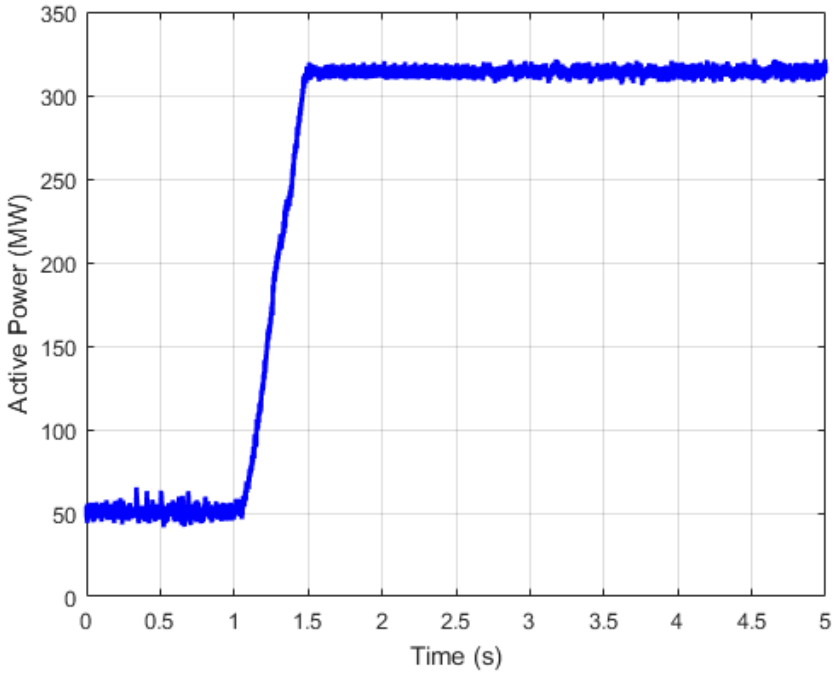

Figure 4.24: Active power step response of 300 MW model at interface with infinite grid (Ramp up).

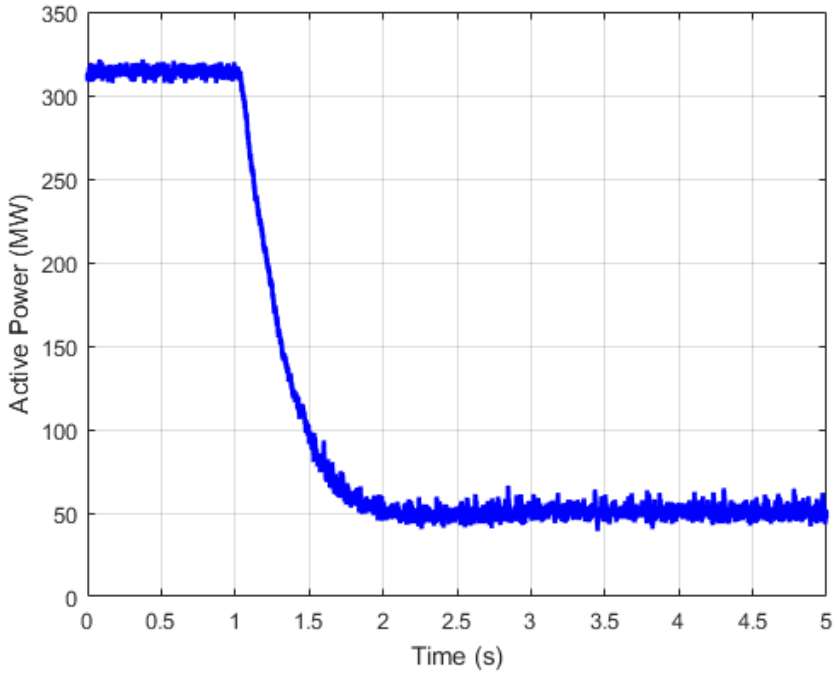

Figure 4.25: Active power step response of 300 MW model at interface with infinite grid (Ramp down).

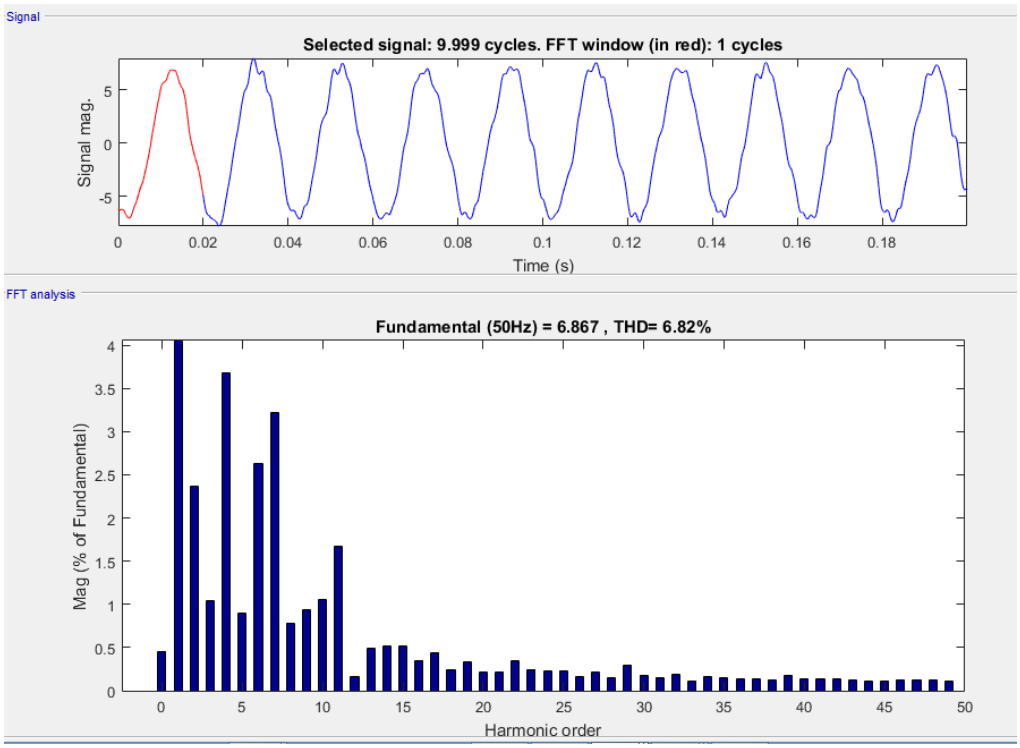

Figure 4.26: Current distortion at PCC with 300 MW unit.

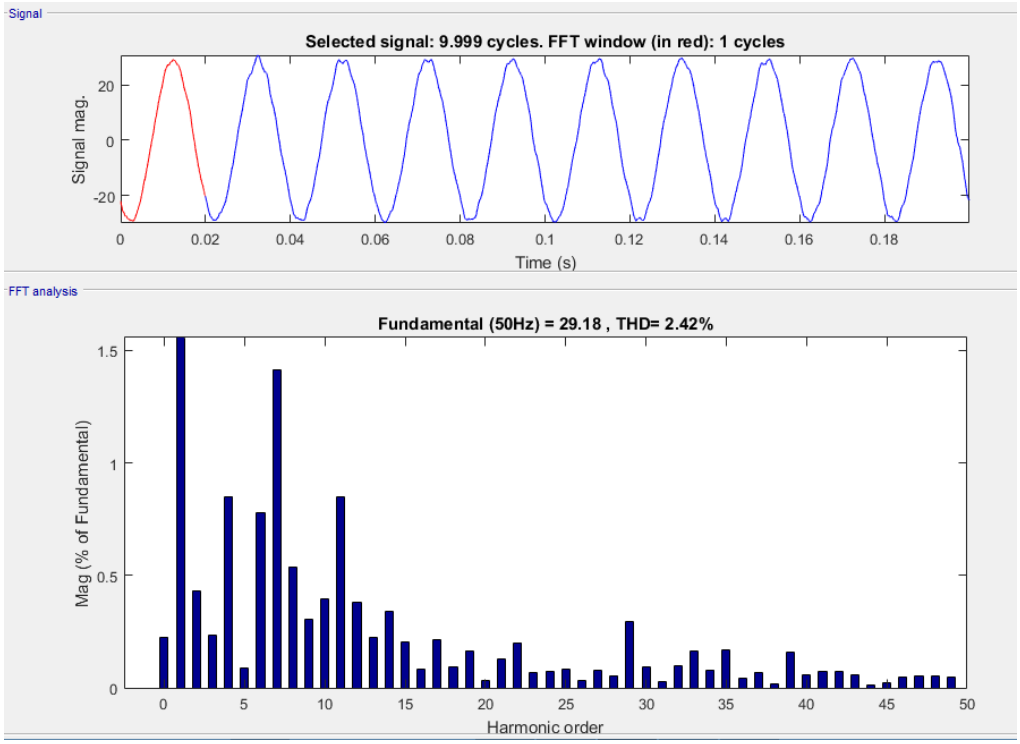

Figure 4.27: Voltage distortion at PCC with 300 MW unit.

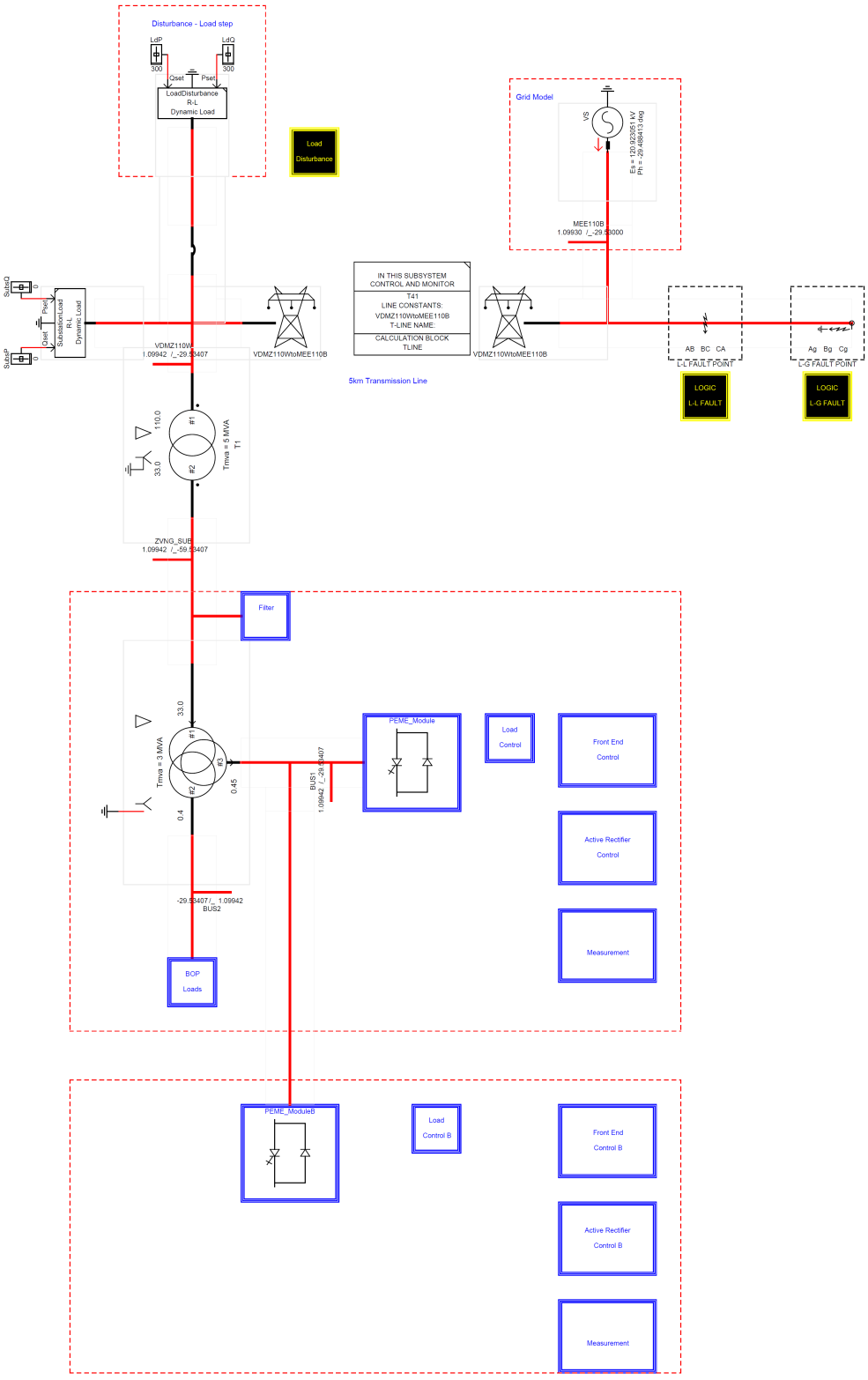

Figure 4.28: Extended model with two separate stacks and control systems, in parallel.

5

Model Application for Ancillary Services Simulation

5.1. Introduction

A balance in generation and load is manifested in a stable frequency. Maintaining this balance is the key to maintaining system stability. Traditionally, the supply side provided the larger part of short term flexibility, however, demand management can also help mitigate the potential destabilising effects of large VRES integration. This can be done in two main ways, load shifting and balancing. Load shifting entails transferring a part of the load to off-peak periods to absorb excess energy generation, whereas balancing services entails fast-acting demand resources that are deployed to help balance generation and load in real time. The use of demand side resources such as electrolysers for purposes of maintaining stability of the power system is the one of the underlying motivations for this thesis project. Previous work done in [45], highlights the potential optimal demand side solutions hold in contributing to improving stability. Recent research highlighting the feasibility of using electrolysers, have yielded some good initial results [14, 15, 46]. However, there are still some remaining aspects that need to be looked into. The size of electrolysers used in previous work range from 40 kW to 312 kW, with varying performance results. It has also been identified that some additional control schemes are required to realise the full potential of electrolysers in the provision of ancillary services. This section aims to highlight the potential of large scale electrolysers with regards to the provision of ancillary services and also congestion management. The potential for electrolysers to act as sources of ancillary services lies mainly in their ability to adjust demand set points very quickly, operate at low loads for extended periods and also allow use of grid side converters for reactive power adjustments (i.e. assuming the AC to DC converter is a controlled converter). The feasibility of ancillary service provision is built on these capabilities. This section demonstrates the feasibility for each type of defined service and also possibilities for congestion management. First a brief overview of ancillary services is given with a description of the ancillary services of interest. The capabilities of electrolysers are then matched to the requirements of each service and a conclusion is drawn on the feasibility or otherwise of delivering each type of service. Part of this chapter is published in [9].

5.2. Overview of Ancillary Services

Power system design and operation aims to ensure resilience against the most likely contingencies. In order to do this reliably, system operators require support from other stakeholders in the form of ancillary services. Definitions for ancillary services vary widely across countries. Some definitions place focus on the role of ancillary services in supporting system security and reliability,

others define ancillary services to support electricity transfers from generation to load and to maintain power quality. Some other definitions also limit the contribution of ancillary services to transmission network domain, while others expand to cover distribution networks. In this thesis, the European Commission definition which states that ancillary services are all services necessary for the operation of transmission and/or distribution networks [8], is used. Maintaining the power system in a secure operating state broadly entails the following:

- Controlling the frequency of the system within set limits
- Controlling the voltage profile of the system within set limits
- Maintaining the stability of the system
- Preventing overloads in the transmission system
- Restoring the system in case of an outage

In order to maintain a stable system in the presence of large amounts of Variable Renewable Energy Sources (VRES), the capability to provide a system support service on short notice is crucial. Work done in [8] categorises the ancillary services under seven broad classifications based on responses to a questionnaire sampled from 17 countries across the world, including The Netherlands. The main classifications are as follows:

- **AS-1 (Primary Frequency Control)** - This service is provided specifically to control system frequency variations, and provides the first response to frequency deviations that follows loss of supply etc. Reaction time is instantaneous and is delivered for up to about 2 minutes.
- **AS-2 (Secondary Frequency Control: Regulation)** - This service deals with services that are usually driven by Automatic Generation Control (AGC). This service handles power system deviations that last for as long as 30 minutes. This service is delivered in response to a continually varying control signal based on the Area Control Error (ACE) of the given area. The goal of secondary frequency control is to restore primary frequency control capacity.
- **AS-3 (Secondary Frequency Control: Spinning Reserves)** - This is an event-driven service focused on recovery from a loss of supply (or demand). It is slower than the primary control response but faster than economically dispatched load-following units. This service is provided by holding an amount of fast responding capacity in reserve. The amount of synchronised reserve is tied to the accepted level of risk.
- **AS-4 (Secondary Frequency Control: Non spinning reserves)** - This is also an event-driven service similar to AS-3, however, the difference is that non-spinning reserves are idle and come with the added risk of a failure to start.
- **AS-5 (Tertiary Network Control)** – Tertiary reserve services are used to restore fast secondary services when they are used up. This ancillary service replaces used energy with economically dispatched units or by slow reserve units which are on standby.
- **AS-6 (Voltage Control Service)** – This service is aimed at ensuring a power system operates within acceptable voltage limits using network arrangements and reactive power compensation. It involves the strategic siting of reactive power reserves in order to facilitate an effective response and maintain the stability of the power system. The voltage control service is a critical ancillary service needed by all system operators. Currently, the definition of this service varies across countries.

- **AS-7 (Blackstart Service)** – This service is recognized as a necessary service to restore systems following power system (or area) blackouts.
- **Congestion Management (CM)** - This is another key responsibility of the system operator. Though not defined as an ancillary service in [8], the potential for delivering this support is also considered in the analysis.

It must be noted that in other literature such as [47], other classifications are used to describe the same services. For example AS-1 is also described as Frequency Containment Reserve (FCR), while the services AS-2, AS-3 and AS-4 are collectively described under the automatic Frequency Restoration Reserve (aFRR) description. AS-5 is also described as Restoration Reserve (FRR).

From the survey of ancillary services in 17 countries, generators (within the control area) and demand side participation (within the control area or from other control areas) were identified as the main sources of ancillary services. To access these services, system operators establish a procurement arrangement with the service providers. This procurement arrangement can be mandatory (paid/unpaid), via bilateral contracting, public tendering or based on a real-time market. The mandatory methods are non-market based, while the remaining methods can be considered as market based mechanisms. Apart from the real-time market, all other methods require agreements in advance. According to [8], mandatory - unpaid procurement method is used mostly for primary frequency control ancillary services, which is the fastest service. Ancillary service products can be instructed automatically or manually. The method of instruction can also be based on closed loop control or real-time optimisation. Primary and secondary (regulation) frequency control are usually instructed automatically. Spinning and non-spinning reserves are usually activated manually.

5.3. CAPABILITIES OF ELECTROLYSERS WITH FRONT END CONTROL

The power system of the future will require fast acting demand side resources to maintain a good level of flexibility. The ability of PEM electrolyser technology to participate in delivery of ancillary services is contingent on response time and duration operating characteristics. This brings to the fore the need to align the following with the service requirements:

- the time it takes to settle after a power setpoint change
- the rate at which the device can change power consumption
- the lower operation limit or the minimum turndown level
- the time it takes to startup and shutdown

Table 5.1 compares each ancillary service with the electrolyser's capabilities. Data for The Netherlands is used as the basis for comparison primarily because the real system of interest will be deployed there and secondly due to variations in requirements in each country. To provide primary frequency (AS-1) support, electrolysers can regulate active power consumption in response to instantaneous deviations of frequency from nominal values. The amount of active power demand adjustment is determined by the droop setting. The reaction time of electrolysers is usually under 1 second and is much faster than generator governors. For secondary frequency control (AS-2, AS-3, AS-4), the electrolysers' operating point adjustment can be utilised to offset short-term variations in demand that might affect the stability of the power system. The reaction time for setpoint changes is less than 1 second and the setpoint can be maintained for unlimited amounts of time. This capability is demonstrated by the model in figure 5.1. The model is able to react within one second and maintain the setpoint for the duration required. This adjustment can be instructed based on events or continuously based on a signal from the system operator (e.g. Area

Service	Reaction	Delivery	Electrolyser capability
AS-1	0	30s	Reaction time < 1 second. Delivery time > 30 seconds.
AS-2	0–30s	15min	Reaction time < 1 second. Delivery time is unlimited.
AS-3	0–15min	15min	Reaction time < 1 second. Delivery time is unlimited.
AS-4	-	-	Cold start for electrolysers typically <10 minutes.
AS-5	-	15min	Fast ramp up/down within 1 second with unlimited delivery time.
AS-6	-	-	Fast reactive power injection/absorption.
AS-7	-	-	Active and reactive power adjustments feasible.
CM	-	-	Active power adjustments possible for unlimited time.

Table 5.1: Ancillary service response time requirement matched with electrolyser capabilities. Electrolysers exceed the requirements for each ancillary service.

Control Error). This capability makes it feasible to emulate spinning and non-spinning reserves and also provide regulation. Tertiary control (AS-5) is also feasible because the power consumption of electrolysers can be partly reduced or curtailed completely for extended durations to create operating reserves. This capability can be used in place of economically dispatched units if the cost of delayed gas production is less than the revenue from the ancillary service. This service can be manually instructed, as with conventional reserves.

The power conversion system of large electrolysers also holds potential to support voltage in the power system. The converter control can be instructed to inject or absorb reactive power. The response time for this capability is tunable to meet the requirements of the application. The limit for reactive power support varies dynamically with the active power setpoint. This ensures the total apparent power rating of the converter is not exceeded. This capability can be utilised to deliver voltage control services (AS-6).

Another possible application of the electrolyser's capabilities is in the area of black start (AS-7) services. Though not a source of energy, the electrolyser can contribute to system recovery procedures. The electrolyser can act as a controlled load in the system restoration stage of the black start process. The electrolyser's active power demand can be precisely controlled in order to maintain a balance between generation and load at each instant of the process. The reactive power capabilities can also be utilised to stabilise voltage during system restoration.

Lastly, congestion management, though not classified as an ancillary service by most countries, can also be realised. This capability is again based on the electrolyser's ability to adjust demand within a short time and maintain partial load or complete curtailment for unlimited periods. Electrolysers can contribute to easing congestion by peak capacity management. Instructing a large electrolyser to reduce active power demand, can contribute to eliminating congestion on transmission lines. Comparing the performance characteristics of electrolysers and the requirements of the various ancillary services shows that participation in frequency support, voltage support and congestion management ancillary services is feasible. It must also be noted that the extended capabilities are enabled by the FEC. The controller allows adaptation of the total electrolyser system's electrical response to the application's requirements.

5.4. ELECTROLYSER SYSTEM REQUIREMENTS FOR ANCILLARY SERVICE DELIVERY

Requirements for ancillary services differ slightly from country to country. Therefore, to ensure goals of stakeholders are met, it is important to establish some generic guidelines for parties interested in ancillary service delivery with large electrolysers. Table 5.2 summarises the proposed set of requirements. The set may only be used as a guide and therefore is not an exhaustive

Service	Requirement
AS-1	1.The system must track frequency in real time and adjust active power. 2. The system must respond within 1 second to a frequency deviation > 10 mHz.
AS-2	1. The system must adjust active power demand in real time based on command. 2. The system must achieve the required set point within 30 seconds. 3.The system must maintain the instructed setpoint for at least 15 minutes.
AS-3	1. The system must decrease active power demand in real time based on command. 2. The system must achieve the required setpoint within 15 minutes. 3.The system must maintain the instructed setpoint for at least 15 minutes
AS-4	1. The system must perform a cold start based on signal from system operator.
AS-5	1. The system must decrease active power demand in real time based on command. 2. The system must achieve the required setpoint instantaneously (<1 s) 3. The system must maintain the instructed set point for at least 15 minutes
AS-6	1. The system must adjust reactive power in real time based on command. 2. The system must track bus voltage magnitude and adjust reactive power.
AS-7	1.The system must track frequency in real time and adjust active power demand. 2. The system must respond within 1 second to a frequency deviation > 10 mHz.
CM	1. The system must adjust active power demand in real time based on command. 2. The system must achieve the required set point within 15 minutes. 3. The system must maintain set points for unlimited duration.
Control	1. The system must be able to process external signals and optimise setpoints.
Link	1. The system must have high speed communications link to transmit instructions.

Table 5.2: Proposed set of requirements for electrolyser configured to deliver ancillary services.

list, since other countries may also impose additional requirements based on specific grid codes. The entries in the table highlight requirements drawn from a combination of the response of the electrolyser and the requirements of ancillary services (based on data from The Netherlands). Additional requirements for high level control and a communications link are also included as basic requirement. It is expected that these requirements will evolve with time as new capabilities are discovered. For example, high and low level control functions may evolve to become a single unit thereby making the inclusion of an additional high level controller unnecessary.

5.5. CONCLUSION

This chapter has highlighted some capabilities of electrolysers integrated with high level controls, within the framework of standard ancillary services as defined by [8]. Some requirements for electrolyser systems planned for use as sources of ancillary services were also proposed. The evidence from the simulations support the view that providing the power system with ancillary services from large electrolysers in the areas of frequency control, voltage control and congestion management is feasible. This goes to further support similar conclusions that have been arrived at in other research [13].

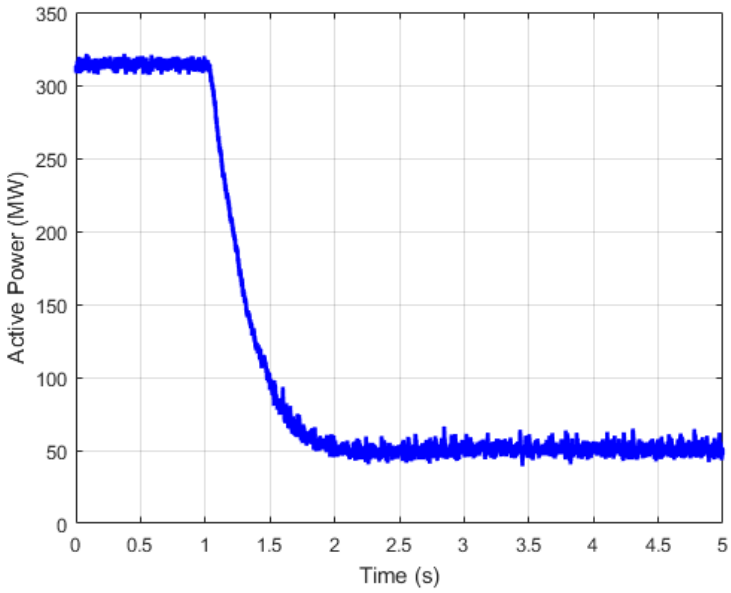

Figure 5.1: 300 MW electrolyser model showing rapid power adjustment in response to external signal from system operator. Setpoint is maintained for up to 5 seconds. Capability to extend this delivery time to meet requirements of ancillary services is possible with the model.

6

CONCLUSIONS & RECOMMENDATIONS

This chapter concludes the report and highlights future work in line with the higher motivation for this area of research. Key contributions made during the course of the research project are also mentioned.

6.1. SUMMARY OF OBSERVATIONS AND KEY INSIGHTS

The generic model's responses to basic commands indicate a capability to emulate a real system. The setpoints are achieved within seconds without any instability. The emulation of low or partial load operation for extended durations is also possible with the model, just like with a real electrolyser. The flexibility also exists to scale the model for different sizes of electrolysers. The model was built on mathematical foundations and implemented in RSCAD using library components. The structure of the model was verified using available literature.
To test the feasibility of using large scale electrolysers to deliver ancillary services, the basic electrolyser model is augmented with a high level controller. The proposed high level control scheme attempts to bridge the gap between the capabilities of the electrolyser model with low level controls and the requirements of the various ancillary services. With the controller in the loop it is possible to simulate the delivery of frequency support (primary, secondary and tertiary), voltage support and congestion management services with reasonably fast response times. The controller has a stable and fast response to typical power system disturbances and also allows controlled changes of setpoints based on external commands and price signals. The model also performs satisfactorily in the presence of stack parameter uncertainties.

In order to leverage the potential of large electrolysers for ancillary services, some basic requirements must be met: key among them being, the ability to adjust active and reactive power level within time limits specified by the system operator and to maintain these setpoints for the duration required. To ensure adequate responses, the system must also have the capability to measure and track the variables of interest in real time at the required accuracy, and react to changes observed. To facilitate the transmission of commands to the electrolyser, there must be a some form of communication path or link. The model is capable of emulating the response required for all the types of ancillary services and also track the system frequency and bus voltage in order to react when the controller settings require that. In this model however, the communications link is not modelled. Overall, the results appear to support the view that creating a scalable generic model of a large scale PEM electrolyser in RTDS is feasible. The various test cases in chapter 4 also provide important insights into the capabilities of large scale electrolysers to participate in supporting the power system with the front end controller being the key enabler. Once the basic set of requirements, together with other operator-specific requirements, are met, the delivery of different types and volumes of ancillary services is possible.

In view of the significant potential large scale electrolyser technology holds for the power system, it is important to reflect on the limitations of this technology. As with all relatively new technology or applications, there are still some aspects which are undergoing research. Broadly speaking, the limitations of the technology can be grouped under the areas of scalability, durability and cost. First, is the issue of the method of scaling. This is of prime importance since the focus is on large scale units. Currently large electrolysers are built up using small units of 1 or 2 MW. A state-of-the-art fully integrated 10 MW unit is housed in building which covers approximately 280 square meters. It is also interesting to note that, the 100 MW unit requires more than ten times the space for a 10MW unit. Clearly, this scaling approach presents a challenge for potential sites where space is limited or expensive. The additional cost of space may lead to a higher total cost of ownership (TCO) which will make the overall project uneconomical. Secondly, the lifespan of the PEM stack also limits the potential of the technology. According to [48], intermittent operation of PEM water electrolysers tends to increase the rate of degradation. Until recently, most PEM water electrolysers used for industrial applications were operated under fairly stable conditions. New applications in the power system will require more flexible and intermittent operating conditions. The impact of these varying conditions can contribute to reduce the life span of the electrolysis stack. Reduced stack life increases failures and leads to higher operational costs and downtime. Lastly, despite the recent advances in PEM cell technology, the overall capital cost of PEM electrolysers is still relatively high. Industry players are still exploring ways to reduce the overall capital expenditure of the technology in order to make it more affordable. With successive decreases in cost, the technology will gain widespread acceptance for large scale projects.

Despite the limitations of the technology, there is still a high level of interest in applications for the power, industrial and transport sectors. It is possible that the demand for large scale electrolyser technology, may spur more efforts to overcome the aforementioned limitations.

6.2. CONCLUSIONS

The main conclusions drawn from the evidence in this research project are outlined as follows:

1. Developing practical RSCAD models of large scale electrolysers connected to transmission networks is important for understanding their overall impacts on the power system. The advantage of being able to test various scenarios on a real time basis cannot be overstated.

2. It is possible to create generic models of different sizes of large scale electrolysers in RTDS. It is possible to emulate the electrical response with a good level of accuracy. Higher capacity units, however, may require more advanced power conversion in order to meet grid code requirements for total harmonic distortion.

3. The dynamic response of the basic generic model matches that for a real electrolyser closely and the proposed control scheme extends the basic capabilities to unlock ancillary service capabilities.

4. In addition to country-specific requirements, some basic requirements such as fast response and ability to maintain reactive and active power setpoints for long durations must be met in order for large scale electrolysers to participate in ancillary services delivery.

6.3. ANSWERS TO RESEARCH QUESTIONS

The answers to the research questions drawn up in chapter 1 are summarised as follows:

1. **Is it feasible to build a suitable model to represent the electrical response of the electrolyser in RSCAD?**
   Feasibility is defined as the possibility that something can be made, done, or achieved. This definition, as applied to this thesis, refers to the possibility of creating a model of a 1 MW electrolyser with built-in RSCAD library components. To this end, a generic detailed architecture of a 1 MW electrolyser was built in RSCAD. The various subsystems identified in the real system, were replicated in detail based on practical assumptions and operating conditions. The dynamic performance of the electrolyser system within an electrical power system, was simulated with the aid of RTDS and the RSCAD software tool. The dynamic response of the basic model is capable of emulating the response time and step response profile of a real electrolyser. It can therefore be concluded that creating a suitable model to represent the electrical response of the electrolyser in RSCAD is feasible.

2. **Which additional control scheme is required to extend the capabilities of electrolysers for ancillary service applications?**
   Controls systems in commercially available electrolysers are designed primarily to support plant automation for production of hydrogen gas. In order to optimise the electrolyser system to support additional objectives such as provision of ancillary services, an additional layer of control is required. The Front End Controller (FEC) is the additional high level control that enables the basic electrolyser to deliver the various types of ancillary services. The front end controller integrates with low level controls to form a hierarchical control scheme with extended capabilities. The proposed control scheme implemented in RSCAD, has the capability to track and respond to price signals and the condition of the power system simultaneously. This capability presents value differently, based on the perspective of each stakeholder. For the plant owner, it enables the accrual of additional revenue from ancillary services and also increased profits from cost-optimised hydrogen production. For the system operator, it enhances power system flexibility (due to the availability of fast demand side resources to support the power system). Another additional value of the proposed scheme lies in its simplicity. This makes it possible to implement its functions on existing plant controllers at a low cost and without significant increase computational burden.

3. **How robust is the controller to disturbances in the power system?**
   Robustness implies an ability to withstand or overcome adverse conditions. Within the context of the electrolyser system (i.e. at the module layer boundary) this means an ability to withstand disturbances in the power system (e.g. faults) and still deliver its functions. A key finding is that the hierarchical control scheme (for both 1 MW and 300 MW versions) is able to improve the response of the electrolyser system to typical disturbances, significantly. The generic model's responses were adequate and stable for the test cases simulated, indicating an reasonably good ability to withstand disturbances in the power system.

4. **What are the minimum requirements needed for delivery of ancillary services (congestion, frequency, and voltage) using electrolysers?** The minimum requirements that must be met by large scale electrolyser in order to be able to deliver ancillary services are broadly summarised as follows:

   - The system must track and respond to frequency and voltage changes in real time.
   - The system must maintain required set points for the minimum duration specified.
   - The system must adjust active and reactive power on command.

- The system must process external signals and optimise setpoints.
- The system must have high speed communications link to transmit instructions.

These requirements are generic and may change depending on country-specific requirements.

6.4. CONTRIBUTIONS TO IEPG

The thesis project has developed models and tested scenarios, thereby enhancing the understanding of large scale PEM electrolyser systems and the potential they hold for supporting the power system. The contribution to IEPG's ongoing research in this field are outlined as follows. This thesis project:

1. Developed a practical model of a large scale electrolyser in RSCAD which can be used for future power system studies by IEPG and other institutions globally. This is potentially the first of its kind.
2. Proposed a control scheme to extend the capabilities of an electrolyser to deliver ancillary services.
3. Produced a conference paper on the modelling of PEM electrolysers which was submitted and accepted at the 3rd International Hybrid Power Conference in May 2018.
4. Contributed to creating course materials for the RSCAD course in modelling and simulation which starts in August 2018.
5. Highlighted the potential of large electrolyses in supporting black start procedures. An area which can be further explored in future research.

6.5. FUTURE WORK

Research on developing large scale electrolysers is still in its early stages and the industry competition is fairly intense. As a result information to facilitate accurate modelling for academic purposes is difficult to access. This notwithstanding, some progress can still be made in the area of bridging the identified knowledge gaps and new challenges. In line with this, a few recommendations are made for future research in this area of modelling:

1. A detailed set of data containing step response profile, controller gains, power conversion and PEM stack component from a real system can be used to fine tune the responses of the basic model. This will improve high level controller design.

2. The hierarchical control system can be improved with stochastic input processing capabilities.

3. The controller can be coded into a custom component in order to reduce computational burden for advanced controllers.

4. Other methods for reducing THD can be explored for use in larger systems.

A

User Guide - Running Sample Simulations

A.1. Introduction

The PEM electrolyser model represents a real large scale electrolyser in RSCAD. The model has two key parts: the basic model comprising the power conversion system, PEM stack and balance of plant components, and the Front End Controller. The model facilitates studies of electrolysers configured as sources of ancillary services, within the power system. This guide will help users of the model identify the key parts of the model, run basic scripts and modify model parameters. This model can be run on a PC which has RSCAD 5.0 installed and an IP (Internet Protocol) connection to an RTDS simulator.

A.2. Objectives

The guide aims to equip users with the basic knowledge to enable them do the following:

- Identify the key components of the electrolyser model in RSCAD.
- Run basic scripts which demonstrate the capabilities of model within the framework of ancillary services.

A.3. Prerequisites

Before using the model, users should:

- Read chapters 4 and 5 of this report.
- Be familiar with the basics of RSCAD software (i.e. opening files in Draft module and compiling and running a simulation in Runtime module).

A.4. Procedure

This section outlines the procedure to prepare and run the test cases. The attached files listed below are the only files required to run the simulations:

- Electrolyser model in RSCAD – Draft and Runtime simulation files
- Runtime script files for test cases 1 to 9
- Transmission line files

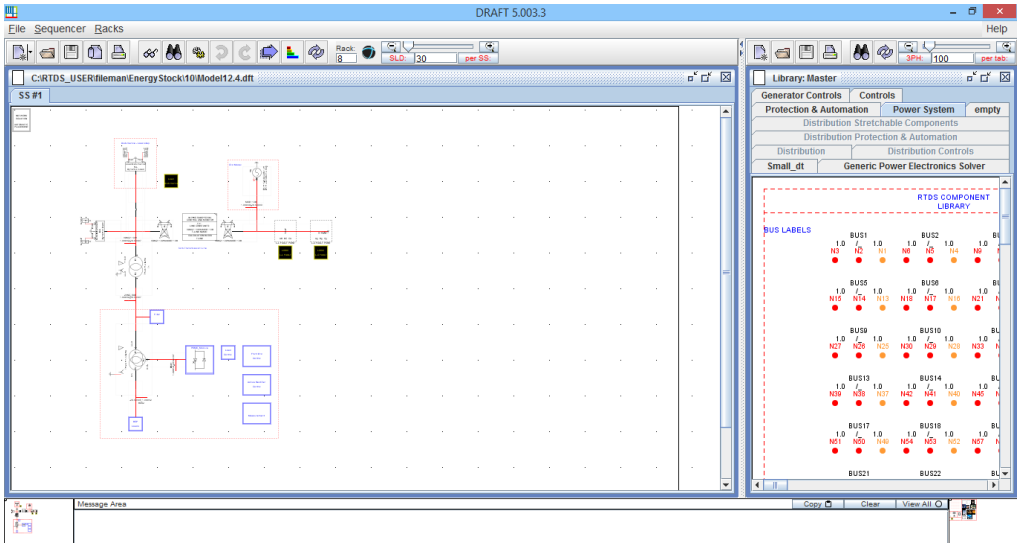

Figure A.1: Electrolyser model loaded in Draft module of RSCAD.

A.4.1. LOADING THE DRAFT FILE

This section describes the loading of the Draft file and identification of key components. Follow the under-listed steps to load the model:

- Launch RSCAD's Draft module by clicking on "Draft" button.
- Create a new folder in the RSCAD folder on Drive C and save the attachments into that folder.
- Launch the RSCAD software and double click on the draft file labelled "Model12.4.dft". The model will load as shown in figure A.1. This is the model as represented in the Draft module of the RSCAD software.
- Proceed to select the rack and compile the circuit

A.4.2. IDENTIFYING KEY COMPONENTS

Figure A.2 shows the electrolyser model along with various other power system components. Each component is labelled accordingly. Within each hierarchy box, there is a detailed circuit. All circuits parameters can be changed to suit the user or application.

A.4.3. RUNNING THE SIMULATION SCRIPTS

The circuit in the Draft module is replicated in the Runtime module along with some additional parts to aid the simulations. In figure A.3, the two additions are shown. The TSO segment sends active and reactive power setpoints to the FEC, while the hydrogen market segment sends price and ramp direction commands. These signals are considered external to the electrolyser system control. To run the simulation scripts follow the under listed steps:

- Launch the Runtime module by opening the file labelled "Model12.4.sib" in RSCAD.
- In the Runtime module, click "Script" and choose one script file in the folder created in the earlier step.
- Open the sample graph related to the chosen test case. Note that additional plots can be created for any other variable of interest.

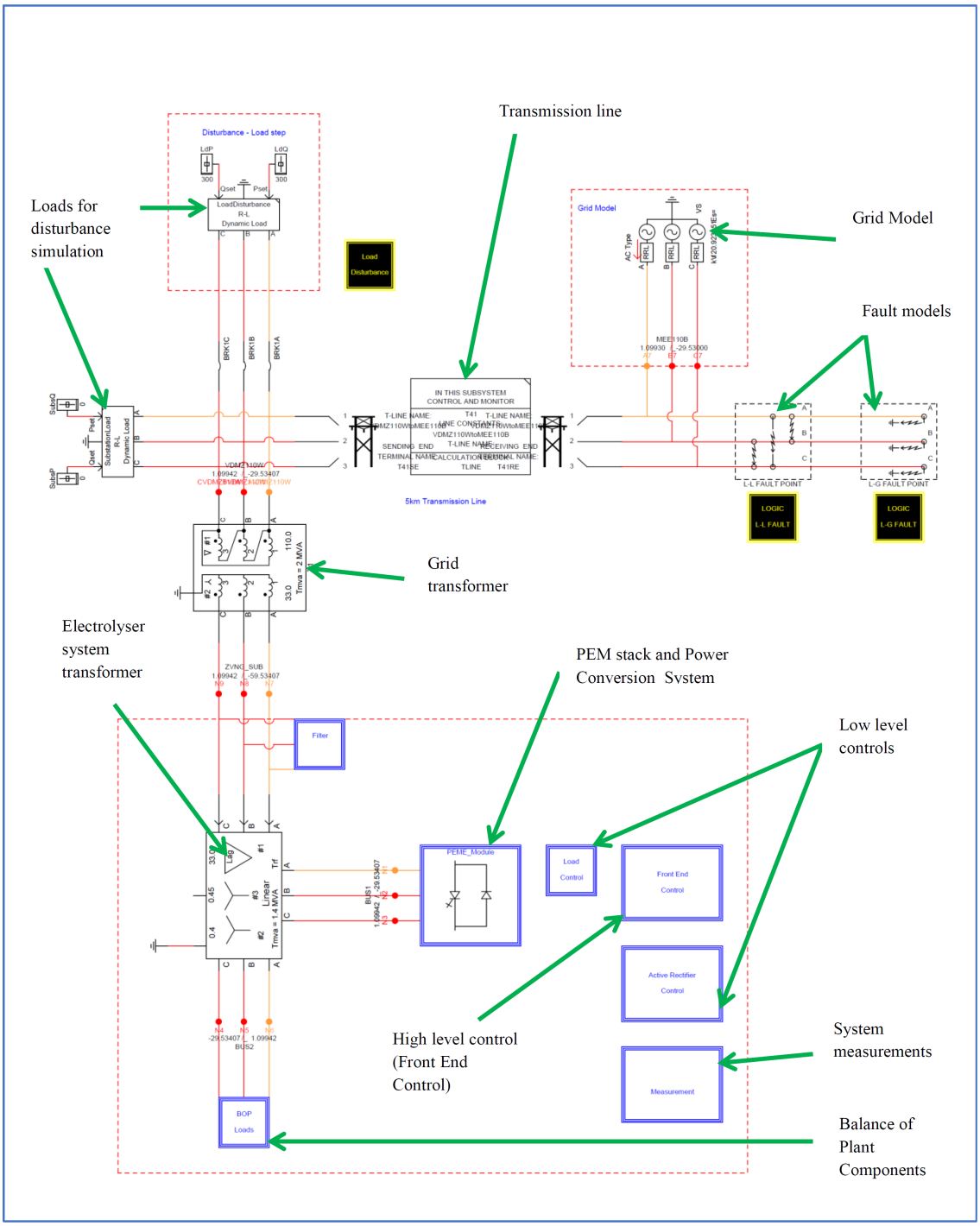

Figure A.2: Electrolyser and grid models highlighting the key parts.

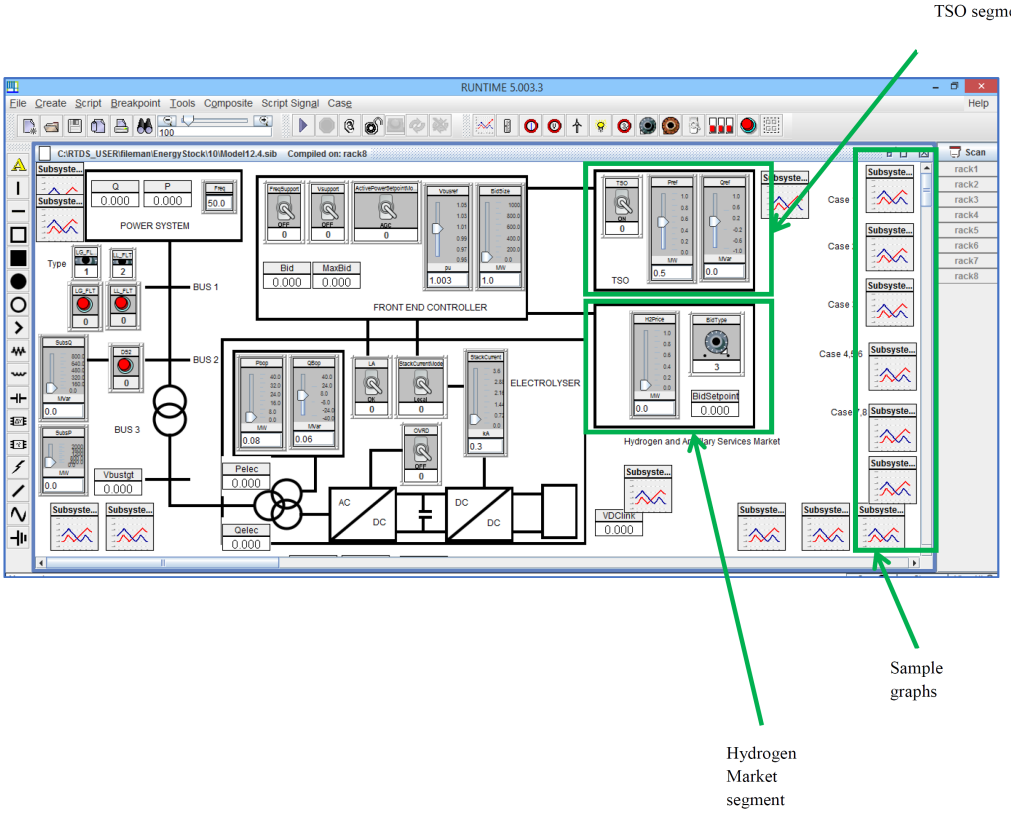

Figure A.3: Runtime module highlighting segments for generating external signals and viewing real time plots.

- Click "Run" and observe the sliders, push-buttons and switches. Note that, depending on speed of connection, refreshing of graphs may take a few seconds.

The key parameters used in these attached model are listed in table A.1.

No	Parameter Name	Parameter Value	Subsystem
1	Proportional gain	20.09	DC link Voltage PI Control
2	Integrator time constant	0.0048	DC link Voltage PI Control
3	Proportional gain	0.6628	Inner current loop PI control
4	Integrator time constant	0.04533	Inner current loop PI control
5	Proportional gain	0	Bus voltage support PI control
6	Integrator time constant	0.06677	Bus voltage support PI control
7	Proportional gain	0	Active power outer loop control
8	Integrator time constant	0.36483	Active power outer loop control
9	Proportional gain	0	Reactive power outer loop control
10	Integrator time constant	1.0576	Reactive power outer loop control
11	Proportional gain	0.0022	Load Current Controller
12	Integrator time constant	0.1944	Load Current Controller
13	PEM stack resistance (Ohms)	0.015	PEM Stack
14	PEM Stack Open Circuit Voltage (Volts DC)	145	PEM Stack
15	Input reactor inductance (H)	0.000325	PCS

Table A.1: Key simulation parameters

B

TOTAL HARMONIC DISTORTION

B.1. THD ANALYSIS RESULTS WITH DUAL UNIT MODEL

This appendix shows the results of the test with dual unit model of the electrolyser. Synchronised operation of the two-unit model had a higher THD than in unsynchronised mode. However, the single unit performed better than the dual unit model for both cases.

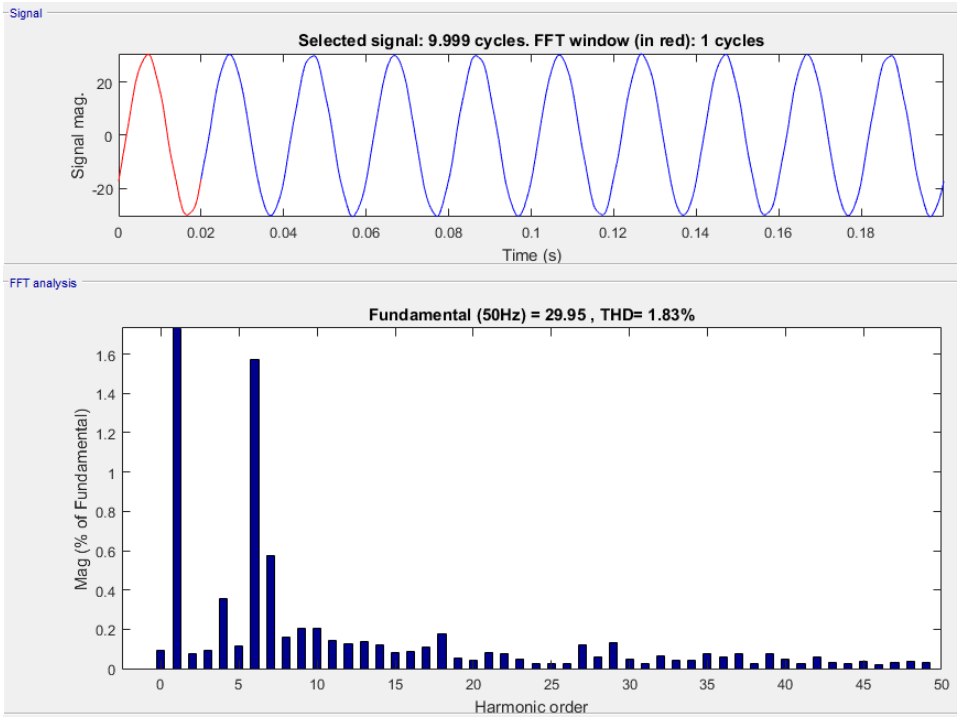

Figure B.1: Voltage THD at PCC with single unit of 1 MW.

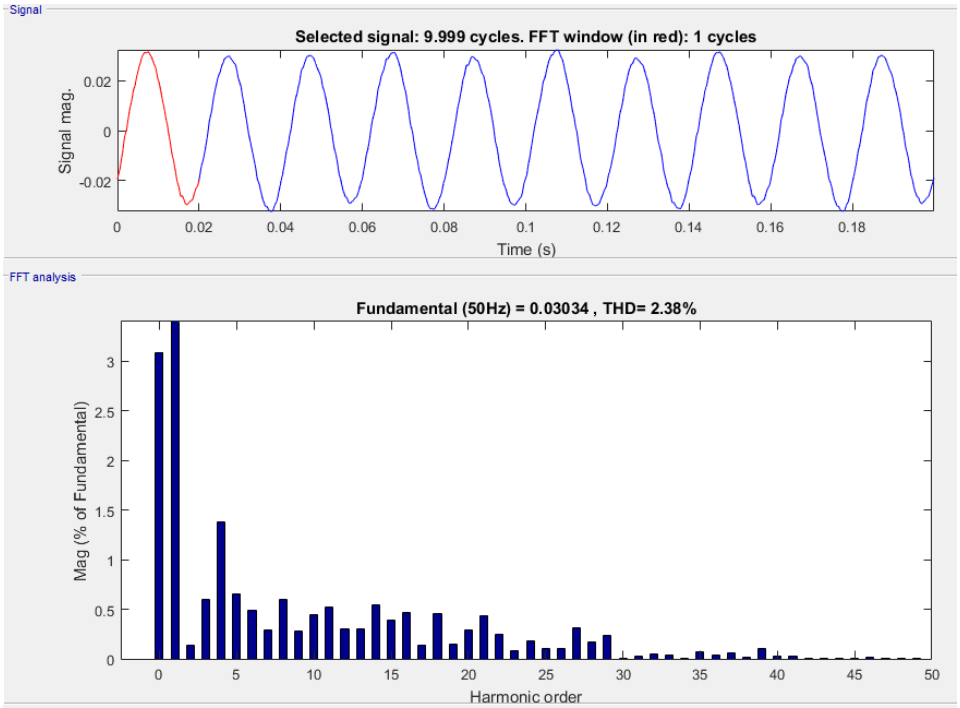

Figure B.2: Current THD at PCC with single unit of 1 MW.

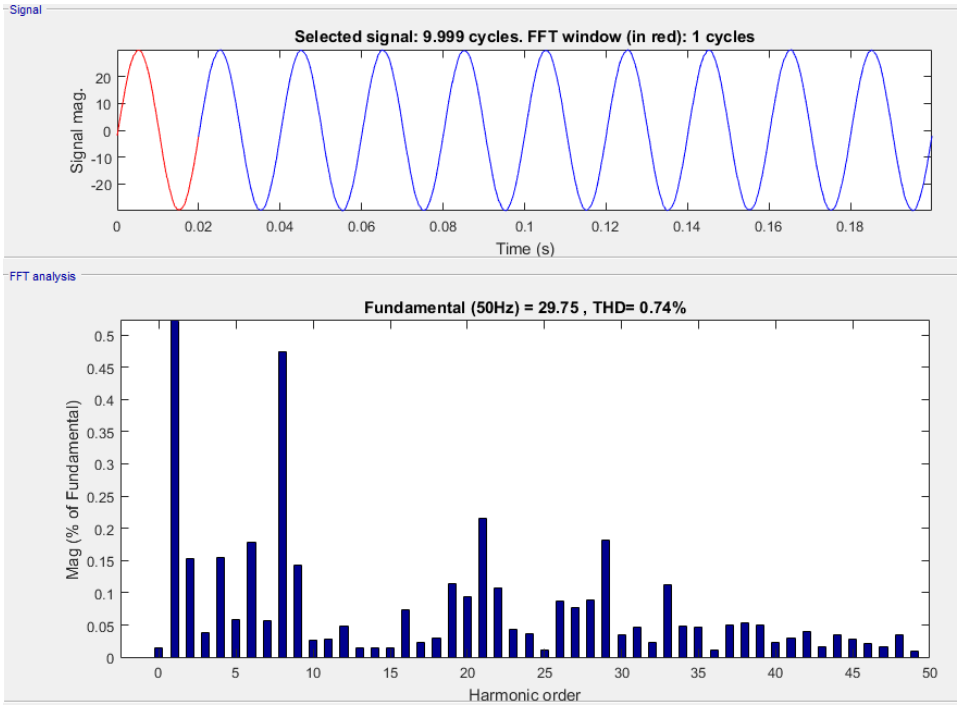

Figure B.3: Voltage THD at PCC with two units of 0.5 MW.

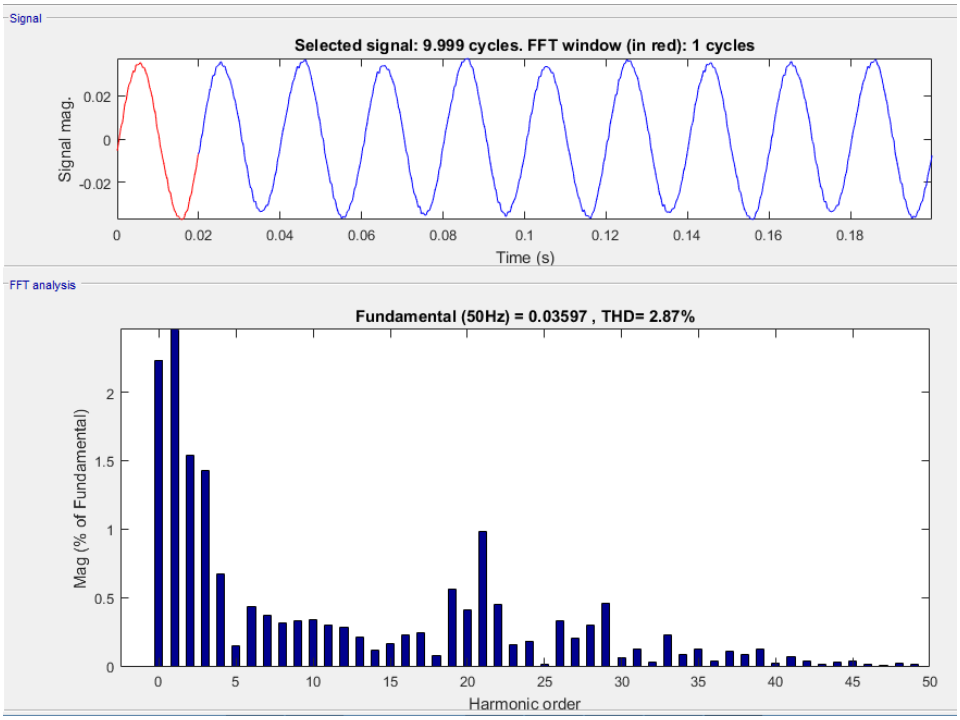

Figure B.4: Current THD at PCC with two units of 0.5 MW.

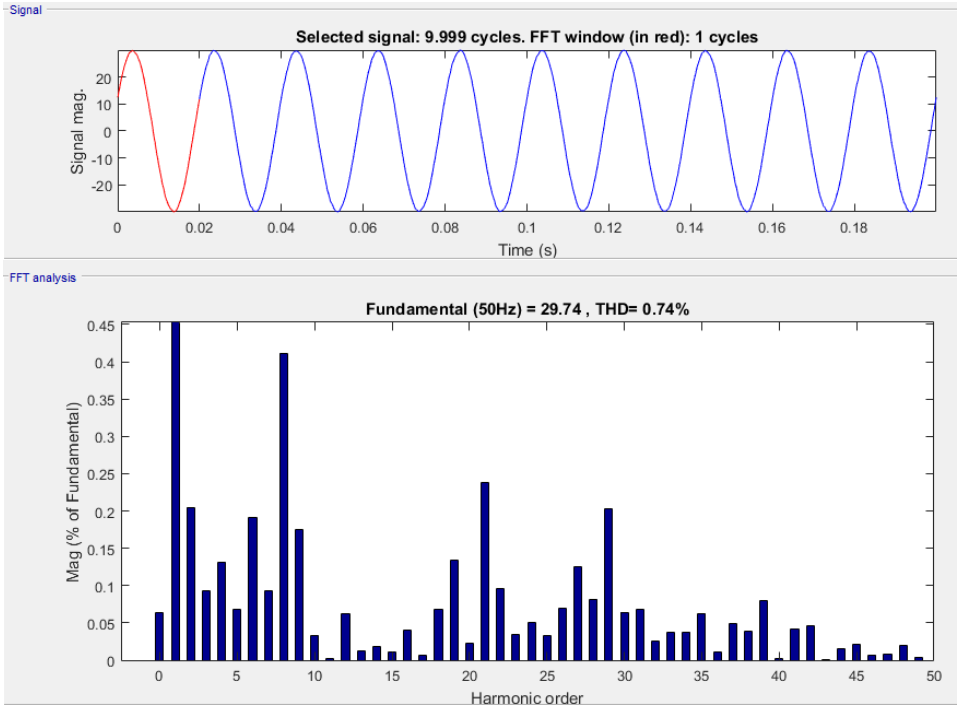

Figure B.5: Voltage THD at PCC with two units of 0.5 MW. Units are synchronised.

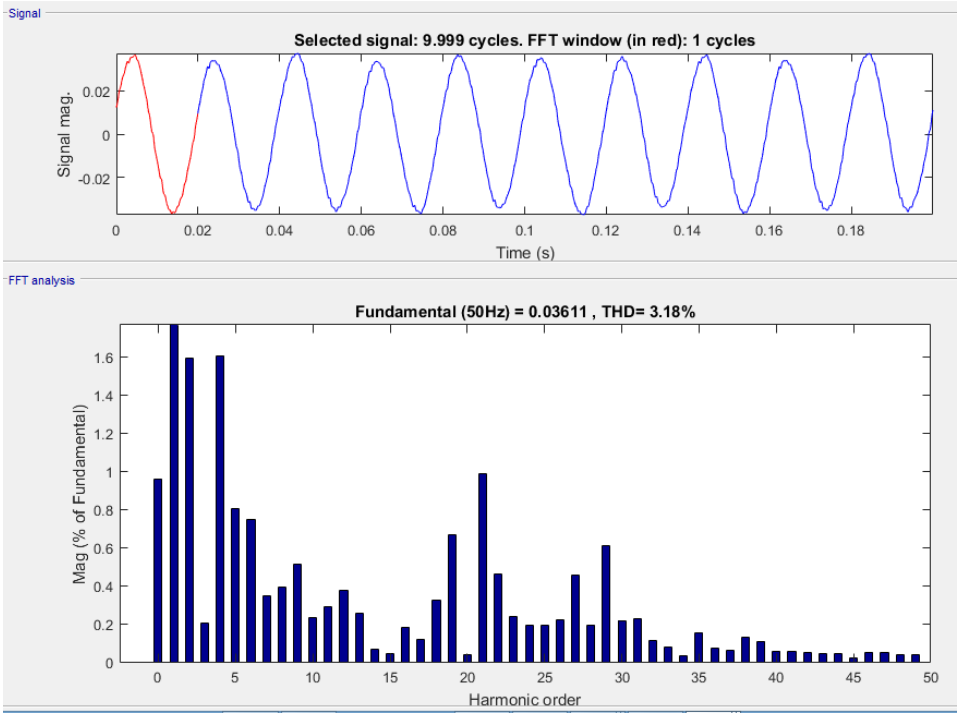

Figure B.6: Current THD at PCC with two units of 0.5 MW. Units are synchronised.

C

ALKALINE STACK MODEL

C.1. INTRODUCTION

This appendix highlights the potential for the application of the RSCAD model to emulate alkaline electrolysers. The approach involves using the electrical equivalent circuit of the stack. It is assumed that the methods used to obtain the parameters in the electrical equivalent circuits adequately characterise the device and also parameters of controllers can be leveraged to emulate the dynamic properties of alkaline electrolysers.

C.2. ELECTRICAL EQUIVALENT CIRCUIT

Milewski et. al. in [7], develop an electrical equivalent circuit model of the alkaline electrolyser using the reduced-order approach. In this approach, the main reactions which take place in the cell can be described by the flows of ions and electrons through an equivalent electric circuit. This results in the model shown in figure C.1. The parameters of the model can be experimentally determined from both static and dynamic operating tests on the electrolyser. In the model, i_1 represents the total electron flow transported by alkaline ions, while i_2 represents electrons which pass through the electrolyte in the same direction as the alkaline ions due to the presence of a small but significant electric conductivity [7]. The model can be simplified by neglecting current i_2 however, this can lead to errors in estimating E_{ideal}. The parameter r_1 models the overall 'permeability' of the electrolyte and electrodes structure to alkaline ions and r_2 models the electric conductivity of the electrolyte. Total ionic resistance of the cell r_1 is calculated using equation C.1.

$$r = \frac{\delta_{KOH}}{\sigma_{KOH}} + r_{other} \tag{C.1}$$

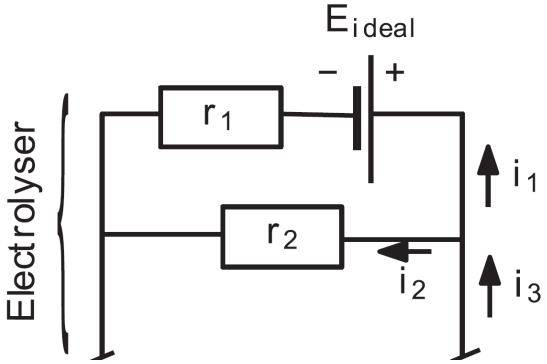

Figure C.1: Electrical equivalent of alkaline cell. Extracted from [7].

where δ_{KOH} is the ionic conductivity and σ_{KOH} the thickness of the electrolyte layer. All other effects are aggregated and modelled with r_{other}. According to [7], the deviation observed from the model and experimental data is below 3%. It must be noted however, that this approach is one of many modelling approaches proposed in literature.

Changing the stack model in the RSCAD model is the key modification that is required. The PEM is stack modelled by a resistor in series with a DC voltage source. As can be seen from figure C.1, the alkaline cell model is also made up of the same circuit but with an additional resistor in parallel. This makes the replacing the stack technically feasible. However, the assumptions for large scale alkaline electrolysers must be taken into account in scaling the model. The overall dynamics of the stack can be emulated with the aid of well-tuned converter controls.

BIBLIOGRAPHY

[1] T. Smolinka, E. T. Ojong, and T. Lickert, *Fundamentals of pem water electrolysis,* PEM Electrolysis for Hydrogen Production: Principles and Applications **11** (2016).

[2] H. Z. Ji, J. J. Sun, M. Huang, L. J. Wei, and X. M. Zha, *A nonlinear large-signal model for DC-dc converters,* in *Proc. IEEE 8th Int. Power Electronics and Motion Control Conf. (IPEMC-ECCE Asia)* (2016) pp. 2183–2186.

[3] S. Leng, *Coordination of multiple active front end converters for power quality improvement,* Ph.D. thesis, The Florida State University (2012).

[4] M. Mohanpurkar, Y. Luo, D. Terlip, F. Dias, K. Harrison, J. Eichman, R. Hovsapian, and J. Kurtz, *Electrolyzers enhancing flexibility in electric grids,* Energies **10**, 1836 (2017).

[5] T. Strasser and et al, *Real-time simulation technologies for power systems design, testing, and analysis,* IEEE Power and Energy Technology Systems Journal (2015).

[6] RTDS-Technologies, *Real time power system simulation,* (2018).

[7] J. Milewski, G. Guandalini, and S. Campanari, *Modeling an alkaline electrolysis cell through reduced-order and loss-estimate approaches,* Journal of Power Sources **269**, 203 (2014).

[8] O. Lavoine, F. Regairaz, T. Baker, B. RONNIE, L. Meeus, L. Vandezande, C. Hewicker, Y. Matsubara, R. Pereira, E. Torres, *et al., Ancillary services: an overview of international practices,* Electra , 86 (2010).

[9] V. Suarez, P. Ayivor, J. Rueda-Torres, and M. van ver Meijden, *Demand side response in multi-energy sustainable systems to support power system stability,* in *16th Wind Integration Workshop,October 25-27, 2017, Berlin, Germany* (Energynautics GmbH, 2017).

[10] P. D. A. van Wijk, *The green hydrogen economy in the northern netherlands,* (2017).

[11] V. der Merwe and J. H. Petrus, *Characterisation of a proton exchange membrane electrolyser using electrochemical impedance spectroscopy*, Ph.D. thesis, North-West University (2012).

[12] R. Harvey, R. Abouatallah, and J. Cargnelli, *Large-scale water electrolysis for power-to-gas,* PEM Electrolysis for Hydrogen Production: Principles and Applications , 303 (2016).

[13] J. Eichman, K. Harrison, and M. Peters, *Novel electrolyzer applications: providing more than just hydrogen*, Tech. Rep. (National Renewable Energy Laboratory (NREL), Golden, CO., 2014).

[14] R. Hovsapian, *Role of electrolyzers in grid services,* (2017).

[15] S. Adams, S. Schnittger, I. Kockar, N. Kelly, H. Xu, F. Monari, M. Edrah, J. Zhang, and G. Bell, *Impact of electrolysers on the network,* (2016).

[16] V. Ruuskanen, J. Koponen, K. Huoman, A. Kosonen, M. Niemelä, and J. Ahola, *Pem water electrolyzer model for a power-hardware-in-loop simulator,* International Journal of Hydrogen Energy **42**, 10775 (2017).

[17] P. Ayivor, J. Rueda-Torres, M. van der Meijden, R. van der Pluijm, and B. Stouwie, *Modelling of large size electrolyzer for electrical grid stability studies in real time digital simulation,* in *3rd Hybrid Power Systems Workshop,May 7-9 2018,Tenerife, Spain* (Energynautics, 2018).

[18] Z. Abdin, C. Webb, and E. M. Gray, *Modelling and simulation of a proton exchange membrane (pem) electrolyser cell,* International Journal of Hydrogen Energy **40**, 13243 (2015).

[19] K. Agbli, M. Péra, D. Hissel, O. Rallières, C. Turpin, and I. Doumbia, *Multiphysics simulation of a pem electrolyser: Energetic macroscopic representation approach,* International journal of hydrogen energy **36**, 1382 (2011).

[20] M. Lebbal and S. Lecœuche, *Identification and monitoring of a pem electrolyser based on dynamical modelling,* International journal of hydrogen energy **34**, 5992 (2009).

[21] O. Atlam and M. Kolhe, *Equivalent electrical model for a proton exchange membrane (pem) electrolyser,* Energy Conversion and management **52**, 2952 (2011).

[22] R. García-Valverde, N. Espinosa, and A. Urbina, *Simple pem water electrolyser model and experimental validation,* international journal of hydrogen energy **37**, 1927 (2012).

[23] N. Chiesa, M. Korpås, O. Kongstein, and A. Ødegård, *Dynamic control of an electrolyser for voltage quality enhancement,* in *proc of* (2011).

[24] P. Millet, *Characterization tools for polymer electrolyte membrane (pem) water electrolyzers,* PEM Electrolysis for Hydrogen Production: Principles and Applications , 179 (2016).

[25] F. da Costa Lopes and E. H. Watanabe, *Experimental and theoretical development of a pem electrolyzer model applied to energy storage systems,* in *Power Electronics Conference, 2009. COBEP'09. Brazilian* (IEEE, 2009) pp. 775–782.

[26] S. Bourne, *Scaling pem electrolysis to 100mw,* (2017).

[27] J. Solanki, N. Frohleke, J. Bocker, and P. Wallmeier, *Comparison of thyristor-rectifier with hybrid filter and chopper-rectifier for high-power, high-current application,* in *Proc. PCIM Europe* (2013).

[28] L. Yanfei, *A unified large signal and small signal model for dc/dc converters with average current control,* Transactions of china electrotechnical society **22**, 84 (2007).

[29] M. A. Shrud, A. H. Kharaz, A. S. Ashur, A. Faris, and M. Benamar, *Analysis and simulation of automotive interleaved buck converter,* World academy of science, engineering and technology (2010).

[30] L. Teshmont Consultants and S. Karim, *Transformer modelling guide,* Alberta Electric System Operator, Revision **2** (2014).

[31] H. Vogelesang, *An introduction to energy consumption in pumps,* World pumps **2008**, 28 (2008).

[32] P. Kundur, N. J. Balu, and M. G. Lauby, *Power system stability and control*, Vol. 7 (McGraw-hill New York, 1994).

[33] O. Rolf, *Engineering Solutions for the Next Millennium. 1999 IEEE Canadian Conference on Electrical and Computer Engineering (Cat. No.99TH8411)*, Ph.D. thesis (2003).

[34] D. E. Rivera, *Internal model control: A comprehensive view,* Arizona State University, Tempe, Arizona , 85287 (1999).

[35] R. W. Erickson and D. Maksimovic, *Fundamentals of power electronics* (Springer Science & Business Media, 2007).

[36] J. Fraden, *Handbook of modern sensors: physics, designs, and applications* (Springer Science & Business Media, 2004).

[37] F. Blaabjerg, R. Teodorescu, M. Liserre, and A. V. Timbus, *Overview of control and grid synchronization for distributed power generation systems,* IEEE Transactions on Industrial Electronics **53**, 1398 (2006).

[38] S. S. Lechat, *Voltage oriented control of three-phase boost PWM converters*, Master's thesis (2010).

[39] D. Jovcic, *Voltage source converter controller design for dc networks,* (2010).

[40] N. Mendalek and K. Al-Haddad, *Modeling and nonlinear control of shunt active power filter in the synchronous reference frame,* in *Proc. (Cat. No.00EX441) Ninth Int Conf. Harmonics and Quality of Power*, Vol. 1 (2000) pp. 30–35 vol.1.

[41] C. Bajracharya, M. Molinas, J. A. Suul, T. U. Undeland, *et al.*, *Understanding of tuning techniques of converter controllers for vsc-hvdc,* in *Nordic Workshop on Power and Industrial Electronics (NORPIE/2008), June 9-11, 2008, Espoo, Finland* (Helsinki University of Technology, 2008).

[42] H. W. Dommel, *Digital computer solution of electromagnetic transients in single-and multiphase networks,* IEEE Transactions on Power Apparatus and Systems **PAS-88**, 388 (1969).

[43] J. J. Grainger and W. D. Stevenson, *Power system analysis*, Vol. 621 (McGraw-Hill New York, 1994).

[44] J. Levene, M. Mann, R. Margolis, and A. Milbrandt, *Analysis of Hydrogen Production from Renewable Electricity Sources: Preprint*, Tech. Rep. (National Renewable Energy Laboratory (NREL), Golden, CO., 2005).

[45] W. Hu, C. Wang, Z. Chen, and B. Bak-Jensen, *Power system transient stability improvement using demand side management in competitive electricity markets,* in *European Energy Market (EEM), 2012 9th International Conference on the* (IEEE, 2012) pp. 1–8.

[46] K. Harrison, M. Mann, D. Terlip, and M. Peters, *Potential for distributed and central electrolysis to provide grid support services,* Hydrogen and Fuel Cell Technical Highlights. NREL/FS-5600-54658. Golden, CO: National Renewable Energy Laboratory (2012).

[47] ENTSO-E, *Operation Reserve Ad Hoc Team Report*, Tech. Rep. (ENTSO-E, Brussels, Belgium, 2012).

[48] P. Millet, *Degradation processes and failure mechanisms in pem water electrolyzers,* PEM Electrolysis for Hydrogen Production, S , 219 (2016).